Capping of Contaminated Marine Sediments

Ebullition of Biogenic Gas and its Impact on the Flux of PAH

Luke Dokter

Master Thesis in Geosciences

Discipline: Environmental Geology & Natural Catastrophies

Department of Geosciences

Faculty of Mathematics and Natural Sciences

UNIVERSITY OF OSLO

June 2005

© Luke Dokter, 2005

Tutor(s): Espen Eek (Norges Geotekniske Institutt)

This work is published digitally through DUO – Digitale Utgivelser ved UiO

http://www.duo.uio.no

It is also catalogued in BIBSYS (http://www.bibsys.no/english)

Researched, written and
compiled at the:

NORWEGIAN
GEOTECHNICAL
INSTITUTE

"The history of any one part of the Earth, like the life of a soldier, consists of long periods of boredom and short periods of terror."
British geologist Derek V. Ager

ABSTRACT

The risk associated with exposure to contaminants has, in recent years, drawn attention to the fate and transport of these contaminants in shallow marine sediments. It has been suggested that the transport of Hydrophobic Organic Contaminants (HOC), such as Polycyclic Aromatic Hydrocarbons (PAH) from the sediments surface, may be enhanced by the existence of mechanisms which complement the diffusive and advective fluxes. Gas bubbles released from the sediment, through the ebullition of biogenic gas is one of these possible mechanisms. Ebullition may theoretically increase PAH transport in the *diffusive boundary layer* (DBL), by introducing additional advection through water filled bubble voids and through the partitioning of PAH to the gas-water interface of the rising bubbles. This enhanced transport may reduce the effectiveness of remediation techniques, such as the isolation of contaminated sediments by engineered capping.

Therefore, a series of one dimensional (1-D) diffusion tests have been conducted, using contaminated marine sediment from Oslo Fjord. Half of the tests had a carbon source added to the sediment to initiate ebullition. The setup consisted of some tests with only sediment, both with and without ebullition and also some with the sediment covered by a capping layer (gravel – 0-2 mm), also with and without ebullition. Tests consisting of only capping material and only sea water were also performed. Ebullition was observed 30 – 60 days after initiation, generating gas filled fissures in the sediment. The diffusive flux of 10 PAH compounds from the sediment or capping phase, through a 1 – 2 cm layer of sea water, was then measured over a period of 7 months.

Results from the uncapped tests showed that the diffusive flux of PAH fitted a linear model described by Fick's first law and increased from $2.1 \times 10^{-4} \pm 0.4 \times 10^{-4} \mu g/cm^2/day$, for those tests without ebullition, to $3.0 \times 10^{-4} \pm 0.4 \times 10^{-4} \mu g/cm^2/day$ for those tests with ebullition. The capped tests showed no significant increase in the diffusive flux of PAH attributed to ebullition. This finding is positive and confirms that the ebullition of biogenic gas from marine sediment, in a laboratory experiment, has no impact on the effectiveness of capping as a remediation method.

Keywords: PAH; ebullition; biogenic gas; capping; diffusional flux; sediment

ACKNOWLEDGEMENTS

TABLE OF CONTENTS

LIST OF FIGURES

LIST OF TABLES

LIST OF UNITS & ABBREVIATIONS

1-D	One dimensional
A	Area (cm^2)
atm	Atmosphere (101325 Pa)
B	Ratio determining effective area of sediment interface
BBL	Benthic Boundary Layer
C	Concentration
C_b	Concentration of PAH_{10} in bubbles (µg/ml)
CH_4	Methane
CO_2	Carbon Dioxide
C_{pw}	Concentration in pore water (µg/ml)
Cr	Chromium
c_u	Undrained Shear Strength (kPa)
D	Diffusion coefficient (cm^2/sec)
d.w.	Dry weight
DBL	Diffusive Boundary Layer
DNA	Deoxyribonucleic acid
E(z)	Eddy diffusion coefficient
E_{cap}	Efficiency of Capping Layer
F	Diffusive flux (µg/cm^2/day)
f	dimensionless factor = 11.6
F_{cap}	Flux from tests with cap
Fe	Iron
f_{oc}	Fraction of organic carbon
$F_{PAH_{10}}$	Flux of PAH10 Compounds as described by Fick's Law
F_{sed}	Flux from tests with no cap in place
g	Gravity (9.8 m^2/s)
GC	Gas chromatograph
H	Henry's Constant
H_2	Hydrogen gas
H_2S	Hydrogen Sulphide
HOC	Hydrophobic Organic Contaminants
$j_{PAH_{10}}$	Mass of PAH_{10} compounds per unit area (µg/cm^2)
K_{bw}	Bubble-water partition coefficient
K_d	Soil-water distribution coefficient
K_{gw}	Methane-water partition coefficient
K_{oc}	Organic carbon-water partition coefficient
Mg	Magnesium
$M_{PAH_{10}}$	Mass of PAH_{10} compounds (µg)

n	Mole fraction
N_2	Nitrogen gas
η_w	Viscosity of sea Water (1.235 cP)
O_2	Oxygen gas
OTP	Ortho-terphenyl
P	Pressure (Pa)
PAH	Polycyclic Aromatic Hydrocarbons
PAH_{10}	Naphthalene, Acenaphthylene, Acenaphthene, Fluorine, Phenanthrene, Anthracene, Fluoranthene, Pyrene, Benzo (a) anthracene and Chrysene.
Pb	Lead
P_{ow}	Octanol-water partition coefficient
R	Reynolds number (8.31 j/mol/K)
r	Radius (cm^2)
R_{OTP}	Concentration ratio
S	Relation between F and z ($\mu g/cm^3/day$)
t	Time
T	Temperature
TOC	Total Organic Carbon
u_*	Shear velocity
u_x	Mean velocity
v	Viscosity
V	Volume
V_B	Molar Volume
z	Length
Z	Dimensionless height
ε	Porosity
κ	von Karmen's Constant
λ	Mean free path
ρ	Density (kg/m^3)
σ_z	Average distance diffused
τ	Tortuosity

1 INTRODUCTION

The identification and remediation of contaminated marine sediments has, in recent years, become increasingly important. In the past these polluted sediments, which are a result of anthropogenic activity, remained out of sight and therefore out of mind to much of the population. After the Love Canal incident (Niagara Falls, New York), in which a residential area was unwitting constructed on top of highly polluted soil, resulting in many health problems for its residents. The US government developed the Superfund Program to identify and cleanup contaminated sites. The lessons learnt from the Love Canal incident also forced many other countries to develop similar schemes, dealing with the past ineptness in waste management. In Norway, seriously contaminated marine sediments have been identified at more than 120 sites (SFT, 1998). With projects such as the New Opera House in Oslo it has been necessary to identify these contaminated sediments and develop remediation techniques, which reduce the overall risk posed to humans and the surrounding ecosystem. One such remediation technique involves the engineering of a physical cap, which isolates the contaminated sediments. The cap can be constructed of sand or gravel and may also utilise geomembranes.

Capping only isolates and does not remove contaminates, therefore a great deal of research has been conducted investigating the effectiveness of different capping materials under varying environmental conditions. Nonetheless, many questions still remain as to the behaviour of the capping materials when placed on the sea floor. Processes such as advective flow (i.e. the movement of groundwater or flow due to consolidation of sediments as they are loaded) and potential diffusive permeation of the capping materials by contaminants are reasonably well understood. However, it has been hypothesised that other processes such as bioturbation (The movement of contaminated sediment by bottom living animals) and the ebullition of biogenic gas (The bubbling of the sediment due to gas produced by microbial activity) may also play an important role in the caps isolating efficiency. Only a small number of attempts have been made to observe and quantify the process of ebullition and even fewer attempts have been made to describe this process. Therefore, an investigation into the process of ebullition, and it influence over the diffusional flux of 10 PAH compounds, has been conducted for both a capped and a non-capped marine sediment. This investigation was performed in the laboratory, over a period of 7 months, and the results together with a description of the main processes are outlined in the following report.

2 BACKGROUND AND AIMS

The isolation of contaminated marine sediments, through the construction of an engineered capping layer, has gained acceptance in recent years as an effective alternative to different processes such as removal by dredging. Research has been conducted into the fate and transport of contaminates in marine sediments isolated by a capping layer (Costello (2003), Eek et al (2003a), Mohan et al (2000), Herrenkohl et al (2001) & Thoma et al (1993)), although questions still remain as to the overall behaviour of these systems.

One question encompasses the effect the ebullition of biogenic gas has, on the transport of contaminates from sediments isolated by a remedial capping layer. This gas ebullition arises from the microbial breakdown of organics in the sediment (discussed in Section 2.2). A small number of attempts have been made to explore and quantify ebullition in sediments (Hughes et al (2004), Huls & Costello (2003), Kesteren & Kessel (2002), Kesteren (2000) & Adams et al (1997)), although these focused mainly on changes in the engineering strength of the sediment or on direct increases in contaminant transport due to ebullition and not the processes. Further research is therefore required if the processes of overall significance in contaminant transport by ebullition are to be understood.

Therefore, the aim of this study has been to augment the present understanding of ebullition in marine sediments, with relation to the transport of contaminates through an engineered capping layer. This was accomplished by measuring the one dimensional (1-D) flux of PAH in a series of simple bench tests, over a period of several months. These bench tests were developed and conducted by this author, between June 2004 and December 2004, as part of a research placement at The Norwegian Geotechnical Institute (NGI). It is hoped that the results from these tests and the discussion accompanying them, will build on and enhance our present understanding of the behaviour of capped marine sediments.

Before discussing ebullition, it is important to consider the main mechanisms involved in the transport of contaminates, including the origins of these contaminants. A short discussion into the generation of biogenic gas in marine sediment is also relevant and therefore the remained of Chapter 2 will explore these topics, setting the scene for the discussions in Chapter 4.

2.1 Sources of Contaminates in the Oslo Fjord

Norwegian industrialisation had its beginnings along the banks of the Akerselva River during the 1850s. The abundant supply of water provided the energy required by earlier industries such as timber mills which, eventually led to larger industries such as ship building yards being developed. The waste generated by this industrial activity, combined with the sewage and runoff from the city itself, ensured that high levels of organic matter, nutrients, and contaminates entered the relatively confined environment of The Inner Oslo Fjord. This eventually resulted in the complete eutrophication of the fjord and a realisation that, measures needed to be taken to prevent further deterioration.

Surveys of the sediments in Oslo Fjord have been performed and results have shown that high levels of all environmental contaminants are present. This includes heavy metals such as lead and mercury, and a wide range of compounds including Polycyclic Aromatic Hydrocarbons (PAH), Polychlorinated Biphenyls (PCB), DDT (Dichlorodiphenyltrichloroethane), Methyl Tertiary Butyl Ether (MTBE) and Tributyltin (TBT). The contaminated sediment exists up to a thickness of 2 meters in some areas and can be visually distinguished from the cleaner natural underlying clay (Sivertsen et al, 2003). Developments in the understanding of the effects these compounds have on the environment, has made it not only necessary to remove or contain them, but also to develop ways in which reduce there emission in the first place.

2.2 Biogenic Gas Production in Marine Sediments

As mentioned the ebullition of microbial gas from marine sediments may influence the transport of contaminates, both directly from the sediment surface or through an engineered capping layer. Experiments by Van Kesteren et al, (2002) have shown that gas bubble nucleation, the precursor to ebullition, occurs when pore waters become saturated with CH_4 at concentrations only slightly higher than saturation. Bubbles in the sediment then grow as the gas that does no escape by convection or diffusion accumulates. And although these bubbles usually remain small in diameter, they have a very high density per cubic meter and are only limited by the gas production rates. Bubble nucleation may eventually lead to crack formation if the fracture energy and stress conditions are favourable. These cracks or fissures, depending on their depth, may eventually open to the sediment surface and the discharge of water and gas will occur (Van Kesteren et al, 2002).

Jepsen et al (2000) has shown that these bubbles also effect the consolidation of the sediment and therefore may influence some of the processes mentioned later in Section 2.3.

A number of studies have been conducted into the production and accumulation of biogenic gas in marine sediments (Davie et al (2004), Bazhin (2003), Heyer & Berger (2000) Vogel et al (1982) & Rice & Claypool (1981)). Findings have shown that in subaqueous cohesive sediments, such as in Oslo Fjord, organic matter is decomposed through the reduction of different electron acceptors. The most energetic of these acceptors are used first, in the order $O_2 > NO_3^- > Mn^{4+} > Fe^{3+} > SO_4^{2-} > CO_2$. Oxygen usually accounts for most of the oxidation at the sediment-water interface, although the depth to which it penetrates is limited by diffusion. Below this penetration depth and in marine sediment systems, sulphate-reducing bacteria usually out compete methanogens and are therefore the dominate species. This dominance is due to an affinity sulphate-reducing bacteria have for H_2 as an electron acceptor compared to that of methanogens. Therefore, methanogenesis in marine sediments is not supported by H_2, as it is in fresh water sediments, but by methylated substrates such as methylamines and methanol. Even though sulphate-reduction dominates in marine sediments, it is the solubility of methane in water which makes it the most likely candidate for the bubble nucleation required for ebullition. At 1 atm, methane has a partial pressure 66 times higher than Hydrogen Sulphide (H_2S) and 22 times higher than Carbon Dioxide (CO_2), therefore making it a likely candidate for bubble nucleation (Sanders, 1999).

To achieve ebullition in this experiment, methanogenesis was initiated through the introduction of an artificial carbon source. This resulted in two distinct phases; the first involved a range of organisms fermenting the large carbohydrate based organic substances down into smaller acidic wastes. For example, glucose may have been fermented leaving formate, hydrogen gas, acetate, and many more compounds as by-products. These organisms are generally anaerobic bacteria and these reactions occur for the most part in the absence of oxygen. Secondly, these bi-products were used by the methanogens which produced methane as a by-product. These types of reactions are found anywhere oxygen is absent and are therefore, ideally suited to the sediments found in Oslo Fjord.

The processes in which the ebullition of gas influences the transport of contaminates are discussed in greater depth later in Chapter 4. First Section 2.3 will discuss alternate processes which, together with ebullition, contribute to the overall transport and entrapment of contaminates in marine sediments. This discussion will also focus on the impact these processes have on the reliability of an engineered capping layer.

2.3 Deposition and Mobilisation of Contaminants

Figure 1 shows the main processes active in the deposition and mobilisation of contaminants in the marine sediment environment. Studies by Brenner et al (2002), Khodadoust et al (2005), Loehr et al (2000) and Headly et al (2001) have described these processes, especially in relation to the fate and transport of PAH compounds. It is obvious from Figure 1 that some of the processes control the deposition and entrainment of contaminates (*sediment is a sink*), while others are active in transport and dissemination (*sediment as a source*). The experiments presented in this report will investigate the transport of PAH through an engineered capping layer and therefore, the source terms are of greatest interest. However, all of the processes in Figure 1 will be discussed throughout the remainder of this chapter.
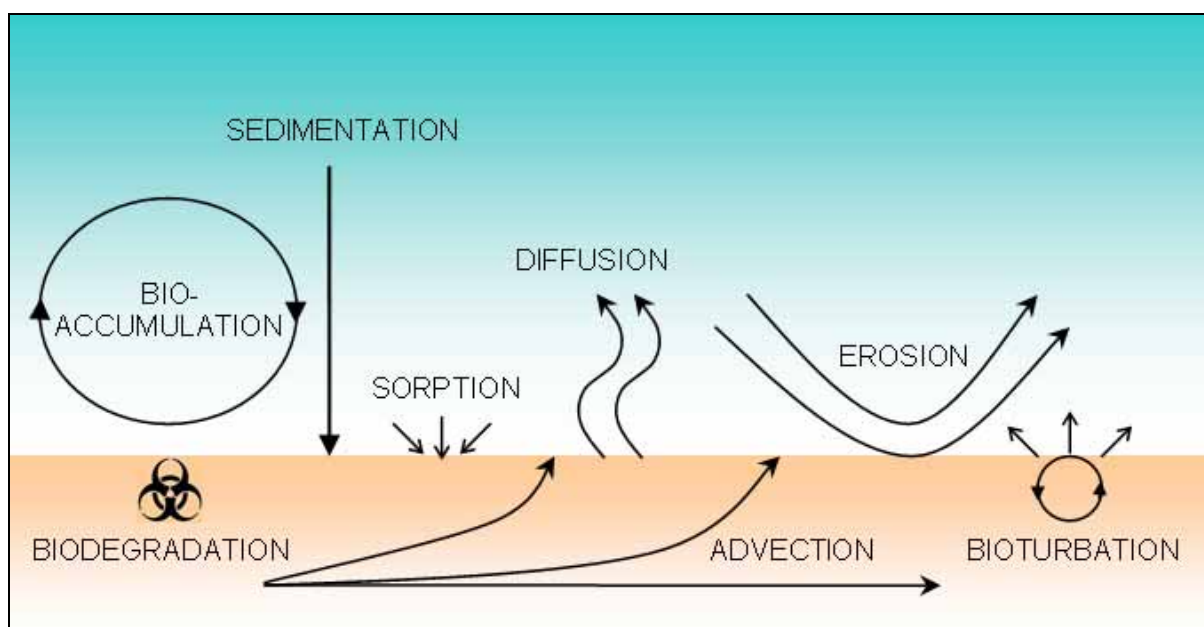
Figure 1: Main processes involved in the deposition and transport of contaminants in the sediment-water interface.

2.3.1 Sedimentation

The settling of suspended particles in the water column is controlled by many factors including the particle diameter, particle density, fluid density and fluid viscosity. An in-depth description of these factors is beyond the scope of this paper. However, it is important to consider sedimentation rates and the concentration of contaminates bound to these particles, when considering remediation methods. It is well known that rates of accumulation can vary from millimetres per 1000 years in the pelagic ocean up to centimetres per year in lakes and near shore oceanic areas (Lerman 1979, p. 333).

Therefore it is of no surprise that the sedimentation rates in Oslo Fjord are quite high and strongly influenced by the outflow of the Arkeselva River. This rate is important when considering capping as a remediation option. If it is too high for the area under consideration, and depending on if the concentration of contaminates on the sediment particles, the isolating properties of the cap may either be increased or diminished. An increase in efficiency will arise from cleaner sediments creating a new barrier to contaminate transport, or oppositely the cap will become worthless if the new sediments are as polluted as those being contained. It is therefore of no use constructing a capping layer if first, actions have not been taken to reduce or remove sources of contaminants in the area.

2.3.2 Erosion

Water passing over seabed sediment may eventually reach a high enough velocity to cause the erosion of the topmost layer. In normally consolidated muddy sediment strength increases with depth and therefore, the sediment will be eroded down to a level at which point the strength in the sediment is sufficient to resist the shear. That is to say that continual erosion will only occur when the shear stress is considerably higher than the critical erosion shear strength of the mud (Dyer 1986, p.220). Norwegian fjords are usually deep anoxic basins (threshold fjords) (Breedveld et al, 2003), and although the velocity at the water sediment interface in deeper areas is usually quite low, it may still be influential in shallower areas such as shorelines and bays.

Erosion forces usually arise from tidal, wave and current forces however other forces may also contribute to the resuspension of contaminated sediments. For example, propeller wake from large boat traffic in Oslo fjord may cause velocities capable of eroding bottom sediments. Furthermore, Thibodeaux & Bierman (2003) have hypothesised that disturbances in the top layer of sediment caused by benthic organisms and gas bubbles generated by microbes (Jepsen et al, 2000), may effectively reduce the shear strength of the sediment leading to higher erosion rates. Thoms et al. (1995) has observed that bioturbation mixing, discussed in later in Section 2.3.5, is limited to the top 15 cm of sediment. Therefore, the construction of a cap may eliminate the enhanced erosion due to bioturbation. Bioturbation may increase the erosion of the engineered cap but as these caps are generally armoured with heavier material this erosion is usually limited.

2.3.3 Sorption

Sorption describes a process where a compound is either absorbed (incorporated) or adsorbed (attracted to surface) to a solid, liquid or gas. Sorption also incorporates the process of ion exchange, in which one chemical species is replaced by another on the surface of a solid. Sorption is an important consideration when investigating sediment-water interfaces as it largely regulates the transport of pollutants between these two interfaces (Appelo & Postma 1999, p.142).

Eek et al. (2003b) has shown that redox reactions do occur between capping materials and contaminated sediments, in which case heavy metals can be dissolved from the sediment into the cap. That is to say that Redox processes have a tendency to perturb the sediment-water partitioning of contaminates. Results show that contaminates once dissolved, are usually re-bound to the mineral phase of the capping material. For heavy metals the key parameter for this rebinding is the distribution coefficient between soil and water (K_d). However for organic compounds such as PAH, partitioning to the capping material is largely dependant on the fraction of organic carbon (f_{oc}) in the solid phase of the sediment or capping layer and the octanol-water partition coefficient (P_{ow}) of the compound.. This is important as it shows that the diffusion or advection of contaminants through the capping material may be retarded by the properties of the mineral phase.

2.3.4 Diffusion

The dispersal of contaminants by the intermolecular nature of gas, pore water, and surface water is known as molecular diffusion. Diffusion will often be the dominant mechanism governing the movement of dissolved contaminants, especially in systems where the advective flow of pore waters is low. In the cohesive sediments of Oslo Fjord, the hydraulic gradient or the hydraulic conductivity is usually fairly low resulting in only small amounts advection (Lim et al 1998, p. 812).

In turbulent systems such as those in nature, the diffusion of contaminants may be referred to as dispersal or turbulent eddy diffusion (Lerman 1979, p.56). In a laminar system, such as in this experiment, the driving force of diffusion is the gradient of the chemical potential of the species. In a turbulent system the driving force also includes the formation of eddies and microscopic velocity fluctuations within the medium. The zone, in which these processes occur, is known as the *benthic boundary layer* (BBL). The BBL is a zone of intense transport of solutes and suspended particles, and of high chemical and biological activity.

Furthermore, eddy diffusion within the BBL dominates due to the turbulent nature of the sediment water interface (Boudreau, 2001).

Diffusive processes within the BBL can be described by a total diffusive flux (*F*) of a solute with a unique diffusivity (*D*) in the direction perpendicular to the sediment surface (*z*)

$$F \approx -\left[D+E(z)\right]\frac{\partial C}{\partial z}$$
(2.3.1)

$E(z)$ describes the eddy diffusion coefficient for a solute and can be determined as a function of a dimensionless height above the sediment surface ($Z = (zu_*)/v$), the viscosity of the water (*v*), the shear velocity of the water (*u*) and the von Karman's constant (*κ*). Empirical equations to calculate $E(Z)$ can be found in work by Boudreau (2001, p. 106). The relationship between *Z* and eddy diffusion $E(z)$ is described in Figure 2, showing that as the surface is approached, *F* is no longer dominated by the turbulent flow of the liquid and $E(Z) \to 0$.
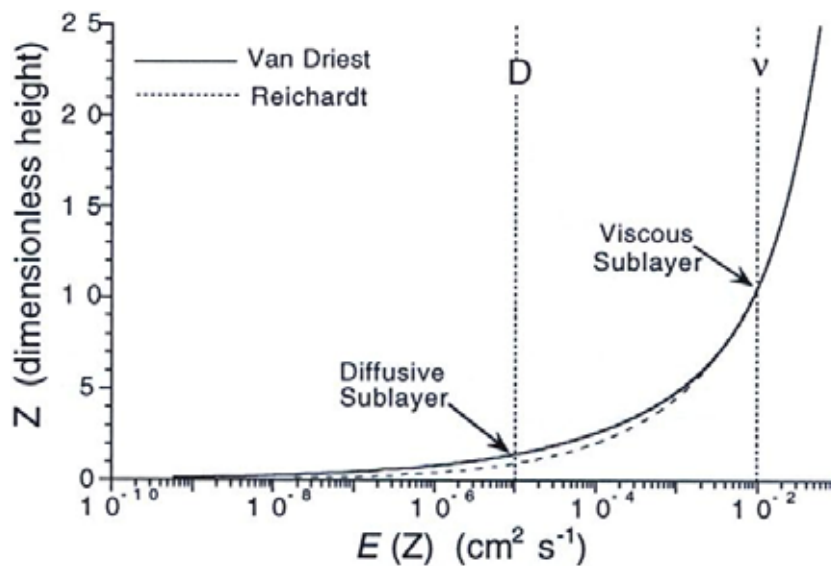
Figure 2: Plot of eddy diffusivity, *E(Z)*, with dimensionless height Z in the boundary layer above an infinite flat plate. Also plotted are vertical lines marking the values of the kinematic viscosity of water, *v*, and a typical molecular diffusivity, *D*, of a solute. The intersections of the curved lines and the vertical lines for *v* and *D* mark the top of the viscous sublayer and diffusive boundary layer respectively (Boudreau, 2001).

The vertical line in Figure 2 labelled viscous sublayer, defines the point a which when $E(Z) = v$. In this area $E(Z)$ falls bellow the kinematic viscosity of the fluid and the water velocity becomes dominated by viscous forces.

Much closer to the sediment, eddy diffusion becomes less than molecular diffusion and a *diffusive sublayer* or *diffusive boundary layer* (DBL) (Jørgansen & Revsbech, 1985) is formed. In this layer molecular diffusion is the dominate transport mechanism. Therefore as $E(Z) \rightarrow 0$ the relation for the flux of a solute from the sediment becomes

$$F = -D\frac{dC}{dz} \qquad (2.3.2)$$

this equation describes Fick's first law and represents a linear concentration gradient from the sediment in the *z* direction. Diffusivity (*D*) can be interpreted in the framework of a random walk model and is related by the parameters, mean free path λ (*Δz*) and mean velocity u_x ($\Delta z / \Delta t$), by the simple relation:

$$D = \frac{1}{2}\lambda u_x \qquad (2.3.3)$$

We can also calculate the average distance (σ_z) a population of molecules has diffused in a one dimensional case as being;

$$\sigma_z = (2Dt)^{\frac{1}{2}} \qquad (2.3.4)$$

A discussion into how equations (2.3.3) and (2.3.4) are related and the theory behind the framework of a random walk model will not be discussed in detail here, but can be found in work by Schwarzenbach et al, 2003.

It is hypothesised that the construction of a cap would remove or reduce the shear velocity generated by water flow thus reducing $E(Z)$ to zero and leaving the DBL as the only active region for solute transport through diffusion.

2.3.5 Bioturbation

The processes discussed up until now have all entail physical or chemical mechanisms. Despite the significance of diffusion and advection, it is now generally accepted that there are a number of more complex processes in the BBL driving solute transport processes. One of these mechanisms "bioturbation" described by Thibodeaux & Bierman (2003) as – an in-bed particle translocation phenomenon driven by the activity of benthic organisms, which move sediment bound pollutants and homogenise surface layers – may have a higher then expected influence on the transport of contaminants. Recent mass balance studies into the chemical release process from marine sediments have shown unexpectedly high release rates.

And it may be bioturbation which accounts for the higher rates of transport during non resuspending flows and even during particle deposition (Thibodeaux & Bierman, 2003).

Simply put benthic organisms deposit pellets of faecal material on the bed surface moving contaminated particles upwards where they settle on the sediment surface, losing a fraction of their contamination. Cleaner, particles subduct downward into the bed, where they sorb contaminates from adjoining contaminated particles. The bioturbation process can persist for decades until the source material is depleted of its reversibly available contaminant loads (Thibodeaux & Bierman, 2003).
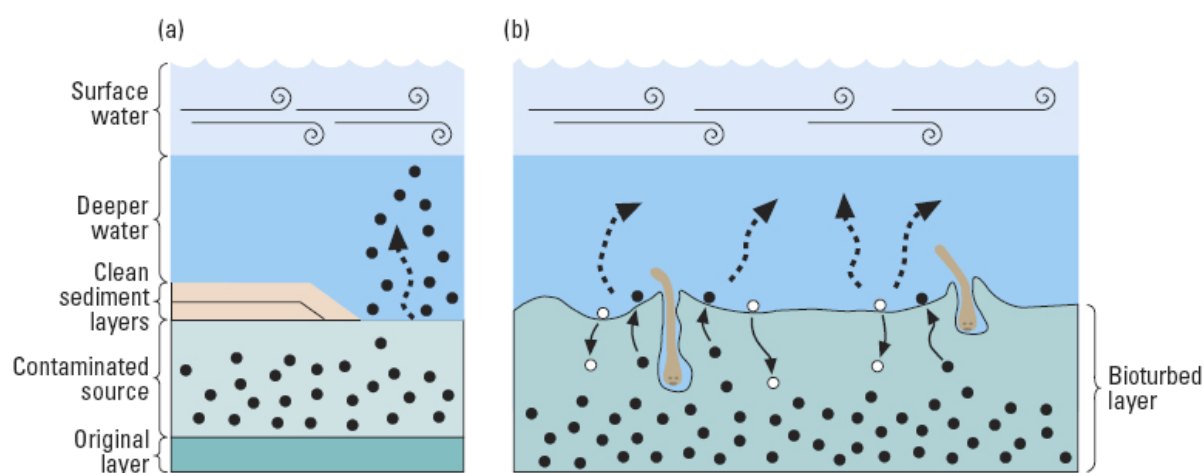
Figure 3: (a) This conventional scenario shows particle resuspension (black dots) and the placement of clean sediment layers on the surface of the contaminated source. (b) Here, the clean layers are gone. They have been disturbed by oligochaete bioturbation, a significant aid to pollutant release. (Thibodeaux & Bierman, 2003).

The process of bioturbation is illustrated in Figure 3(b) with the extra transport mechanisms depicted against the more conventional scenario of contaminate transport shown in Figure 3(a). Particle resuspension through erosion and advection (Sections 2.3.2 & 2.3.6) (black dots) and the placement of clean layers through sedimentation (Section 2.3.1) are visible in Figure 3(a). However in Figure 3(b) the clean layers are gone, having been disturbed by bioturbation.

Tens of thousands of small earthworms and related animals may inhabit one square meter of sediment and their continual feeding circulates buried pollutants to the surface and disrupts newer cleaner deposits. Studies (Write et al, 1997) have also shown that the BBL and seabed micro-morphology may be biologically dominated, resulting in changes in hydraulic roughness compared to when only physical processes such as erosion are present

It is believed that the construction of a capping layer would neutralise the effects of bioturbation, as benthic organisms usually only occupy the first 10 to 15 cm of sediment. However, Reible (1996) has mentioned that the bioturbation layer is thought to provide little or no resistance to mass transfer through the cap, thus effectively reducing a caps active thickness. Therefore, the bioturbation layer needs to be taken into consideration when discussing the thickness of an engineered cap.

2.3.6 Advection

The flow of water through porus sediment can be described by a flux relationship in which, the volume of water flowing per unit area of the porus bed is proportional to hydrostatic pressure difference across the bed (Darcy's Law) (Lerman, 1979 p.44). It is obvious that advective flow is driven by forces, in which the magnitude of flow does not strongly depend on the chemical composition of the sediment in which the material is being transported. That is to say, that the transport of contaminants through advection is largely driven by the flow of pore water and therefore the hydraulic gradient present.

The potential causes of these gradients could be currents, waves, tidal ebb, density changes or subaqueous groundwater flow (Huettel & Webster, 2001 p.146) within the aquatic system. In sandy, permeable sediments, these types of interstitial water motions can be an effective transport mechanism and may exceed molecular diffusion by many orders of magnitude. However in muddy, cohesive sediments such as those found in Oslo Fjord, advective flow is not thought to play a major role in the mobilisation of contaminants. However, as caps are generally constructed from sandy material these interstitial water motions may influence the transport of solutes once they have entered into the pore water of the capping material. Furthermore, the velocities generated by these motions may reintroduce the eddy diffusivity term discussed in Section 2.3.4, further influencing solute transport.

There has also been discussion into the effects of advective flow generated during the consolidation of marine sediments after the application of a remedial cap (Kesteren et al, 2002). Although, under steady state conditions the influence of advection is not of concern, since it only represents the transit effect of consolidation which, in comparison to diffusion is a relatively fast process.

2.3.7 Degradation

The degradation or alteration of contaminants through both chemical and microbial oxidation is one way in which contaminants can be demobilised or removed. Hinga (2003, p. 466) has shown that in most marine sediments, microbial degradation is probably the main mechanism for decreases in concentration of contaminants over time, especially decreases in PAH. However, the micro-organisms ability to degrade contaminants is largely dependant on the types of microbes present and the environment in which they inhabit (Hinga 2003, p 466).

For example, in sediments where little light penetrates to the sea floor photolysis is not a significant process. Temperature also has an influence on degradation and therefore these rates may vary seasonally. In environments rich in oxygen the main species will be aerobic and in environments devoid of oxygen anaerobic species will dominate.

The system present in Oslo Fjord consists of largely anaerobic sediment devoid of photolysis. Tests preformed by this author (Section 3.1) and the discussion in Section 2.2 shows that processes such as sulphate-reduction and methanogenesis are present in these sediments. These types of anaerobic degradation may generate anoxic conditions resulting in sulphatic pore water and subsequent precipitation of sulphide minerals, thus resulting in the strong binding of many heavy metals like Pb, Mg and Cr to the capping material (Eek, 2003b). Micro-organisms degrade PAH in marine sediments and this degradation may also occur in an engineered capping layer and this is discussed again in Section 4.2.3.

2.3.8 Bioaccumulation

Bioaccumulation describes the accumulation or uptake of contaminates or toxins in a biological system. Most substances, such as PAH have a short half-life, as they are usually metabolized, or excreted as waste. However, some compounds may stay in a system for a much longer period of time for example, DDT or tetra-ethyl lead (TEL), and this is where the problem arises. Generally these compounds are not acutely poisonous but are associated with chronic poisoning. Contaminates such as PAH are known carcinogens and can mutate the DNA structure of bottom filter feeding organisms such as mussels, oysters and worms. Furthermore, these contaminants have the capacity to potentially change the community structure of naturally occurring benthic organisms. These changes may in turn impact on local fish stocks or the general health of the local aquatic ecosystem (Crane et al, 2002). In addition to changing local ecosystem the bioaccumulation of contaminants in the base of the aquatic food chain, can have disastrous effects for organisms higher up such as humans.

This was proven in the 1950s in Minamata, Japan where more than 900 people died in severe pain due to mercury poisoning through the consumption of contaminated fish and shellfish taken from the local bay. Unfortunately the bay was also used for the discharge of wastewater from an industrial plant producing, in which high levels of mercury were present.

The introduction of cleaner capping material on top of contaminated marine sediments, reduces the rate of bioaccumulation in benthic feeding organisms by isolating the contaminate source. However, as mentioned in Section 2.3.1, if suspended particles in the surface waters are highly polluted the cap will have no long term effect in reducing the rates of bioaccumulation.

3 EXPERIMENTAL PROCEDURES

Four experiments were conducted to investigate the ebullition of biogenic gas and it influence on the overall flux of 10 PAH compounds, from contaminated marine sediment covered with an isolating layer of gravel or 'cap'. The first examined only the production rates of biogenic gas in the sediment and the results were used in the development of the final three experiments. The remaining experiments all investigated the flux of 10 PAH compounds from contaminated sediment under a variety of circumstances. The following sections describe the methods and materials used in the production of all four of the experiments.

3.1 Measurement of Microbial Gas Production Rates in Sediment

Before the experimental procedures for the 1-D diffusion tests mentioned in Chapter 2 are discussed, a short presentation of gas production rates in the sediment is required. These rates of production are very important, because without sufficient gas production to provide ebullition the investigation of ebullition would be impossible. Furthermore, as it is the production of gas and not the processes behind this production which are of most relevance, the overview in this section will give a description of both the investigation method and a short presentation of the results.

As discussed in Section 2.2 the production of gas which leads to crack formation in marine sediment, is a complex process involving many geneses of micro-organisms. Although, as most polluted marine sediments exist in environments devoid of oxygen, it assumed that anaerobic process are dominant. One of these gas forming processes, methanogenesis, has been investigated as a potential source of ebullition.

Two trials were performed to determine if sufficient gas could be produced in the sediment, through microbial respiration. The first trial involved the initiation of microbial respiration by the introduction of various weights of carbon equal to 1%, 2%, 4% and 6% of the dry weight of the sediment. This was done to determine an optimal percentage of carbon required to achieve the highest possible production of methane. As carbon makes up 44% of the weight of starch ($C_6H_{10}O_5$), 0.023 g, 0.045 g, 0.9 g and 1.4 g of starch per gram of dry sediment was added. The trials were kept at a constant 21ºC and were prepared by placing approximately 220 g of the sediment-starch mixture into 1 litre glass jars (area of 60 cm^2 perp. to the vertical axis) and flushing them with Nitrogen (N_2), before sealing the jars with rubber membranes.

A one litre laboratory gas bag fitted with a rubber valve connected to a 2-way syringe was then inserted into the membrane of the jar. The bag allowed for an increase in gas volume without an increase in pressure inside the jar. Furthermore, by measuring the change in volume of the bags the amounts of gas produced could be determined.

The bags also made it possible to periodically measure the mole fractions of a number of compounds in the gas. The mole fractions were measured using a mini-portable gas chromatograph calibrated for CH_4, CO_2, N_2, H_2 and O_2 and the concentrations and volumes were calculated using the Ideal gas equation

$$PV = nRT \tag{3.1.1}$$

Where P is pressure (*Pa*), V volume (*m³*), n is the mole fraction of the compound (*mol/mol*), T temperature (*K*) and R is Reynolds number (*8.31 j/mol/K*). Figure 4 displays the results from the first trial and shows that 2% carbon per dry weight of sediment produced by far the most CH_4.
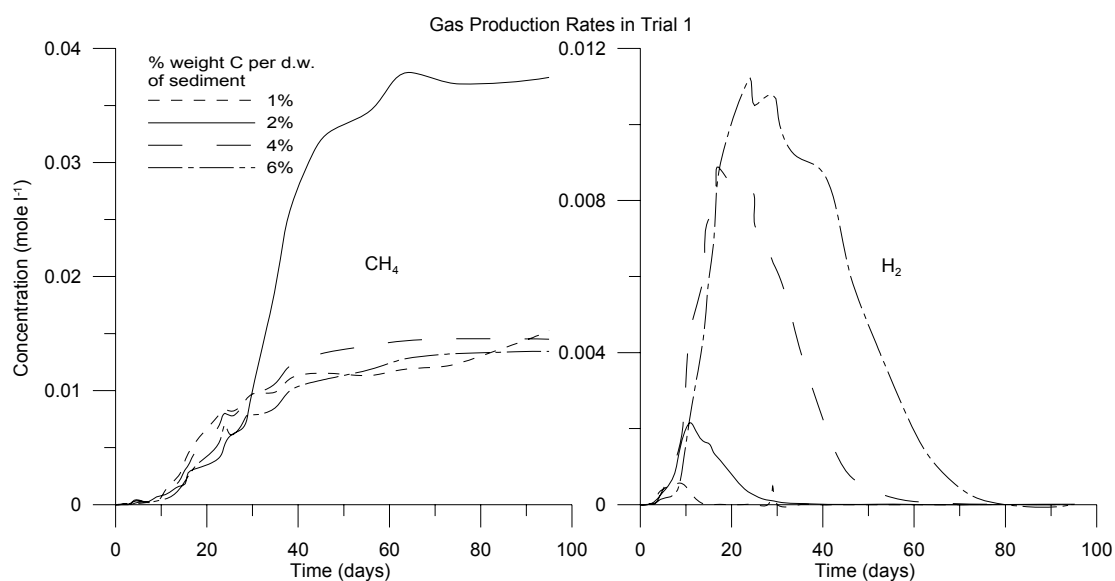
Figure 4: Gas production rates in trial 1 for CH_4 and H_2 from marine sediment maintained at 21°C

The second trial was constructed using the same methods as trial 1 however, the jars were now placed in a temperature controlled room at 12°C and only 2% carbon per dry weight of sediment was added (see Appendix A). Figure 5 displays that the rates of production for CH_4, CO_2 and H_2 from the second trial, showing that all increased rapidly and thereafter decreased again. The decrease in production and concentration is likely due to the microbes exhausting the energy source.

It is also quite likely that other processes, which for example consumed CH_4, were present after the 80 days.

Gas Production Rates in Trial 2
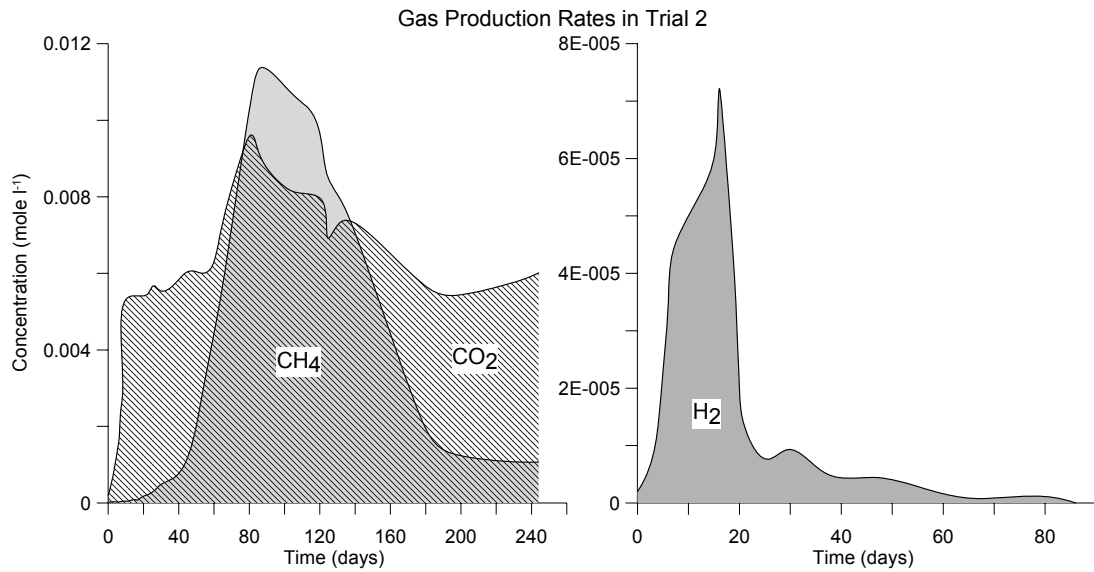
Figure 5: Concentration of CH4, CO2 & H2 in gas released from sediment in trial 2 at 12ºC.

The high levels of H_2 recorded during the first 20 days, gives a very good indication that fermentation was the main process at work during this period. One example of this process is the reduction of glucose to acetate:

$$C_6H_{12}O_6 + 4H_2O \rightarrow 2CH_3COO^- + 2HCO_3^- + 4H^+ + 4H_2$$
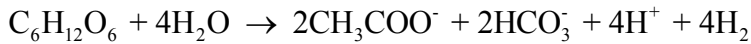
Once fermentation had broken down the larger starch molecules, methanogenesis became the dominate process in which acetate can be transformed into CH_4 through:

$$Acetate + H_2O \rightarrow CH_4 + HCO_3^-$$

Culmulative Volume of Gases Produced in Trial 2
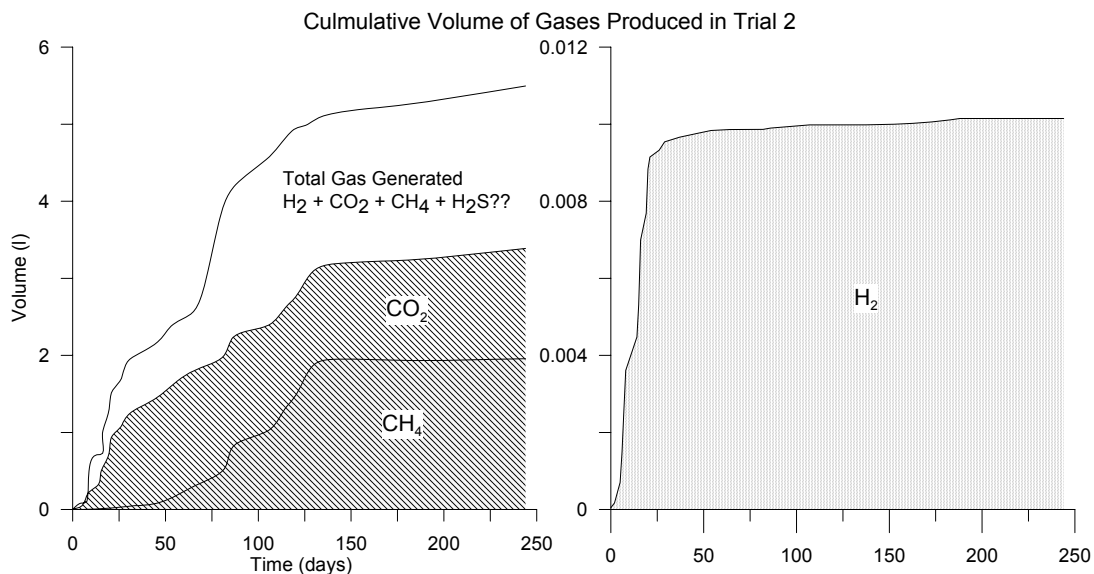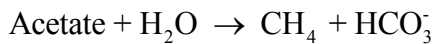
Figure 6: Volumes of gas produced during the gas production rate trials.

The total volumes of gases generated in trial 2 are presented in Figure 6, which shows that the generated volumes of CO_2 and CH_4 alone are approximately 60 times greater than that of the sediment volume. Figure 6 also shows that at $12^{\circ}C$ approximately 3.8×10^{-1} ml/cm^2/day of gas was released from the sediment. The results from these preliminary tests showed that it was possible to generate enough microbial gas for the production of bubbles and eventual ebullition of gas from the sediment.

3.2 Bench Tests Investigating the 1-D Flux of PAH

The trials and results presented in Section 3.1 showed that it was possible to artificially initiate, the enhanced production of gas in marine sediment through microbial respiration. This finding is important as the production of gas leading to ebullition is a prerequisite in both bench tests 2 and 3, which are described in the following sections. A total of 3 bench tests were designed and implemented to examine the 1-D flux of PAH from marine sediment into an overlying water phase and these were.

Bench Test 1 – Examined the molecular flux of 10 PAH compounds (F in Equation (2.3.2)) from a marine sediment to an organic phase with a varying thickness of water (dz in Equation (2.3.2)) between these 2 phases. The theory is that if dz increases and dC and D are constant than F should decrease.

Bench Test 2 – Was a preliminary test examining the influence ebullition of biogenic gas has on the flux of 10 PAH compounds from marine sediment to an organic phase. This bench test also investigates the effectiveness of a capping layer in reducing the flux of these PAH in the presence of ebullition.

Bench Test 3 – Was the most complete investigation of the influence gas ebullition has on the flux of 10 PAH compounds from marine sediment to an organic phase. Included in this trial were systems with and without caps and systems with and without gas ebullition. Also examined in this test was the flux of PAH from only the capping material and only the water phase.

As the basic setup for all three tests are the same, the methods and materials used in the tests will be discussed together in Section 3.2.1.

3.2.1 Description of Bench Test Procedures

A series of bench tests were created to determine the diffusional flux of 10 PAH compounds (hereafter referred to as PAH_{10}) from contaminated marine sediment. The experimental setup is based on a 1-D diffusion experiment developed at the Norwegian Geotechnical Institute (NGI, 2004). The test assumes a 1-D diffusion gradient through a thin layer of water and the scavenging of PAH from the aqueous phase by an organic solvent, which in this case was either hexane or cyclohexane (referred to as organic phase for the remainder of the report). The concentration of PAH at the water-organic phase interface is assumed to be zero and the concentration of PAH at the sediment-water interface and within the sediment porewater is assumed to be high and therefore a steady state diffusion can be calculated following Fick's first law (see Equation (2.3.2)). Thoroughly homogenised sediment from Bjørvika ('vik' is Norwegian for cove or inlet and therefore Bjørvika is actually Bjør Cove) in Oslo Fjord was used and the chemical and physical properties of the material are shown in Table 1.

Table 1: Water content, TOC and concentration of PAH_{10} compounds in sediment from Bjørvika in Oslo Fjord (NGI, 2004).

Parameter	Unit	Sediment Bjørvika
Water content	% d.w.	102.8 – 122.6
TOC	%	4.39
Mineral oil (C_{10}-C_{40})	mg/kg d.w.	3870
Naphthalene	mg/kg d.w.	0.67
Acenaphthylene	mg/kg d.w.	0.13
Acenaphthene	mg/kg d.w.	0.14
Fluorene	mg/kg d.w.	0.31
Phenanthrene	mg/kg d.w.	0.97
Anthracene	mg/kg d.w.	0.56
Fluoranthene	mg/kg d.w.	2
Pyrene	mg/kg d.w.	3
Benzo(a)anthracene	mg/kg d.w.	1.2
Chrysene	mg/kg d.w.	0.82
PAH_{10}	mg/kg d.w.	9.8

The capping material used was originally well sorted gravel (0 – 20 mm) from Aasmund Rock stone crushing plant in Sandefjord, Norway. So as to obtain an evenly distributed capping layer with a thickness of only 10 mm, all fractions larger than 2 mm were removed by sieving. More detailed properties of the sediment and capping materials including TOC can be found in Appendix B. The water phase consisted of sea water taken from Oslo Fjord.

The test containers utilised were ordinary glass jam jars with a Teflon pad inserted into the top of the lid, which prevented reactions with the metal cap and to create a tighter seal. The jars had an internal area of 37.7 cm^2 perpendicular to the vertical axis. The sediment was well mixed and approximately 100 g was injected into the jars, with care being taken not to contaminate the sides of the jars higher than the eventual level of the sediment. The sediment was then artificially consolidated by vibrating until a flat surface had formed.

Sea water was carefully injected into the jar, while trying to keep the amount of resuspended particles of sediment to a minimum (see Figure 8). A thin film of lighter material usually formed on the surface of the water and this was removed by overfilling the jar, allowing the film to run off. The water was then removed again until the jar was filled to the required level, or if a capping layer was to be added all of the water was removed. If the test sample required a capping layer, this was then applied by spooning approximately 55 g of gravel onto the surface of the sediment. The capping material was spread evenly over the sediment layer and the same procedure of filling the jar to overflowing was repeated. This removed the lighter material which arose from the capping material and reduced the risk of unnecessary contamination of the water-hexane interface.
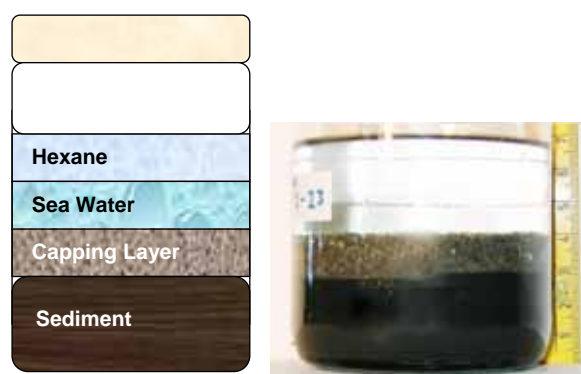
Figure 7: Diffusion test setup

When the sediment, capping and water phases were in place, 50 ml of organic phase was carefully pipetted onto the surface of the aqueous phase. So as a concentration ratio could eventually be determined, an internal standard was added to the organic phase prior to this step, this being 2.5 μg/ml of ortho-terphenyl (OTP). The organic phase had a much lower density than water the two interfaces were relatively easily achieved. The system was then sealed and positioned in a temperature controlled room (12ºC). To reduce the possibility of photolysis, the lights in the room were always switched off while nobody was present. A finished test sample can be seen in Figure 7 with the sediment, water and organic phases clearly visible.

The organic phase was analysed for concentration of the 10 PAH compounds listed in Table 1 using a gas chromatograph (GC) (located at the NGI Environmental laboratory). In order to achieve a concentration of PAH_{10} in the organic phase above the detection limits of the GC, the samples were first required to be concentrated. This was achieved by evaporating the extracted hexane from it initials extracted volume (40 - 50 ml), down to a volume of 1 ml.
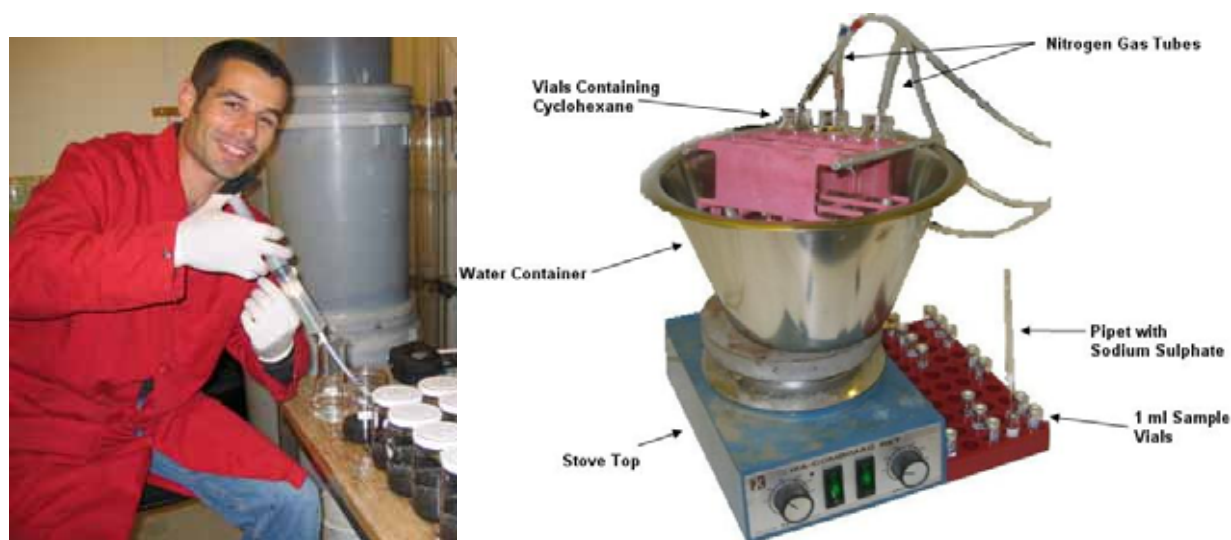
Figure 8: Injection of water into test jars in a controlled temperature environment and the setup used for the evaporation and concentration of the extracted organic phase.

The evaporation process was completed by hand and assisted by placing the vials containing the organic phase in warm water (60ºC) and irrigating with N_2 gas. The remaining 1 ml was then extracted and filtered through 0.3 g of sodium sulphate, so as to remove any water which may have contaminated the samples. This took approximately half an hour to complete for each sample and the setup for the procedure can be seen in Figure 8. The organic phase samples were then analysed using the GC and the area under the OTP peaks determined. Once this area was known it was possible to determine a concentration ratio (R_{OTP}) between the concentrated samples and the original samples (R_{OTP} values for each sample are found in the relevant Appendix for each bench test). The significance of the R_{OTP} parameter will become apparent in Section 3.3.

Three different diffusion tests were carried out using these materials and procedures and are described in the following sections. Following the descriptions of all of the tests a short discussion into the calculations and assumptions behind the calculation of the results will be given.

3.2.2   Bench Test 1 – Flux of PAH_{10} with change in distance (dz)

A series of 12 1-D diffusion tests were created using the procedures described in Section 3.2.1 and developed at NGI. Four different thicknesses of the aqueous phase (*dz*) were used (10, 20, 30 & 40 mm) with three parallel tests of each (labelled 1-1 to 1-12), the test was run for a period of 218 days (see Figure 9 and Appendix C for information). The bench test was created so as to determine a relationship between the flux of PAH_{10} between the sediment and organic phases ($F_{PAH_{10}}$) and the separation distance (*dz*). Further discussion on the results of this test and the related theory will be given in Section 4.
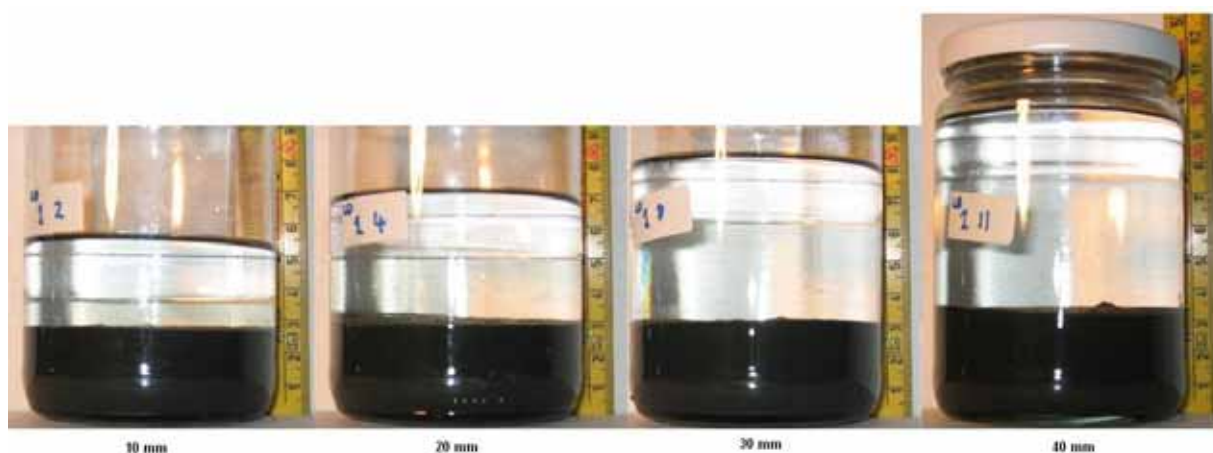
Figure 9: Bench test 1 with varying separation distances (z) visible.

3.2.3   Bench Test 2 – Flux of PAH_{10} with ebullition present

Bench test 2 consisted of 36 samples, 18 of which had a cap in place (labelled 2-19 to 2-36) and 18 without a cap (labelled 2-1 to 2-18). There were 6 different sample times and therefore 3 parallel tests at each time interval. The test jars were completed using the procedures described in Section 3.2.1, although in this experiment an artificial carbon source (starch - $C_6H_{10}O_5$) was introduced into the sediment phase. A mix of 1.5% carbon per dry weight of sediment, as discussed in Section 3.1, was well mixed into the Bjørvika sediment. Samples of the organic phase were then taken at 9, 50, 108, 126, 218 and 238 days and analysed for concentrations of PAH_{10} listed in Table 1 (see Appendix D for information). The test jars were sealed and therefore the internal pressure variation due to microbial gas production inside the jars was unknown.

3.2.4   Bench Test 3 – Flux of PAH_{10} with and without ebullition

As ebullition occurred in bench test 2, the pressure inside the jars increased to above ambient levels. It was unknown if this pressure increase diminished bubble production or actually enhanced it, therefore bench test 3 was designed to remove the uncertainty of pressure changes present in bench test 2. A total of 52 tests jars were created following the procedures in Section 3.2.1, with 4 time intervals and 3 parallel tests per time interval. The tests consisted of 6 different combinations as listed below (see Appendix E for information);

1) Sediment + Carbon Source + Sea Water (labelled UC-1 to UC-12)

2) Sediment + Carbon Source + Cap + Sea Water (labelled CC-1 to CC-12)

3) Sediment + Sea Water (labelled U-1 to U-12)

4) Sediment + Cap + Sea Water (labelled C-1 to C-12)

5) Only Cap (labelled BC-1 to BC-3)

6) Only Sea Water (labelled V-1 to V-3)

Only those samples containing an artificial carbon source were fitted with a device, which allowed the pressure to remain at ambient levels. This device was a simple tube which released generated gas through a water interface so as to reduce the diffusion of O_2 from the atmosphere into the jars. The gas was then ventilated into a 1 litre laboratory gas bag, which allowed the whole system to remain at atmospheric pressure and further reducing the possibility of O_2 diffusion into the system (see Figure 10).
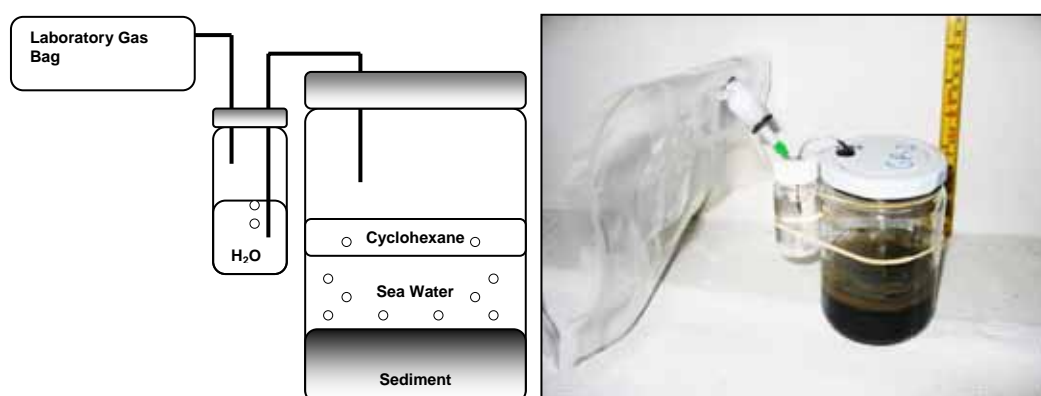
Figure 10: Setup which allowed the release of gas produced in bench test 3.

Test samples of the organic phase were then taken at time intervals of 29, 63, 121 and 149 days, after which they were prepared for analysis using the methods discussed in Section 3.2.1.

3.3 Calculations & Related Assumptions

As discussed in Section 2.3.4, diffusion is often the dominant mechanism governing the movement of dissolved contaminants in environmental systems when advection is absent. Section 3.2 has described the construction of the 1-D diffusion tests. However, the basic calculations and assumptions behind these tests must first be expressed. Section 2.3.4 described Fick's first law, which is the basis for all calculations performed in this experiment and is described again as

$$F = D\frac{dC}{dz} \tag{3.3.1}$$

It was assumed in all bench tests that the flux (F) was constant through the whole duration of each test and that dC/dz or the spatial gradient of the concentration (C) through the water phase and along the z axis was described by a linear function as shown in Figure 11.
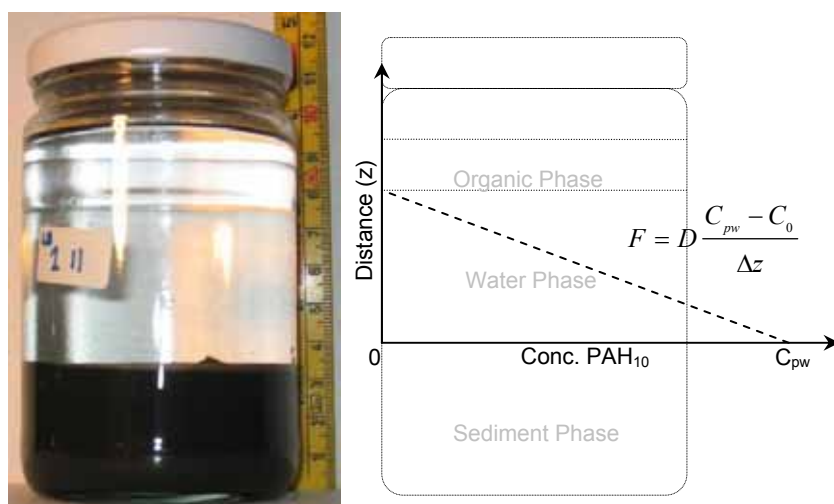
Figure 11: Experimental setup and diagram displaying the assumed
theory behind diffusion in an uncapped system.
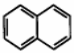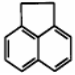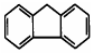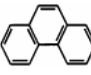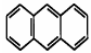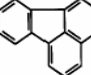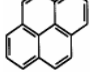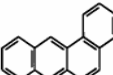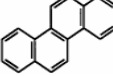
The diffusion coefficient (D) is also constant for each compound of PAH at a constant temperature of 12ºC. The diffusion coefficients were calculated using the relation by Hayduk and Laudie (1974)

$$D = \frac{13.26 \times 10^{-3}}{\eta_W^{1.14} V_B^{0.589}} \tag{3.3.2}$$

where η_W is the viscosity of the sea water at 12ºC (*1.235 cP*) and V_B is the molar volume of the solute (*cm³/mol*).

A list of calculated diffusion coefficients are given in Table 2 along with the molar volumes, Henry's constants, molecular weights and physical structures for each compound.

Table 2: Various properties of the PAH_{10} compounds including calculated diffusion coefficients.

Compound	Structure of PAH Compounds[4]	Henry's Constant @ 12ºC[1] (dimensionless)	Molecular Weight [2] (mol/g)	Carbon-water coefficient log(K_{oc})[3]	V_B [2] (cm^3/mol)	Diffusion Coefficient (cm^2 sec^{-1})
Naphthalene		0,0075	128,17	3,30	148	4,7×10^{-1}
Acenaphthylene		-	152,2	3,16	165,7	4,4×10^{-1}
Acenaphthene		0,0019	154,21	3,94	173	4,3×10^{-1}
Fluorene		0,0008	166,22	4,14	188	4,1×10^{-1}
Phenanthrene		-	178,22	4,45	199	4,0×10^{-1}
Anthracene		0,0007	178,23	4,45	197	4,0×10^{-1}
Fluoranthene		0,0001	202,26	4,99	217	3,8×10^{-1}
Pyrene		0,0001	202,26	4,84	214	3,8×10^{-1}
Benzo(a)anthracene		0,00002	228,29	5,57	248	3,5×10^{-1}
Chrysene		0,0006	228,29	5,61	251	3,5×10^{-1}

[1] EPA, 2003 [2] Jinno Laboratory, 2001 [3] Di Toro & McGrath, 2000 [4] Rogers et al, 2002

Although Equation (3.3.1) describes the flux of PAH, it is important to consider the overall mass balance of the system. Figure 12 describes the basic mass balance of the system present in Figure 11 and shows the parameters, which will be determined throughout the following sections of this report.
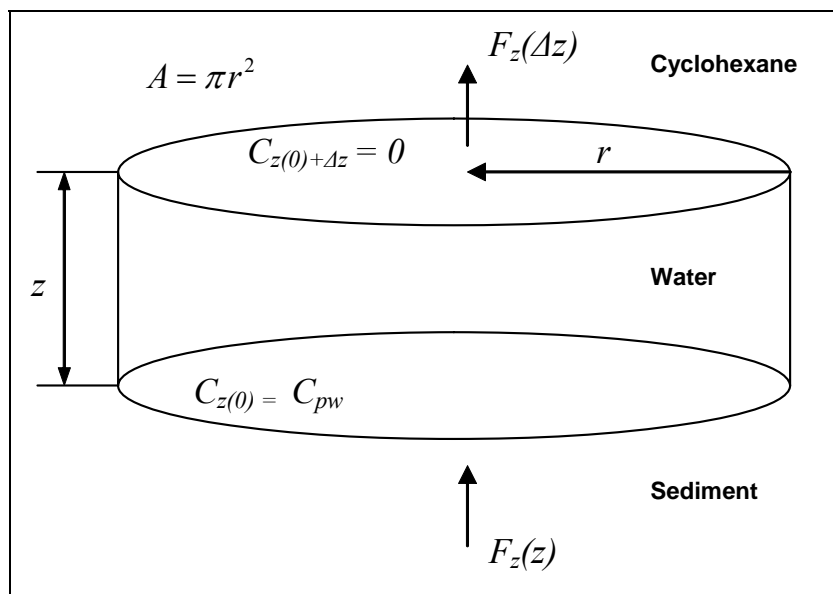
Figure 12: Circular test volume of size and mass flux along the z axis

In all bench tests the values for area (A), length (z) and the radius of the jar (r), seen in Figure 12 can be calculated or measured. It is also assumed that the concentration of PAH_{10} at the water-organic phase interface ($C_{z(0)+\Delta z}$) is zero. As stated the flux ($F_z(z)$) between the sediment at $z = 0$ and the organic phase at $z = \Delta z$ is constant. Furthermore, the steady state flux is assumed to occur immediately after the organic phase is placed on the water surface. Therefore, the mass of the PAH_{10} compounds ($M_{PAH_{10}}$) that have been transported between the water-organic phase interface during time t can be determined as

$$M_{PAH_{10}} = \sum \frac{C_{PAH_i}}{R_{OTP}} V_{hex} \tag{3.3.3}$$

where $M_{PAH_{10}}$ is the total mass of PAH_{10} accumulated in the organic phase (μg), C_{PAH_i} the concentration of each of the 10 individual PAH compounds in the organic phase ($\mu g/ml$), V_{hex} the volume of the organic phase (ml) and R_{OTP} is the ratio calculated from the internal standard of OTP as discussed in Section 3.2.1.

A new value can now be calculated which describes the mass of PAH_{10} accumulated in the organic phase per unit area of the sediment-water interface

$$j_{PAH_{10}} = \frac{M_{PAH_{10}}}{A} \tag{3.3.4}$$

By plotting the $j_{PAH_{10}}$ against the elapsed time Δt between the experiment start, and when the organic phase was extracted from the jar, a flux of PAH_{10} between $z = z(0)$ and $z = z(0) + \Delta z$ can be determined (hereafter described as $F_{PAH_{10}}$).

This is proven by examining the units of each parameter, which for $j_{PAH_{10}}$ is (M A^{-2}) and for Δt is (T). So the slope of the line of $\Delta j_{PAH_{10}}$ against Δt is equal to

$$\frac{\Delta j_{PAH_{10}}}{\Delta t} = \frac{\text{M A}^{-2}}{\text{T}} = F_{PAH_{10}} \tag{3.3.5}$$

the unit for flux is (M A^{-2} T^{-1}) which corresponds with the known unit for the flux of a chemical solute described by Fick's first law.

It is now possible to estimate the concentration of PAH_{10} at $C_{z(0)}$ by using the relationship in Fick's first law to obtain

$$\Delta C = \left(C_{z(0)} - C_{z(0)+\Delta z} \right) = C_{pw} = \sum \frac{F_{PAHi} \Delta z}{D_i} \tag{3.3.6}$$

where C_{pw} is the concentration of PAH_{10} in the pore water of the sediment phase. The i in Equation (3.3.6) indicates that the flux and diffusion coefficients (found in Table 2) for each individual compound must be used. This calculation can also be used to approximate the concentration of PAH_{10} in the pore water of the capping material.

As part of this study involves the assessment of the effectiveness of a capping layer it is helpful to introduce a non-dimensional parameter which gives an indication of this effectiveness. The effectiveness or efficiency (E_{cap}) of a remedial cap can be represented as a percentage and defined as (Talbert et al, 2001)

$$E_{cap} = 100\% \frac{\left(F_{sed} - F_{cap} \right)}{F_{sed}} \tag{3.3.7}$$

where F_{sed} is the flux from the tests with only sediment and F_{cap} is the flux from those tests with a cap in place.

The final assumption made in these tests involves the results obtained by analysing the samples using the GC. The GC had a detection limit of 0.01 µg/ml, so it was therefore decided that all results equal to zero would be given a value of 0.005 µg/ml or half of the machine's detection limit.

4   RESULTS & DISCUSSION

The results from all three bench tests are presented and discussed throughout Chapter 4. As bench test 1 was designed to determine a relationship between $F_{PAH_{10}}$ and dz and did not include any investigation into gas ebullition, the results from this test will be presented and discussed first (Section 4.1). Bench tests 2 and 3 were very similar in setup although bench test 3 was considered the most complete and relative setup for investigating the influence of ebullition on $F_{PAH_{10}}$. Therefore the results from bench test 2 will be presented together with only a preliminary discussed in Section 4.2.1. As stated bench test 3 was the most complete trial as it included all possible scenarios, both with and without ebullition and with and without a capping layer. Therefore, the results from this test will be discussed in greater depth in Section 4.2.2 along with the processes which are suspected to have caused the results obtained.

4.1   Bench Test 1 – Flux of PAH$_{10}$ with change in distance (dz)

After a period of 218 days, the organic phase from all 12-test jars was extracted and analysed. During the test period, no bubbles or disturbances had formed in the sediment phase and only a small amount of material had accumulated on the water-organic phase interface. This material took the form of bacterial growth rings, common to what is seen when cultures are prepared on a petri dish. Therefore, it is possible that some types of bacteria had existed on this interface. The sediment phase had also formed a thin grey layer on the surface, presumably due to redox processes present between the sediment-water interfaces.

Figure 13(a) displays the calculated concentration of PAH$_{10}$ in all 12 samples. It shows that there is no significant difference between the individual results, excluding sample 1-12, in which a concentration of 0.26 μg/ml of Benzo (a) anthracene was recorded (600 times higher than the average). This is the cause of the outlier seen in Figure 13(a) and can be explained by inaccuracies in the GC measurements. Therefore, series 1-12 was eliminated from further calculations. Bench test 1 was run parallel to bench test 2 and was constructed using the same materials and at the same time. As bench test 1 did not have gas ebullition present and bench test 2 did, bench test 1 will also be used to help discuss the observations made from bench test 2.
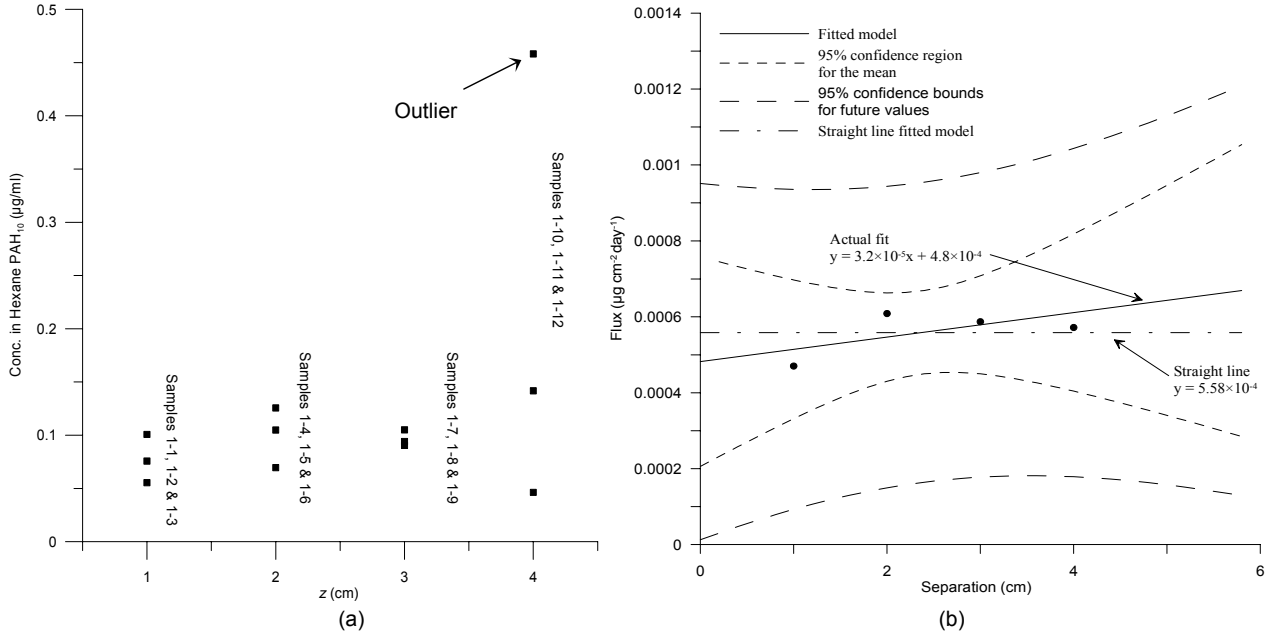
Figure 13: (a) Concentration of PAH_{10} in extracted organic phase samples after 218 days. (b) Calculated flux of PAH_{10} compounds.

The data in Figure 12(a) was adjusted using Equation (3.3.3) so as an actual mass of PAH_{10} in the organic phase ($M_{PAH_{10}}$) could be determined. To calculate the flux of PAH_{10} from the sediment the mass of PAH_{10} accumulated in the organic phase per unit area of the water-organic phase interface ($j_{PAH_{10}}$) was divided by the duration of the experiment (t). Taking the distance of separation in tests samples 1-1, 1-2 and 1-3 as 10 mm, 1-4, 1-5 and1-6 as 10 mm, 1-7, 1-8 and 1-9 as 30 mm and 1-10, 1-11 and 1-12 as 40 mm, a flux vs. length graph was plotted. The results are displayed in Figure 13(b), along with two fitted linear models and the 95% confidence bounds, for both the mean and future values. The method used for calculation of the linear models and confidence intervals can be found in Appendix G.

Test 1 produced a relationship between the flux of PAH_{10} ($F_{PAH_{10}}$) and the length of the water phase (z). Although as discussed it was initially thought that if the flux was constant and that all samples were taken at the same time, the relation between $\Delta F_{PAH_{10}}$ and Δz would yield

$$S = \frac{\Delta F_{PAH_{10}}}{\Delta z} \tag{4.1.1}$$

where S ($\mu g/cm^3/day$) is a constant describing a relation between $F_{PAH_{10}}$ and z for this particular setup. The parameter S could have been useful in describing a relationship between the constant fluxes described later in bench tests 2 and 3 and the width (z) of the water between the sediment and organic phases.

The flux should have decreased with an increase in length, if diffusion (D) and concentration (C) were constant. It is seen in Figure 13(b) that the calculated fluxes for each change in z are very similar. Furthermore, an F-test comparing each of the sample groups revealed there was an 80 to 20 percent (%) chance that the results were not statistically different ($\leq 5\%$ represents statistical individuality) and must therefore be considered constant with S equal to zero. This result is incorrect if the above stated conditions are correct. Furthermore if the simple assumption is made that the relationships between diffusion (D), velocity (u) and average distance travelled (σ) are true and that only molecular diffusion is present (described by Equations (2.3.3) and (2.3.4)), then the PAH molecules would have diffused at an average velocity of 6.6×10^{-2} cm/day. PAH molecules in tests 1-1 to 1-3 would have therefore reached the water-organic phase interface 45 days before they reached the same interface in tests 1-10 to 1-12.
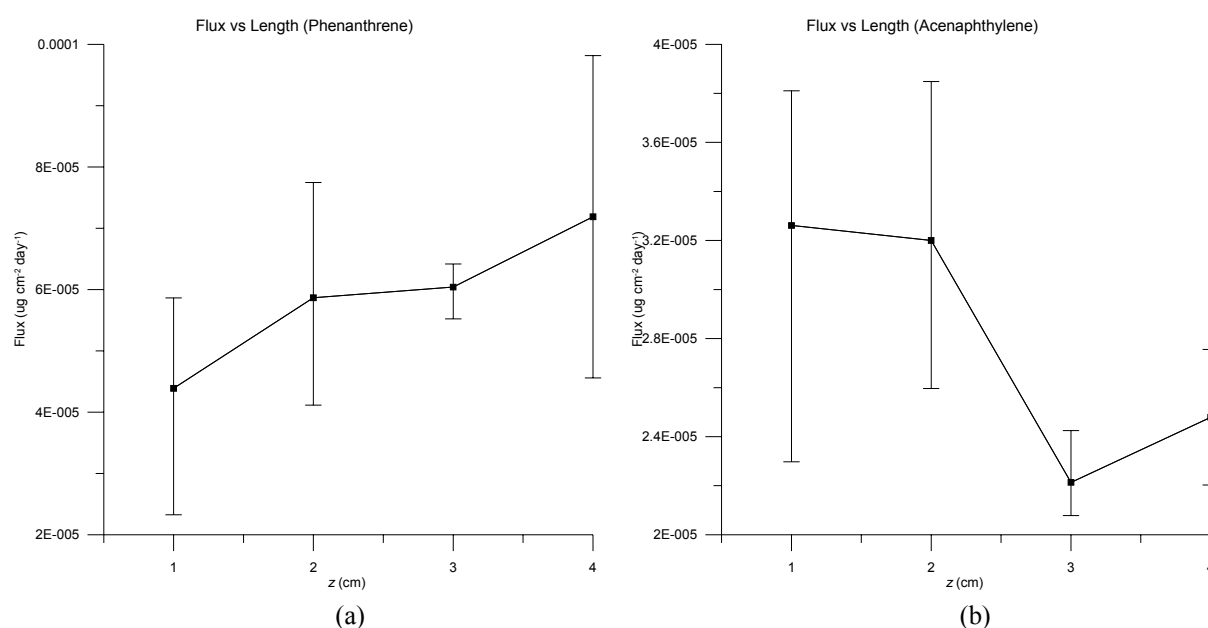
Figure 14: Results from bench test 1 for 2 PAH10 compounds, (a) Phenanthrene and (b) Acenaphthylene, with error bars indicating the average flux with 1st and 3rd quartiles of each parallel test

An investigation into the flux of the individual PAH_{10} compounds showed that almost all behaved differently. This is illustrated in Figure 14 by two compounds, Phenanthrene and Acenaphthylene. It is not known why some individual PAH compounds, such as Acenaphthylene shown in Figure 14(b) complied with the theory discussed above, while others such as Phenanthrene (Figure 14(a)) behaved in exactly the opposite way. It is uncertain whether the duration of bench test 1 (218 days) had an effect on the results, or if a shorter test duration (for example <60 days) may have resulted in a value for $S \neq 0$.

For that reason the results in bench test 1 are considered to be preliminary, and further more in depth tests are needed before the theory discussed in this section can be confirmed.

4.2   Flux of PAH$_{10}$ and the Influence of Gas Ebullition

Both bench test 2 and bench test 3 investigated the influence ebullition had on the overall flux of PAH. As previously discussed, bench test 2 was of a more preliminary nature and did not include all of the systems listed in Section 3.2.4. Therefore, bench test 3 will be used as the primary investigation when discussing the theory behind gas ebullition, although references will be made to bench test 2 where appropriate. For clarification a short summary of the differences between both bench test 2 and bench test 3 is given in Table 3

Table 3: Comparison of behaviour and properties of bench test 2 and bench test 3

Behaviour	Bench Test 2	Bench Test 3
Length of trial period.	238 days	148 days
Time first bubbles appeared.	30 days	60 days
Vigour of bubble formation.	Substantial	Moderate
Thickness of grey sediment surface layer.	1 - 2 mm	≥2 mm
Change in water colour.	Substantial (yellow)	Moderate (foggy)
Constant pressure.	No	Yes
Deposited material in the hexane phase.	Substantial	Moderate
Mixing of sediment-capping phases	Substantial	Light
Organic Phase Used	Hexane	Cyclohexane

Although there were a number of differences between bench tests 2 and 3, the final observations and results of both tests were quite similar. Sections 4.2.1 and 4.2.2 will discuss these observations and results, followed by Section 4.2.3 where a discussion into the processes behind these results will be entered into.

4.2.1 Bench Test 2 - Flux of PAH_{10} with ebullition present

Samples were extracted from bench test 2 at times 9, 50, 108, 126, 218 and 238 days after the start of the test and analysed for PAH_{10} content. The plots generated by the GC were analysed and adjustments made so as the correct peaks were selected. Two test samples at 108 days were not analysed, these were sample 2-7, as there was not enough organic phase to extract from the test jar and sample 2-26, as the sample was not concentrated correctly an therefore was below the detection limits of the GC. All jars experienced changes during the test period and this is illustrated by the time sequence presented in Figure 15.
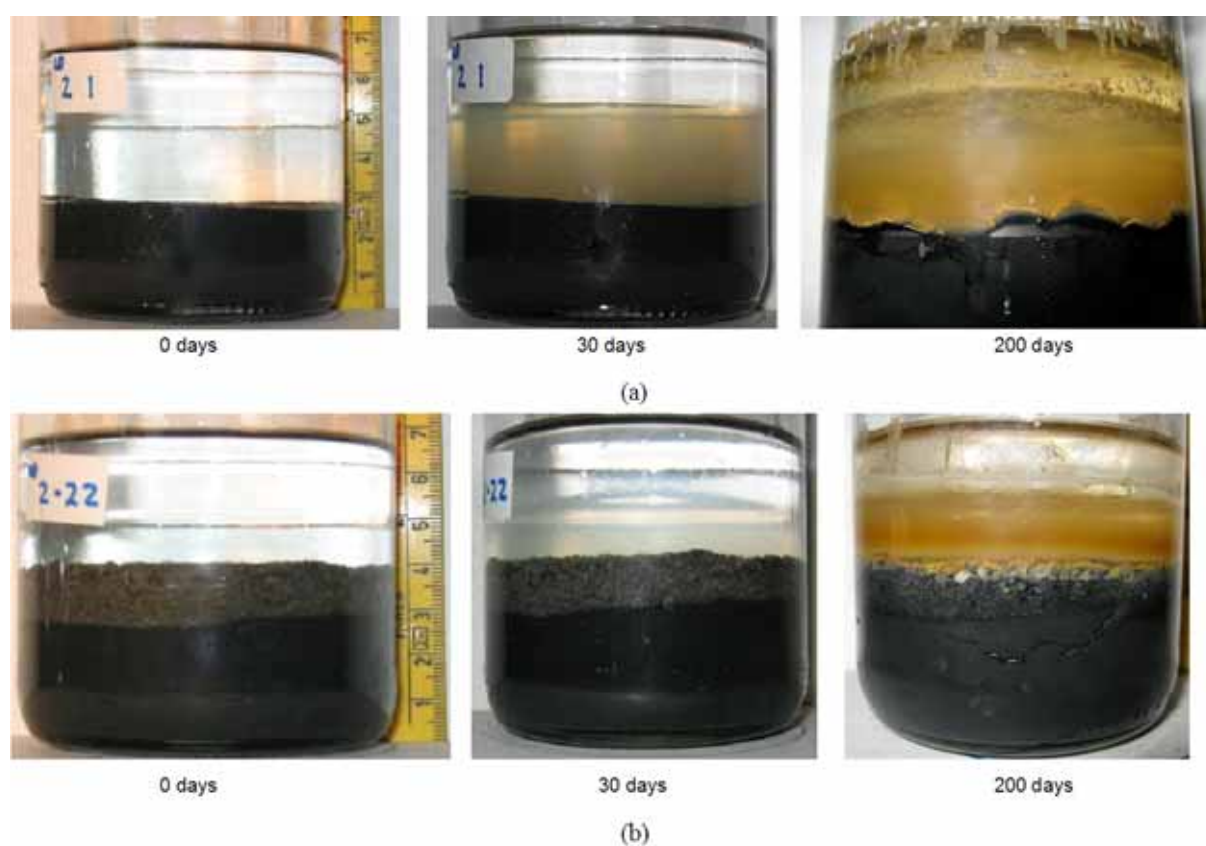
Figure 15: (a) Test jars without a capping layer and (b) with a capping layer, 0 to 200 days.

It can be seen that the first changes occurred after approximately 30 days at which time the water phase became foggy in appearance. This was less enhanced in those tests with caps and totally absent in those tests without ebullition from bench test 1. Soon after this occurred, all tests showed the presence of bubbles forming in the sediment phase. The bubbles were tied to a gradual darkening of the water phase and a heaving of the sediment surface. This heaving only occurred in those tests without caps and can be seen in Figure 15(a) after 200 days.

Some form of oxidation may have also occurred on the surface of the sediment and capping material, causing the yellow colour in the water, although this was only present after approximately 150 days. Again this yellow colour only appeared in bench test 2 and not bench test 1, which didn't have an artificial carbon source added. This also applies to the formation of bubbles in the sediment in which none were seen to be present in bench test 1.

The bubbles in bench test 2 took the form of fractures seen in Figure 16, and were usually larger and more numerous in those tests without a capping layer. Gas released from the sediment rose through the water phase as bubbles and material which was presumable attached to the bubble surface was shed in both the water and organic phases. This is illustrated by the small tube like structures visible in Figure 16 after 200 days. These tubes were more numerous in those tests without capping layers and were completely absent in bench test 1.

(a)   (b)
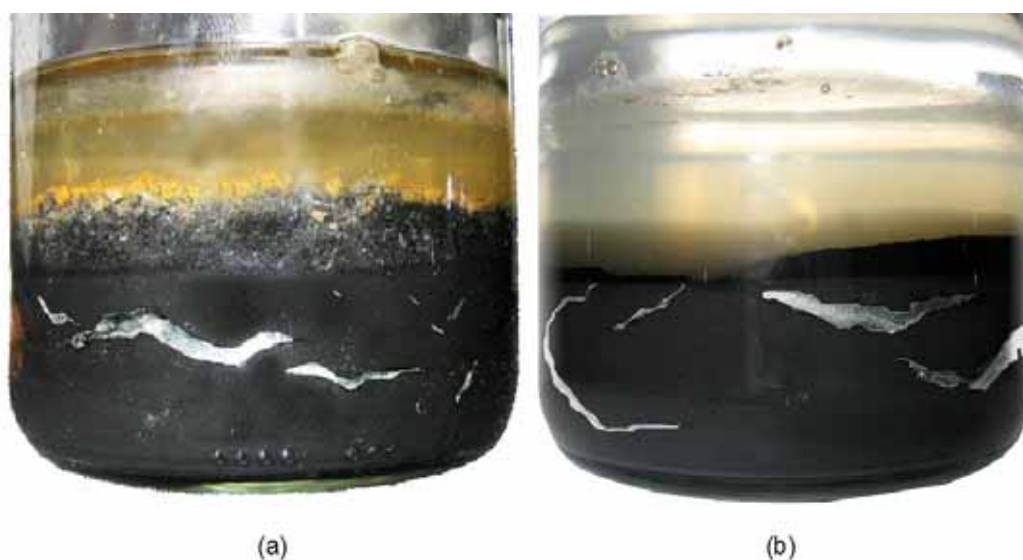
Figure 16: Fracture formation in sediment (a) with capping layer in place and (b) without a capping layer (bubbles are digitally enhanced for viewing purposes).

The continuous release of gas through ebullition seems also to have had a detrimental effect on the sediment-cap interface. This is visible in Figure 15(b), which shows that the distinct interface at 30 days has almost completely disappeared at 200 days. It is believed this is caused by the mixing effect of rising bubbles in the sediment. This mixing of sediment and capping material was witnessed extending up into the cap but never onto the surface of the cap. That is to say that sediment was never witnessed escaping through the capping layer. Figure 17 shows the amount of PAH_{10} accumulated in the organic phase per square centimetre of the sediment-water interface (see Equation (3.3.4)).

Included are the fitted linear models, error bars indicating the 1st and 3rd quartiles of the parallel tests and the 95% confidence regions for the mean (calculations found in Appendix G) , the complete list of results can also be found in Appendix H.
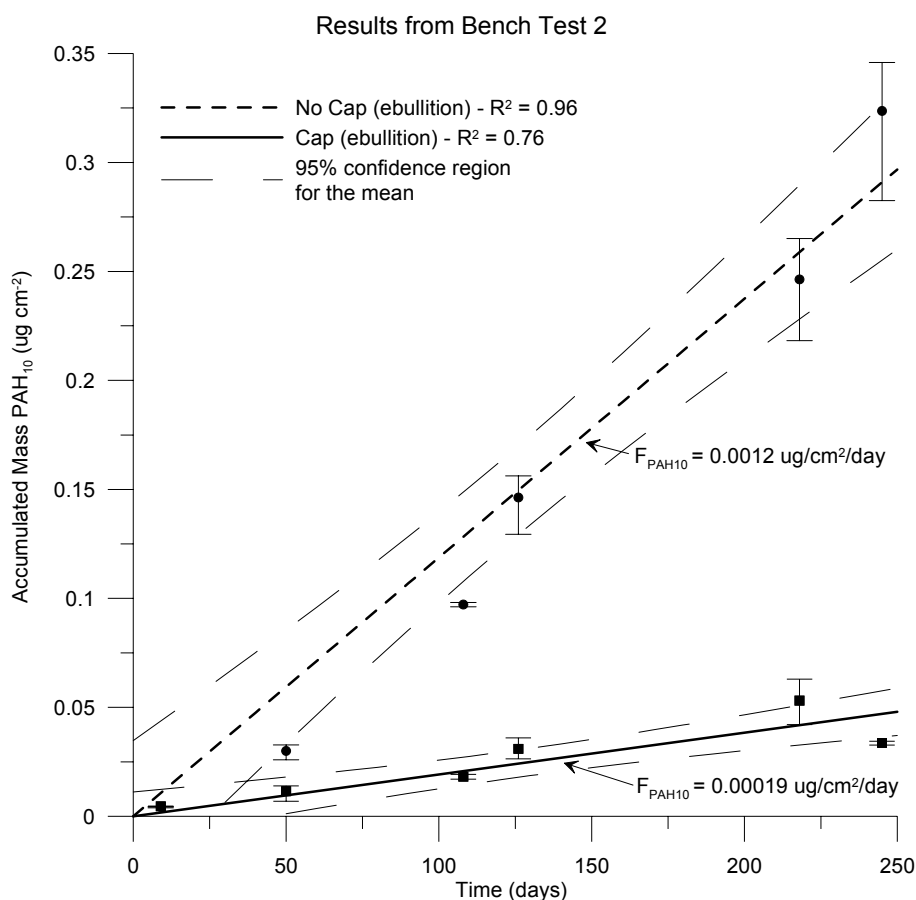
Figure 17: Results from bench test 2 together with the fitted linear model, 1st and 3rd quartiles of the data and the calculated 95% confidence intervals.

The observations fit the hypothesised linear model described by Fick's first law quite well and the R squared values for both linear models are reasonably close to 1. The confidence regions for both tests are also far enough apart to safely assume that the flux of PAH_{10} is greatly reduced by the inclusion of a capping layer; in fact the flux is a factor of 10 lower.

Figure 18 shows the accumulation of PAH_{10} for each individual compound. Showing that some compounds have a larger influence over the overall flux and also that some uncertainty still remains over some of the results. This is represented by the concentration of Naphthalene at 218 days in Figure 18(a), which is much higher that all other results. Furthermore, the results in Figure 18 show that the behaviour of the caped tests is more erratic than the results from those tests without caps. Graphs showing the calculated fluxes and 95% confidence intervals for each individual PAH compound can be found in Appendix J. Two possible explanations may exist, which account for the behaviour of the caped tests.
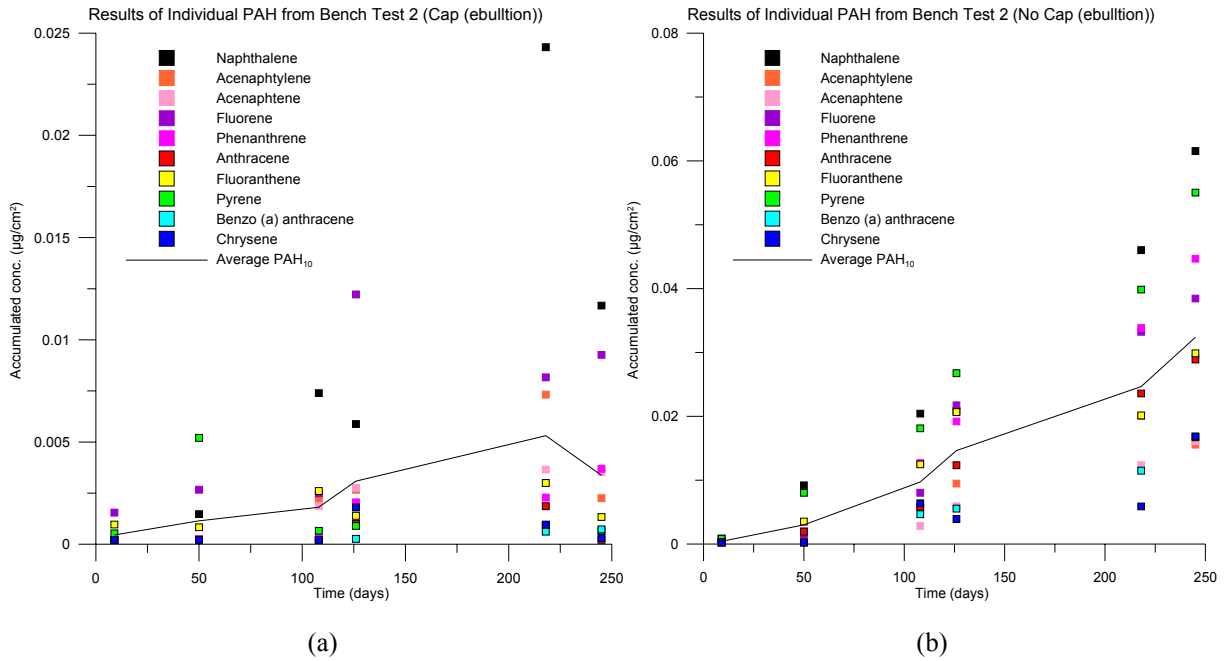
Figure 18: (a) Accumulated mass of individual PAH compounds from bench test 2 and displayed as (a) those tests with a cap in place and (b) those tests without a cap in place.

The first being that the lower concentrations present in those tests may have been more difficult for the GC to analyse and second may be the existence of some mechanism which trapped bubbles in the capping phase and inhibited the continual and steady ebullition from the sediment resulting in more concentrated periods of PAH release. These processes will be discussed further in Section 4.2.3 of this report. By comparing the results in Figure 17 with the calculated flux for those tests with a thickness of water phase equal to 1 cm from bench test 1 (shown in Figure 13), it can be reasonably assumed that the flux of PAH_{10} is also increased due to the introduction of ebullition.
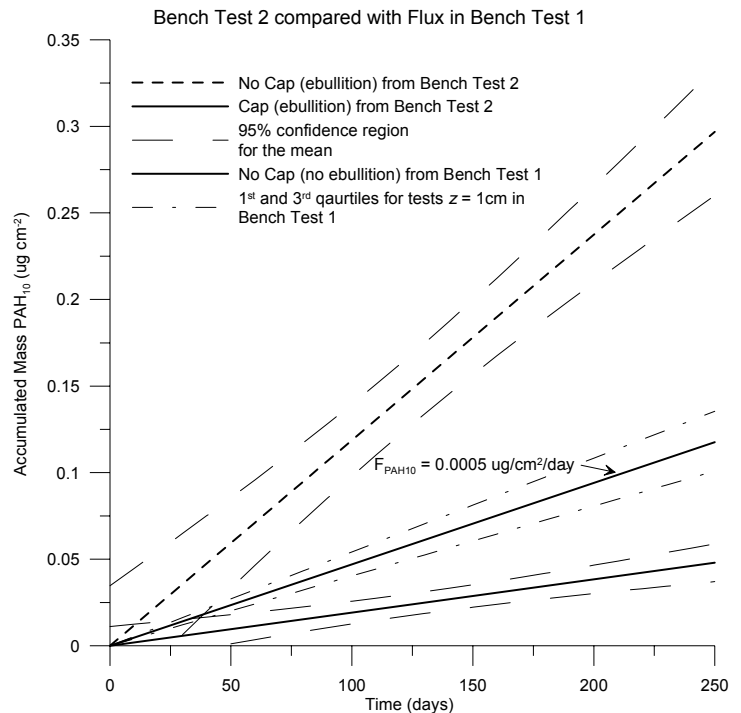
Figure 19: Resulting fluxes from tests with a water phase thickness of 1 cm in bench tests 1 and from bench test 2, including confidence intervals.

This is visualised in Figure 19, which displays the flux of PAH_{10} from both bench tests 1 and 2. As stated the reduction in accumulation of PAH in the organic phase due in those tests with a capping layer, resulted in lower fluxes. Applying Equation (3.3.7) to the fluxes calculated in bench test 2 results in a calculated efficiency of 84% for the reduction in PAH accumulation by 1 cm of capping material. The efficiency of the capping is therefore quite high and the factors behind this efficiency will be discussed throughout the remainder of this section.

4.2.2 Bench Test 3 – Flux of PAH_{10} with and without gas ebullition

Samples were taken from bench test 3 at 29, 63, 121 and 148 days and analysed for concentrations of the PAH_{10} compounds. The final concentrations in the organic phase, after being adjusted for the concentration ratio (R_{OTP}), can be seen in Appendix H. Unexpectedly the formation of bubbles in bench test 3, occurred much slower than previously experienced in bench test 2.
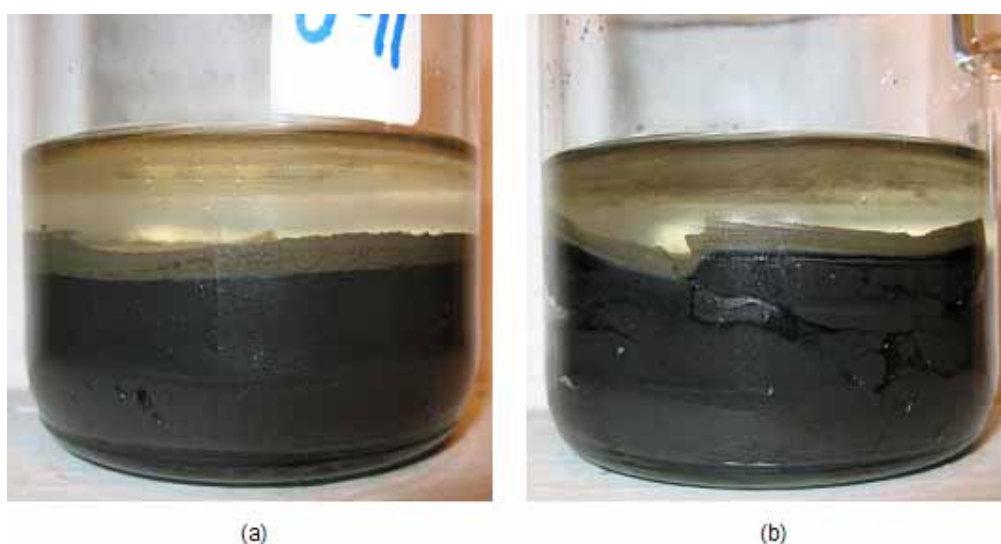
Figure 20: Test jars without capping and (a) without ebullition and (b) with ebullition.
Also visible is a the thin grey layer which has formed on the surface

Bubbles did not appear until after 60 days, twice the time required in bench test 2. Even though the bubbles formed slower they still managed to have the same influence as in bench test 2. These bubbles can be seen in Figure 20 together with the thin grey layer which formed on the sediment surface. This grey layer was also more enhanced in bench test 3, when compared to the other tests, and may explain some of the results discussed later in this section. Furthermore, the samples in bench test 3 did not exhibit the same yellow colour seen in bench test 2. Although as mentioned, the yellow colour did not appear in bench test 2 until 150 days after the start, at which time bench test 3 had been completed.

As mentioned the bubble formation in bench test 3 was observed to be less erratic and this test also recorded lower concentrations of PAH_{10} in the organic phase. By less erratic it is meant that bubbles did not form as quickly as in bench test 2 and that the sediment surface was not as disturbed by ebullition. The results of bench test 3 are shown in, Figure 21 along with error bars that indicate the 1st and 3rd quartiles of the parallel tests. Data for test samples UC-12, CC-4 and U-5 were excluded from the results due to their outlying nature. These outlying results may have arisen from the incorrect analysis of the graphs produced by the CG. This sometimes occurs when too many compounds are analysed together, which causes noise resulting in individual peaks combining to make one large peak and therefore calculating an artificially high concentration.
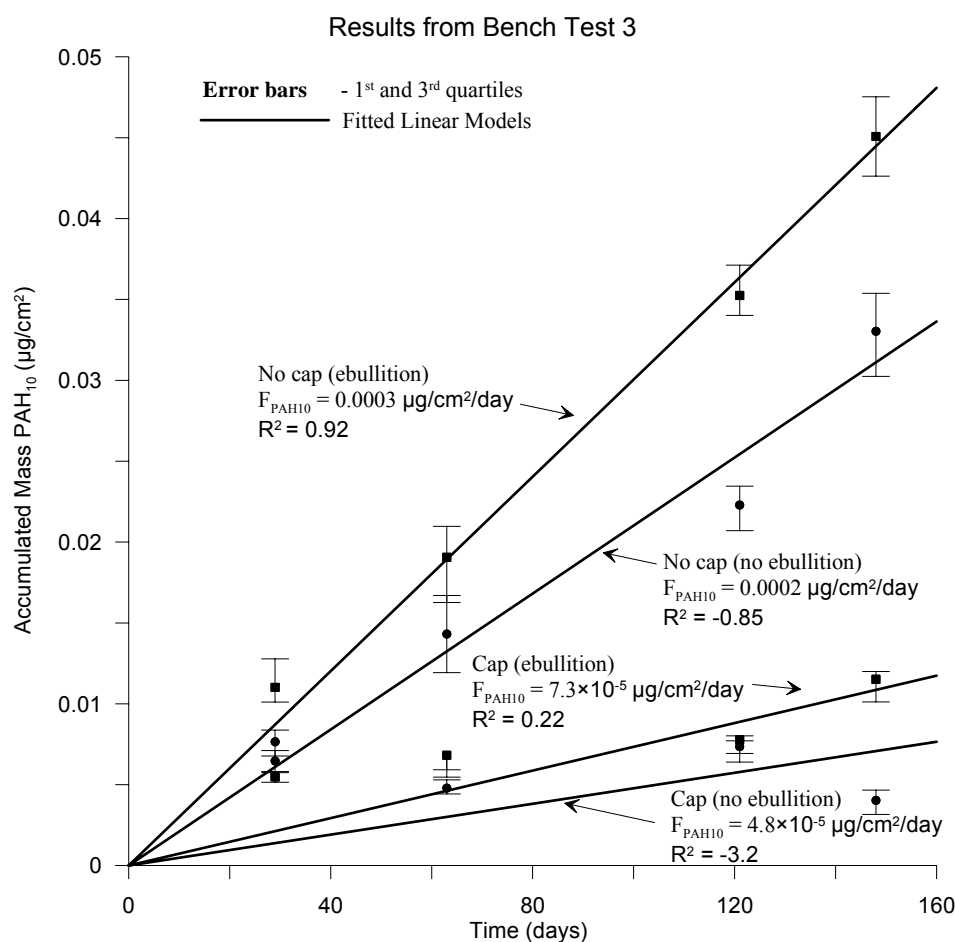
Figure 21: Flux of PAH_{10} recorded from Bench Test 3 with error bars indicating the 1st and 3rd quartiles of the 3 parallel samples for each point.

It was mentioned that the accumulated mass of PAH in bench test 3 was lower than in bench test 2 and one possible explanation for this may involve the organic phase used. In bench test 2 the organic phase consisted of hexane but in bench test 3 it consisted of cyclohexane.

Unfortunately no analysis was performed to investigate possible differences in the scavenging of PAH by these two substances and therefore, it is uncertain what caused this change. However, the amount of PAH_{10} again accumulated in the organic phase linearly with time. And the linear model is again acceptable for those tests without caps but does not fit so well for the capped tests. This is shown by the residual sum of squares (R^2) for both of the capped tests being not very close to 1. This again suggests (as in bench test 2) that the behaviour of the tests with a cap, is more unpredictable than the results from those tests without a cap. The 95% confidence intervals have also been calculated for all of the tests and are seen in Figure 22. Figure 22(a) is a plot of the two tests which had no cap present and Figure 22(b) a plot of the two tests which did have caps. The 95% confidence intervals in Figure 22(a) overlap only when a prediction over a longer time period is made. It can therefore be said that ebullition again had a magnifying effect on the flux of PAH_{10} in those tests without a cap in place. As for Figure 22(b) it is apparent that there is less certainty as to whether there is a substantial difference between those samples with ebullition and those samples without.
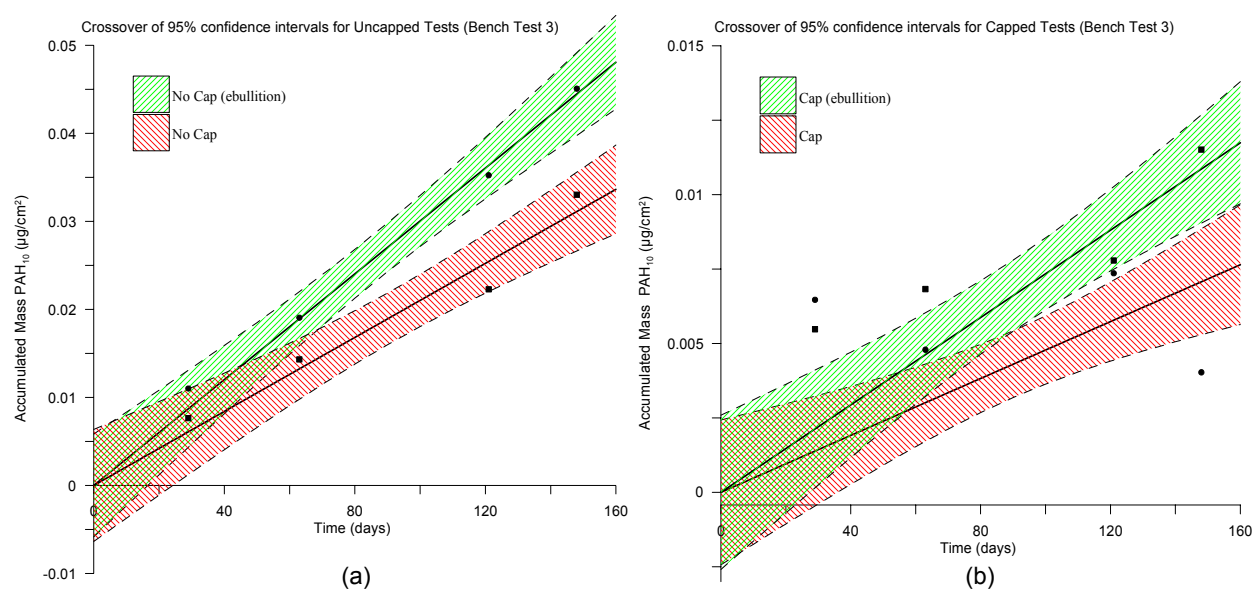
Figure 22: Accumulation of PAH_{10} in the tests with ebullition (a) and those without ebullition (b), including the 95% confidence intervals.

The efficiency of the capping material in bench test 3 was calculated using Equation (3.3.7) and was found to be 76% for both those tests with gas ebullition and those without. Therefore, the cap efficiency in bench test 3 is approximately the same as the efficiency calculated in bench test 2 (84%).
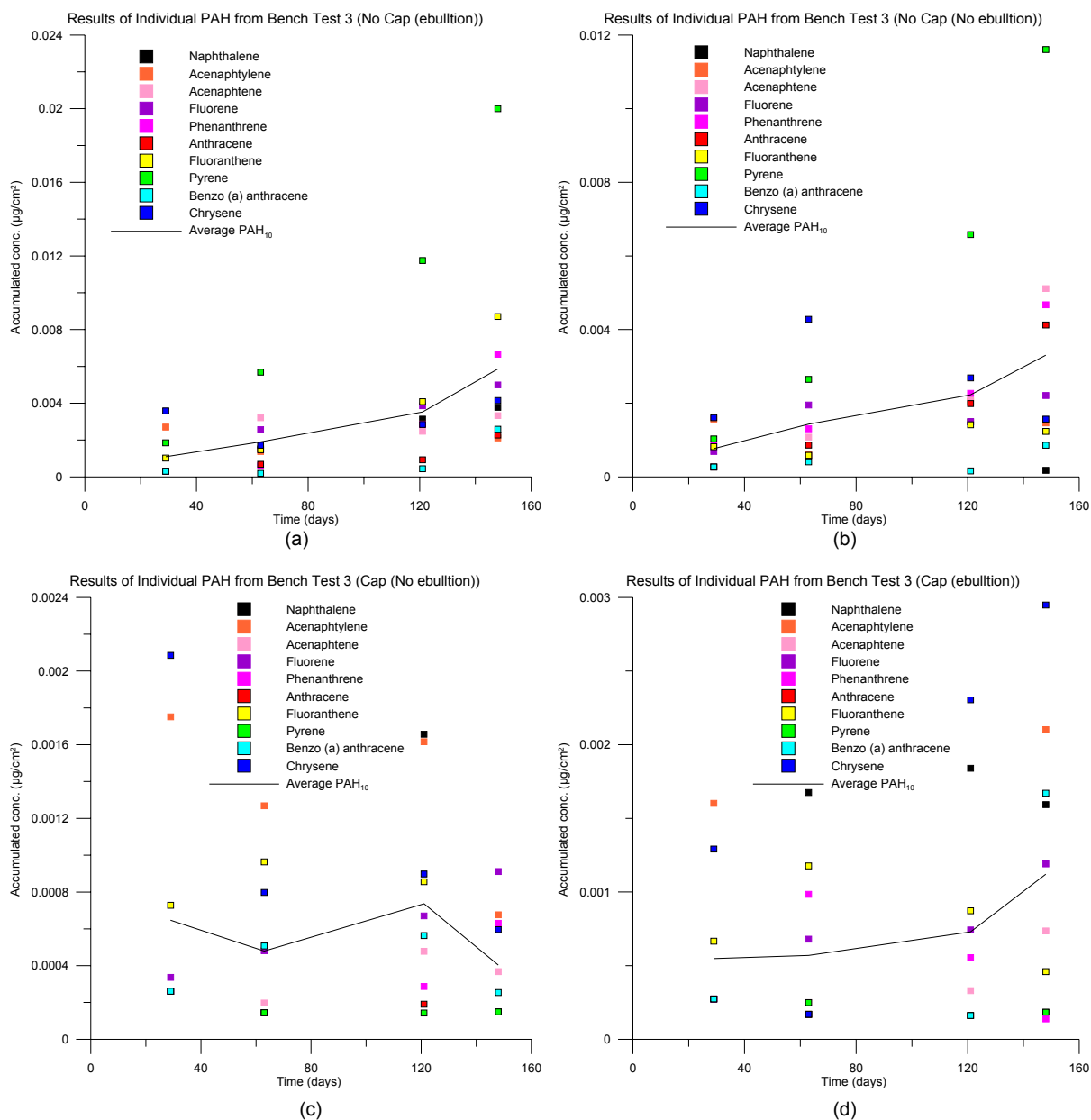
Figure 23: Accumulated mass of the 10 individual PAH compounds from bench test 3 (a) with no cap and ebullition, (b) with no cap and no ebullition, (c) with a cap and no ebullition and (d) with a cap and with ebullition.

Figure 23 shows the accumulated mass of the 10 individual PAH compounds and it is again visible, as in the results from Figure 18, that some PAH compounds have a larger influence over the overall flux (for example Pyrene in Figure 23(a) & (b)). Graphs showing the calculated fluxes for each individual PAH compound in bench test 3 together with the 95% confidence intervals can be seen in Appendix K. These fluxes were used to calculate the concentration of PAH $_{10}$ in the pore water of the sediment and the cap material using Equation (3.3.6) and the results are seen in Table 4.

Table 4: Calculated pore water concentrations (C_{pw}) for each individual
PAH compound from bench test 3.

Compound	Unit	C_{pw} (cap) Bench Test 3	C_{pw} (sediment) Bench Test 3
Naphthalene	µg/l	$1,2 \times 10^{-2}$	$1,3 \times 10^{-2}$
Acenaphthylene	µg/l	$2,3 \times 10^{-2}$	$3,0 \times 10^{-2}$
Acenaphthene	µg/l	$7,4 \times 10^{-3}$	$6,2 \times 10^{-2}$
Fluorene	µg/l	$1,5 \times 10^{-2}$	$3,7 \times 10^{-2}$
Phenanthrene	µg/l	$8,8 \times 10^{-3}$	$6,6 \times 10^{-2}$
Anthracene	µg/l	$3,7 \times 10^{-3}$	$5,6 \times 10^{-2}$
Fluoranthene	µg/l	$1,3 \times 10^{-2}$	$2,7 \times 10^{-2}$
Pyrene	µg/l	$3,5 \times 10^{-3}$	$1,7 \times 10^{-1}$
Benzo(a)anthracene	µg/l	$1,0 \times 10^{-2}$	$1,2 \times 10^{-2}$
Chrysene	µg/l	$2,1 \times 10^{-2}$	$5,6 \times 10^{-2}$
Total PAH$_{10}$	**µg/l**	**$1,2 \times 10^{-1}$**	**$5,3 \times 10^{-1}$**

The calculated concentration of PAH$_{10}$ in the pore water of the sediment phase is a realistic estimate for what is known of the sediment in Bjørvika (E Eek 2005, pers. comm., 25 May). This result strengthens the assumption that the processes present in these bench tests can be sufficiently described by Fick's' first law.

Figure 24 shows the results from the blank tests in bench test 3, which consisted of only sea water and capping material (V-1 to V-3 & BC-1 to BC-3), compared against the results of the capped samples without ebullition (C-1 to C-12). It is interesting to note that some compounds have approximately the same flux in all three tests, for example Fluoranthene, Fluorene and Chrysene. Furthermore, the overall flux from all PAH$_{10}$ compounds is approximately the same for all of the tests and surprisingly also for the blank sea water tests. This therefore raises the question of where the flux of PAH from the capped tests arose from the underlying sediment or the cap and water phases. Therefore, the calculated fluxes for all of the capped tests may be lower if the flux of PAH$_{10}$ from the cap and the water phases are taken into account. This will be discussed further in Section 4.2.3. No series of blank tests were completed in bench test 2 and therefore it cannot be confidently said that the results in Figure 24 apply also to this test.
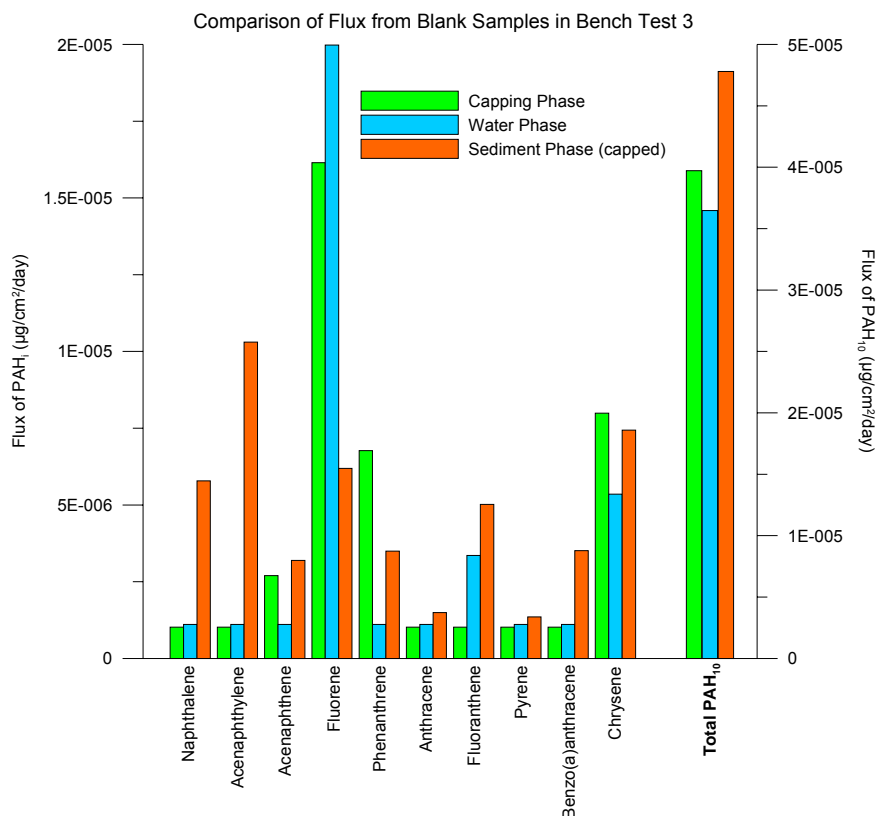
Figure 24: Flux of individual PAH_{10} compounds from both of the blank tests containing only capping material and only sea water compared against the capped test with no ebullition in bench test 2

The results from bench test 3 and bench test 2 will be discussed in greater depth throughout the next Section of this Chapter.

4.2.3 Physical and chemical processes in bench tests 2 & 3

As mentioned previously the general theory and assumptions behind both bench tests 1 and 2 is the same. Therefore, the results from both bench tests will be discussed further in this section. The main processes transporting contaminates into the water phase, from the sediment surface, have already been discussed in Section 2.3. For that reason, only those processes which are of importance in explaining the results in Sections 4.2.1 and 4.2.2 will be elaborated upon here. Four (4) different systems have been studies in bench tests 2 and 3 namely;

1) Sediment with no capping layer and no ebullition present.

2) Sediment with no capping layer and ebullition present.

3) Sediment with a capping layer and no ebullition present.

4) Sediment with a capping layer and ebullition present.

So as the individual processes of importance for each system can be studied, the following discussion will be broken down into these four categories. Many of the processes have already been discussed in Section 2.3 and these are again listed in Table 5. The relevance of each process for the transport of PAH in both a natural system and a laboratory system has also been indicated.

Table 5: List of important processes involved in the transport of PAH and there relevance to both natural systems and the laboratory system used in this experiment.

Process	Is the Process Important in the Transportation of PAH?	
	In Natural Systems	In Laboratory Systems
Sedimentation	Yes	No
Advection	Yes	No
Molecular Diffusion into Overlying Water Phase	Yes	Yes
Molecular Diffusion through the Pore Water Phase	Yes	Yes
Eddy Diffusion	Yes	No
Degradation	Yes	Yes
Sorption to Solids	Yes	Yes
Erosion	Yes	No
Bioturbation	Yes	No
Bioaccumulation	Yes	No

Only those processes which are important in the transport of PAH in the laboratory system will be discussed in this section together with processes tied to ebullition, which have not been listed in Table 5. Furthermore, no processes involving the interaction of contaminates with the actual marine sediment will be discussed in depth.

System 1 (Flux - No Capping Layer - No Ebullition of Gas)

System 1 describes tests U1 to U12 in bench test 3 and represents the simplest of the systems studied. This is emphasised by the results in Figure 23, which showed a very linear accumulation of PAH in the organic phase over time. The processes which are thought to result in this linear flux are seen in Figure 25 and are not so numerous. Even though consolidation has been included, it is uncertain if this process is of any importance.

Bearing in mind the sediment was manually consolidated prior to the test and that advection is usually driven by consolidation. It is therefore assumed that the total consolidation and advection in this system is zero. Redox processes in the sediment were observed as a thin layer of grey sediment, which formed on the surface of the sediment (see Figure 20). It is not known which processes caused the lightening of the surface sediments as no measurements concerning redox were made. This layer was more profound in bench test 3 indicating the possibility of a different redox regime than in bench test 2, which developed a yellow colour on the surface of the sediment possibly indicating iron (Fe) reduction.
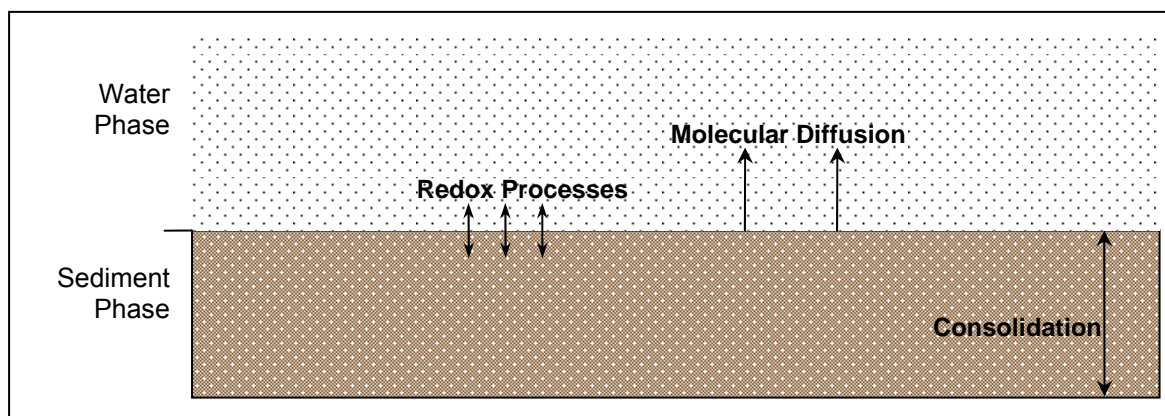
Figure 25: Main processes present in system 1 with transport occurring directly from the sediment surface and with no ebullition present.

The redox processes may have had an impact on the overall diffusion of PAH_{10} from the sediment phase. This could be especially true if the microbial degradation of PAH in the sediment was occurring. The processes involving the degradation of PAH by microbes in marine sediments will not be discussed here, other than to say that the use of bacterial biodegradation of PAHs in remediation techniques is well known and studied (Tabak et al, 2001).

Results from tests with this setup should more closely represent the actual pore water concentrations of PAH_{10} calculated in Section 4.2.2 (*5.3×10^{-1} µg/l*). As discussed this concentrations is quite reasonable for what is known of the sediments in Bjørvika and will therefore be considered a realistic estimate. It is therefore possible to assume that the linear model used gave a realistic estimate of the processes present in this system. This confirms that eddy diffusion discussed in Section 2.3.4 is not of importance in these tests. Although, these were closed systems and eddy diffusion in a real world system would be much more influential.

System 2 (Flux - No Capping Layer – Ebullition of Gas)

The processes influencing the transport of PAH in those tests with ebullition and without capping layers, such as Tests UC-1 to UC-12 in bench test 3 and 2-1 to 2-18 in bench test 2 are described in Figure 26. The processes discussed in system 1 are also of importance but have been neglected so as to avoid repetition. Firstly, a quick discussion on bubble nucleation and behaviour is needed, so as the transport of PAH due to these processes can be better understood.
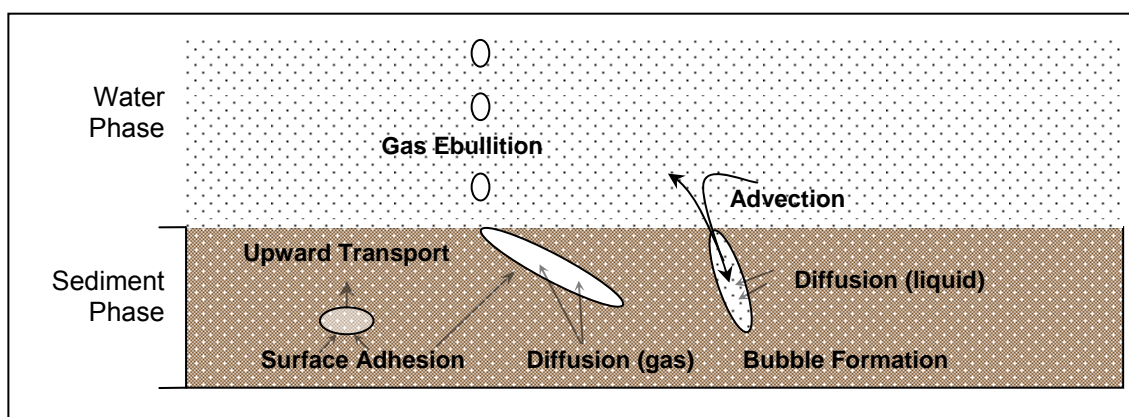
Figure 26: Main processes in System 2 with transport being influence not only by the processes in Figure 26 but also by the ebullition of biogenic gas.

As discussed in Section 3.1, sufficient gas was produced for the nucleation of bubbles to occur. Owing to the large density difference between the bubbles and the sediment, they should tend to rise. Although, research by Nguyen and Borger (1992), Schotmeyer (1998) and models developed by Cazwmier and Visschedijk (1997) have shown that bubbles with a radii of up to 0.84 m are required before a bubble will rise in a sediment with an undrained shear strength $c_u = 1$ kPa and density $\rho = 1400$ kg m^{-3}. This radius is dependant on the shear strength and density of the sediment and is calculated as

$$r = \frac{fc_u}{\rho g} \tag{4.3.1}$$

where f is a dimensionless factor defined to be 11.6 (Kesteren & Kessel 2002, p. 9). Vaneshear tests performed by Cappelen (2003) showed that the shear strength of the sediment from Oslo Fjord was approximately 0.1 kPa with a density of 1400 kg/m^3. Bubbles would therefore theoretically require a radius of 8 cm before they would begin to rise in this sediment. Even if the shear strength was a low as 0.05 kPa, a radius of 4 cm would still be required.

A radius of 4 cm may be reasonable in natural sediment, but in this experiment bubbles were observed at no more that 2 cm in diameter. These large bubble radiuses owe to a 'hardening' of the material above the bubble, which therefore makes the rising of gas bubbles through the grain matrix unlikely (Van Kesteren, 2002). As a result it can be presumed that the upward transport of bubbles due to buoyancy in the sediment and partitioning to these bubbles does not enhance the transport of PAH through the sediment matrix. However in natural systems, zones of weaker shear strength may exist in the sediment allowing bubbles to rise in these areas of reduced resistance.

It is unlikely the molecular diffusion of gas through the sediment matrix enhanced the desorption of PAH from the sediment phase. And although supercritical CO_2 has been used extensively as a solvent for desorbing PAH from sediments (Hawthorne et al, 2001), this form of CO_2 does not exist in this system. It is more likely that changes in pH due to increased levels of CO_2 would be more important. The pH may have had an influence over redox processes and the types and rates of biodegradation of PAH in the sediment. Although as no measurements have been made investigating these effects this is very speculative.

The biodegradation of PAH in the sediment was not studied, although it is interesting to note that bench tests performed by Quantin et al (2005) found that PAH in sediments under aerobic and anaerobic conditions enhanced by the introduction of cellulose could be degraded. This was limited to microbial communities under aerobic conditions, and anaerobic metabolism based on iron and sulphate reduction was not coupled with PAH degradation. It was also discovered that cellulose addition stimulated both aerobic and anaerobic respiration, but had no effect on PAH dissipation. Therefore it can be assume that the initiation of gas ebullition through the introduction of starch had no impact on the biodegradation rates of PAH in any of the tests.

The diffusion of gas in the pore water of the sediment and the rising of bubbles though the sediment does most likely not influence the transport of PAH from the sediment. And if it is assumed that biodegradation does not have a major influence, therefore some other physical or chemical processes must account for the increases in flux seen in Sections 4.2.1 and 4.2.2. One physical process recognised in both bench test 2 and 3 was the formation of cracks or fissures due to bubble formation. Crack formation differs from the physical rising of bubbles in that gas trapped in cracks can only escape if these cracks propagate towards the surface or towards other crack.

Crack formation occurs due to discontinuities in the sediment phase, where bubbles may deviate from a spherical shape and grow in the direction of the smallest principal stress. Experiments by Van Kessel (1998) have shown that this growth is usually in the horizontal direction and this horizontal formation was evident during both bench tests 1 and 2 (Figure 16 & Figure 20). When these bubbles reach a critical radius, the cracks they form create pathways for gas transport to other bubbles and to the surface of the sediment (Van Kesteren, 2002). Once a fracture reaches the surface of the sediment, gasses are released and rise as bubbles in the water phase.

The escape of bubbles through cracks, which had propagated to the surface, was witnessed many times during the length of this experiment. It is possible that these bubbles, after being trapped for an extended period of time, held PAH in the form of vapour and as part of a surfactant attached to the bubble surface. It is possible to obtain a rough estimate of the concentration of PAH_{10} in the gas phase of the bubble, since we already have an estimate of the pore water concentration in the sediment from Section 4.2.2. Assuming the concentration of PAH_{10} in the vapour space (C_b) is in linear equilibrium with the concentration in the pore water (C_{pw}) and is dependent on the PAHs vapour/liquid distribution (Henry's constant, H) then

$$C_b = H \cdot C_{pw} \qquad (4.3.2)$$

Referring to the Henry's constants in Table 2 the resulting concentration of PAH_{10} in the bubbles can be approximated at 5.4×10^{-4} µg/l, a concentration much lower than the actual concentration in the porewater (5.3×10^{-1} µg/l). From Section 3.1 it is known that approximately 3.8×10^{-4} l/cm^2/day of biogenic gas was released from the sediment (see Figure 6). Therefore, a very preliminary approximation of 2.1×10^{-7} µg/cm^2/day of PAH_{10} would have accumulated in the organic phase due to gas bubbles escaping through cracks. This increase in flux has been plotted together with the actual increase in flux due to ebullition shown in Figure 27. This shows that the additional flux due to PAH_{10} in the vapour phase does not account for the actual increase in flux due to ebullition in bench test 3. It must also be mentioned that in natural systems generally less than 10% of the sedimentary bubble reservoir is released through ebullition and therefore, the approximation of increased flux due to ebullition may be overstated (Hughes et al, 2004).

Research by Raja et al (2002) and Smith and Valsaraj (1997) has suggests the existence of a bubble-water partition coefficient (K_{bw}) which may significantly exceed the conventional Henry's constant used in Equation (4.3.2) and could partly explain the increase in flux seen in Figure 27. This higher partitioning coefficient is thought to arise from the accumulation of hydrophobics at the bubble water interface. Preliminary research by Hughes et al (2004) has also shown that it is possible to obtain a value for the true equilibrium partitioning coefficient

Figure 27: Increase in PAH_{10} accumulation in the organic phase of Bench Test 3 assuming that Henry's constant is correct and that 5 litres of microbial gas was released from the sediment over a period of 150 days.

for PAH and bubbles of methane (K_{gw}). This coefficient takes into account the volume per area and volume fraction of gas bubbles in the sediment and includes a term for the water-interface partition coefficient. The experiment by Hughes et al (2004) was preliminary and utilised high methane gas flow rates (4 to12 ml/min) through slurry. These flow rates are 10^2 times higher than those experienced in this experiment and would therefore give K_{gw} values lower than would most likely be found in this experiment. The lowering of the K_{gw} results from the shorter residence time of the bubbles in the sediment in the experiments by Hughes et al (2004) and therefore lower partitioning.

The experiments by Hughes et al (2004) also involved bubbles of methane rising through sediment however as discussed previously, the rising of bubbles in the sediment in these bench tests is unlikely. Again emphasising that the transport of PAH due to gas ebullition must originate from bubbles escaping through fractures not rising through the sediment. It was demonstrated that escaping bubbles do not dramatically influence the flux of PAH themselves, however there may be mechanisms tied to these escaping bubbles which account for the flux increases seen. These mechanisms could in effect also enhance the transport of PAH through the capping layer, although this will be discussed later in system 4.

In addition to small amounts of PAH partitioned to the rising bubbles, the enhanced flux may arise from an increase in surface area between the sediment-water interface. A great deal of research has shown that the transport of contaminates in the BBL can be enhanced by advection through sedimentary structures created by benthic macro-fauna (Aller, 2001). The common themes among these structures include disruption in the sediment fabric, the creation of voids, and the residence time and local advection of water through such voids. Fluid transport in these systems promotes solute exchange between different pore fluid regions, and it is the irrigation of these structures which is often one of the most important process when determining the exchange of contaminates between overlying water and sediments (Aller, 2001).
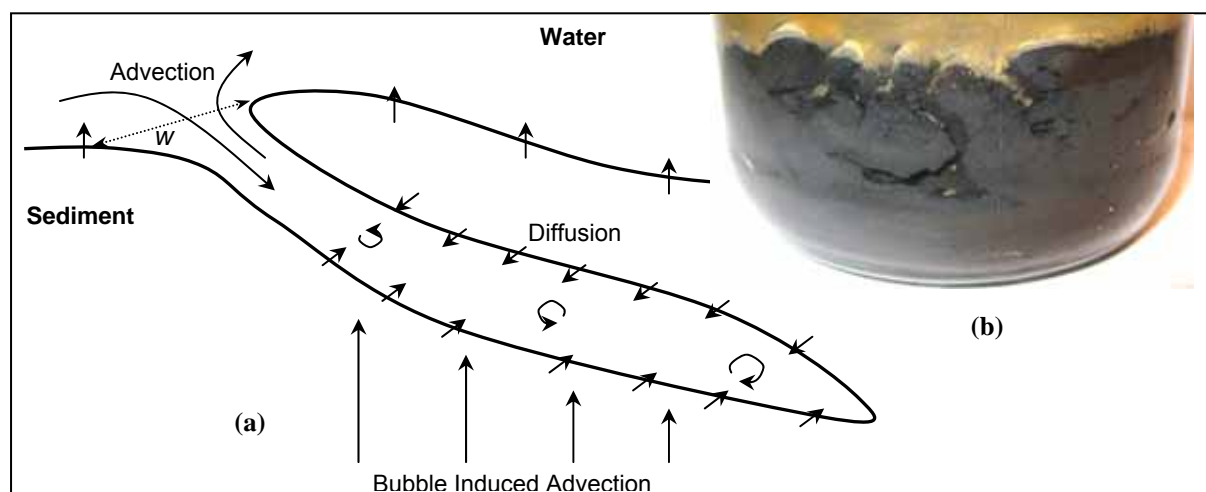
Figure 28: (a) Diagram displaying the diffusion of PAH into water filled cracks driven by bubble induced advection and (b) an actual bubble void filled with water.

It is hypothesised that the irrigation of the voids spaces left behind after crack formation may be one of the driving factors behind the increased flux of PAH_{10}. This is visualised in Figure 28(a), where diffusion occurs not only directly from the surface of the sediment but from those new surfaces created in the crack voids. One of these voids is visible in Figure 28(b) where it is actually possible to see where surface particles have fallen down into the space. However, some manner of flushing of these voids must occur before they can contribute to the overall flux of PAH. If flushing does not occur, then the net increase in flux from the void will only be equal to a surface area of sediment equal to the area of the void entrance shown in Figure 28 as *w*. This flushing must facilitate the transport of diffused PAH into the over-head water column and replace the water in the void with fresh water, thus maintaining the concentration gradient required for molecular diffusion.

From observations made during bench tests 2 and 3 it is possible to say that there may be processes occurring in the sediment matrix which allows this flushing to occur. These processes are summarised in Figure 29 and include;

- A pumping effect generated by the continuous nucleation and dissipation of bubbles in the sediment matrix.

- Microscopic water currents created by bubbles as they escapes through the water filled crack or fissure.

- Water flow induced by pressure gradients created by the escaping bubbles.

Research conducted into the mechanical response of sediments to gas bubbles (Johnson et al, 2002; Gardiner et al, 2004; Scardina & Edwards, 2001 & Sills & Gonzalez, 2001), has described some of these processes.
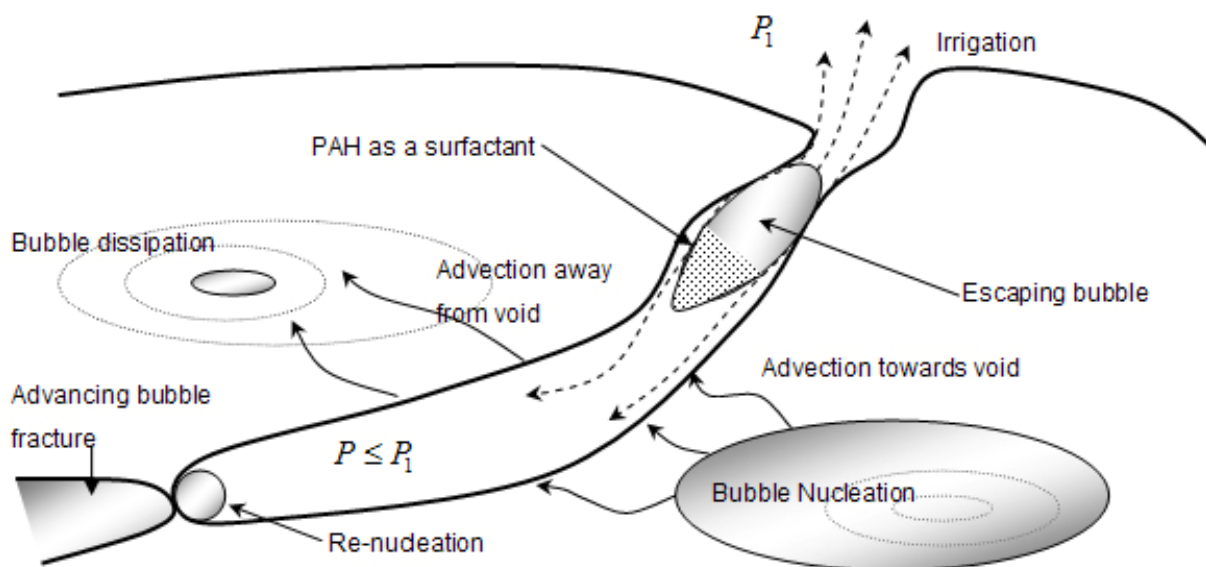
Figure 29: Description of pumping action and pressure differences possibly creating advective fluxes in bubble voids.

Tests performed by Sills and Gonzalez (2001) showed that sediments go through a number of phases due to the effects of biogenic gas production. They observed, as was observed in this test, that when gas production reached a critical threshold it began to escape through cracks in the sediment. This cracking marked a new phase, in which the escaping gas lowered the over-all concentration of biogenic gas in the sediment. As this lowering of concentration occurred the consolidation of the sediment increased and the cracks provided a quick route for pore water dissipation.

They also showed that as gas bubbles formed in the sediment they expelled water, and that most of the volume of new bubble growth was accommodated by expelled water and not the expansion of the sediment matrix. This finding supports the hypothesis presented in Figure 29, that porewater must move away from a growing bubble and inversely, towards a dissipating bubble, and in doing so generating a pumping effect.

As discussed previously, PAH partitioned to surface film on bubbles as they rise through the fissures may slightly increase the overall flux. This partitioning has been discussed by Alves et al (2005), who based on assumptions by Griffith (1962), has modelled the accumulation of contaminates on bubble surfaces as they rise through water. The model follows that if surface convection is fast compared to both bulk diffusion and both absorption and desorption, that the adsorbed surfactant will be collected in a stagnant cap region, leaving the frontal region of the bubbles uncontaminated. A discussion into the theory behind the model developed by Alves et al (2005) is beyond the scope of this report however, it is important to note that this stagnant cap region shown in Figure 29 may have a large influence on the flux of PAH to the water column.
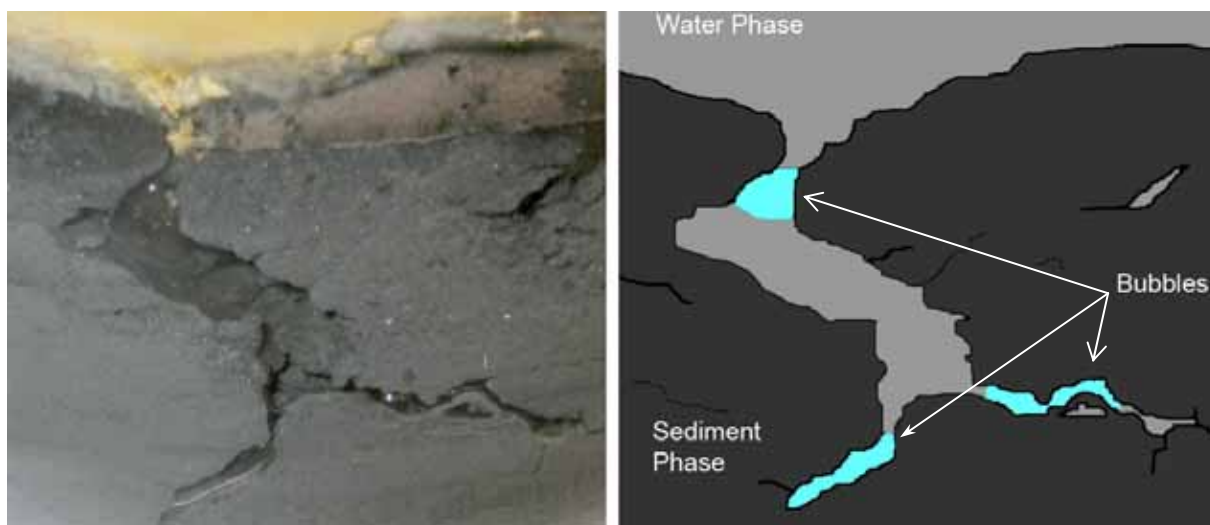
Figure 30: Fisher in sediment exiting into the water phase. It is believed that bubbles seen rising though fishers such as this one enhance the overall flux of PAH_{10}.

Also visible in Figure 29 is a fissure containing a trapped gas bubble located lower in the sediment matrix and advancing upwards into the crack positioned closer to the surface. As this crack advances new bubbles are nucleated in the upper crack. This was observed in both bench tests 1 and 2 and in experiments by Sills & Gonzalez (2001) and can be seen occurring in Figure 30. It is hypothesised that as this newly formed bubble escapes, it creates a very slight under-pressure or suction as it moves through water filled fissure.

This suction force combined with turbulence created by the escaping bubble and the already mentioned dissipation of pore water, combined should allow the irrigation of the fissure to occur. This would therefore allow cycling of the water into this void, thus enhancing the diffusion of PAH into the water phase. If this irrigation is occurring then theoretically the surface area from which diffusion can occur is greatly increased.

It is possible to calculate this increase by determining a ratio (B) between the flux of PAH_{10} from those samples with ebullition (F_b) and those without ebullition (F_{nb})

$$B = \frac{F_{nb}}{\left(F_b - F_{gw}\right)} \quad (4.3.3)$$

F_{gw} is the theoretical flux of PAH_{10} partitioned to the bubble phase and calculated as

$$F_{gw} = \frac{C_b}{a_{gas}t} \quad (4.3.4)$$

where a_{gas} is the volume of gas produced per unit area of the sediment interface (l/cm^2), t is time and C_b is the concentration of PAH_{10} partitioned to the bubble phase and calculated in Equation (4.3.2). It was seen in Figure 27 that the increase in flux due to gas partitioning (F_{gw}) was very small, therefore it will be assumed that $F_{gw} \ll F_b$. A value for B for bench tests 2 has been calculated arriving at 0.7 (B is dimensionless). Assuming that the flux of PAH_{10} from the sediment surface is the same for both tests (with and without ebullition) an effective area (A_{eff}) can be determined as

$$A_{eff} = \frac{A_{sw}}{B} \quad (4.3.5)$$

where A_{sw} is the actual surface area of the water-sediment interface. We therefore have an approximate effective area of the sediment-water interface in bench test 3 of 54 cm^2 compared with the actual area (A_{sw}) of 38 cm^2. These calculations and assumptions are only speculative and more research is required if they are to be certified.

System 3 (Flux - Capping Layer - No Ebullition of Gas)

It is seen by the results presented in Section 4.2 that the introduction of a capping layer onto the surface of the sediment has a large influence over the processes discussed in Systems 1 & 2. This influence involves a reduction in the overall flux of PAH_{10} into the water phase and eventual accumulation in the organic phase. The results showed that the capping layer had an efficiency of between 76 to 84% in reducing this flux. Figure 24 in Section 4.2.2 also showed that a certain quantity of the PAH_{10} accumulated in the organic phase actually arose from the capping and water phases, therefore the efficiency of the capping layer may be actually higher than already mentioned. This actual efficiency is expressed in Figure 31 where the flux from the cap and water phase has been subtracted from the flux in the capped tests (no ebullition) in bench test 3. By subtracting the flux of PAH_{10} originating from the cap and water phases, a new efficiency of 95% is achieved. Furthermore, the confidence regions in Figure 31 overlap introducing uncertainty as to whether the slightly higher fluxes in the capped tests are real or arise simply from errors in the analysis. This also raises the important question as to where the PAH arose from in the capped tests, the sediment or the cap? Figure 31 tends to suggest that the answer is that there has been no detectable flux of PAH_{10} from the sediment through the capping material during the length of the experiment. This finding has also been mirrored by research into the effectiveness of thin capping layers by Talbert et al (2001).

There are a number of processes which contribute to this effectiveness, at both the molecular and mass transport scales, and these are shown in Figure 32.
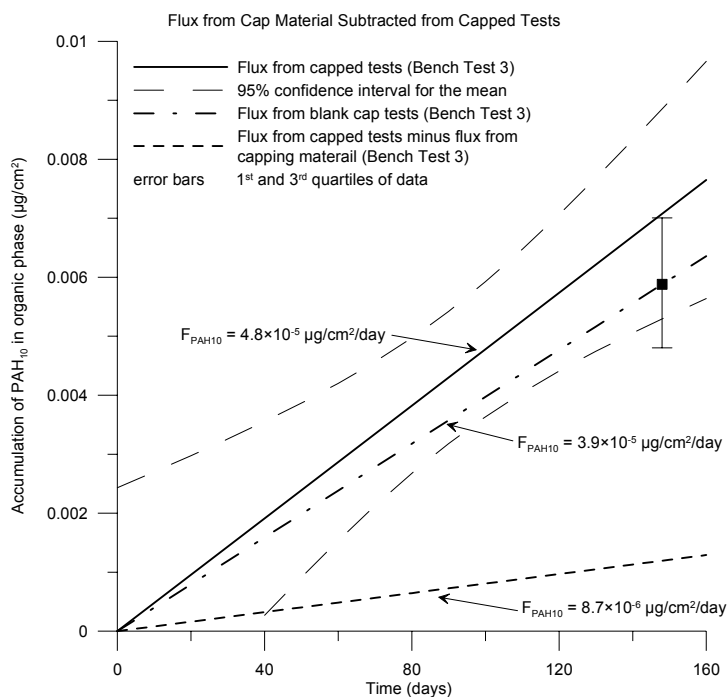
Figure 31: Figure showing the resulting actual flux from the sediment after subtracting the flux from the capping material itself in bench test 3. The 95% confidence interval for the mean is given for the flux of PAH_{10} from those tests which were capped while the error bars indicate the 1st and 3rd quartiles for the result of the blank cap tests representing the results in Figure 24.
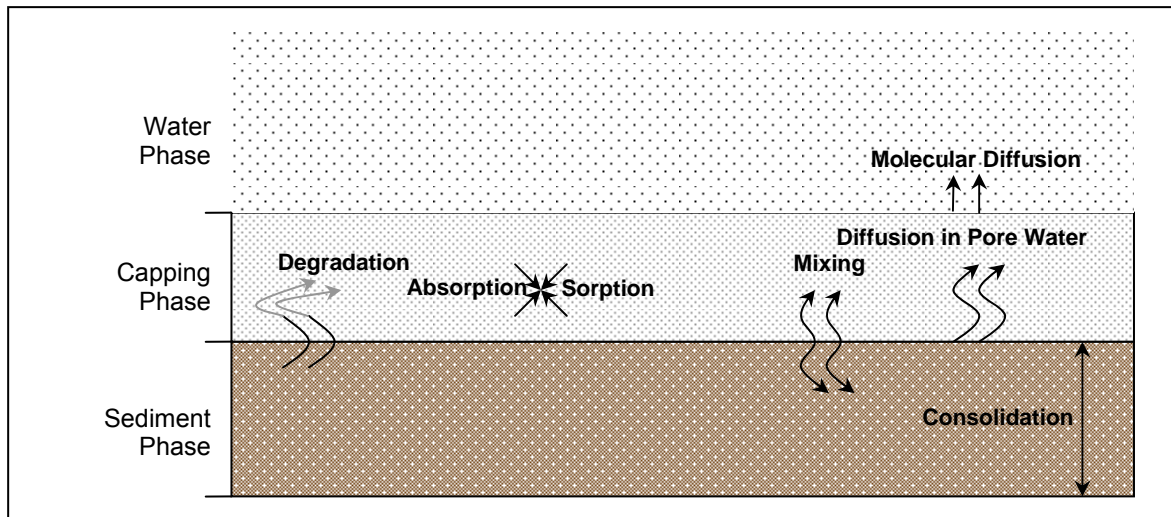
Figure 32: Main processes in System 3 where the transport processes from the sediment surface are further influenced by the inclusion of a capping layer.

Consolidation in Figure 32 has been included as there may have been a small amount of pore-water advection in this system due the introduction of the cap. However research suggests that water flow during compaction of fine grained sediments is very slow and in the sandy material of the cap almost non existent (Bear, 1982). Furthermore, since no consolidation was noticed in any of the tests, it can be concluded that advection due to dissipating porewater again had very little or no influence on the capped systems. It is more likely that the main processes were the diffusion of PAH in the water filled pore spaces of the capping material and the adsorption of PAH to the mineral phase of the cap. This conclusion is also shared by Wang et al (1991) in their studies into the diffusion and adsorption of contaminates in capping layers, in which they concluded that a caps porosity and depth were the dominating factors behind contaminate transport.

The transport of hydrophobic compounds such as PAH through a cap, has also been investigated by Karickhoff et al, (1985) Formica et al (1988) & Baron et al (1990) who all concluded that the process is a combination of molecular diffusion and adsorption in the cap material. The transient motion of PAH in the pore water is therefore highly influenced by partitioning between these two phases. Sorption isotherms have not been investigated for the PAH_{10} compounds and capping material in this experiment, although an estimate of the soil-water partition coefficient (K_d) can be made by

$$K_d = K_{oc} \cdot f_{oc} \qquad (4.3.6)$$

where f_{oc} is the fraction of organic carbon in the cap and K_{oc} the organic carbon-water partition coefficient estimated by

$$\log K_{oc} = 1.04 \cdot \log P_{ow} - 0.84 \qquad (4.3.7)$$

P_{ow} is the octanol-water partition coefficient of the PAH compound. The log K_{oc} value for each of the 10 PAH compounds are listed in Table 2. If the f_{oc} for the capping material is known it is possible to determine the concentration of PAH_{10} bound to the capping phase (C_{solid}) by the relation

$$C_{solid} = \sum C_{soild_i} = \sum K_{d_i} \cdot C_{pw_i} \qquad (4.3.8)$$

where i represents the pore water concentration, solid phase concentration and soil-water partition coefficient for each individual PAH compound. Applying Equation (4.3.8) to the pore water concentrations calculated in Section 4.2.2 together with the fractions of organic carbon in Table 6 and soil-water partition coefficients in Table 2, a concentration of PAH_{10} bound to the solid phase can be calculated. The results of this calculation are displayed in Table 6.

Table 6: Calculated and analysed concentration of PAH_{10} compounds partitioned to the solid phase of the sediment and capping material.

	Units	Sediment Phase	Capping Phase
Fraction Organic Carbon (f_{oc}) [1]	-	0.0403	0.0001
Sum of Partition Coefficients (K_d) [2]	-	4.1×10^4	1×10^2
Analysed PAH_{10} on Solid Phase [3]	mg/kg	9.8	?
PAH_{10} in Pore Water (C_{pw}) [4]	mg/l	5.3×10^{-4}	$1,2 \times 10^{-4}$
Calculated PAH_{10} on Solid Phase [5]	mg/kg	1.9	1.5×10^{-3}

[1] from Appendix **B** [2] from Equation (4.3.6) & Table 2 [3] from Table 1 [4] from Table 4 [5] from Equation (4.3.8)

By comparing the actual analysed concentration of PAH_{10} on the sediment particles (from Table 1) with the calculated concentration in Table 6 it is possible to conclude that Equation (4.3.8) gives a fairly good approximation of the phase distribution of PAH_{10} compounds. Therefore, the concentration of PAH_{10} bound to the capping material is approximately 0.0015 mg/kg. Even though the capping material has a lower partitioning coefficient, it is still sufficient enough to retard the flux of the 10 PAH compounds and account for the results in Figure 17 and Figure 21.

The sorption of PAH to the capping material is a very important processes in the isolation of contaminates. However there will always remain some PAH in the pore water phase and therefore molecular diffusion will still always be present. However, the process of molecular diffusion through the pore water of a cap material is more complicated than through a simple free water phase. The diffusion of PAH through the capping material has been studied by Wang et al (1991) and is shown to be influenced by the porosity (ε) of the material and the tortuosity (τ) of the grain matrix. Inserting these factors into Fick's first law (Eq. (3.3.1)) gives

$$F_{PAH_{10}} = \sum D_i \frac{\varepsilon}{\tau} \left(\frac{\partial C_i}{\partial z} \right) \tag{4.3.9}$$

Tortuosity can be taken as a function of the porosity calculated as $\tau = \varepsilon^{-1/3}$ as described by Millington and Quirk (1961). By simply plotting the calculated concentrations of PAH in the pore water phase (C_{pw} *(cap)* and C_{pw} *(sediment)* found in Table 4) against the thickness of the capping material (*z*) in Figure 33 we can see the impact the cap has on concentration gradient.
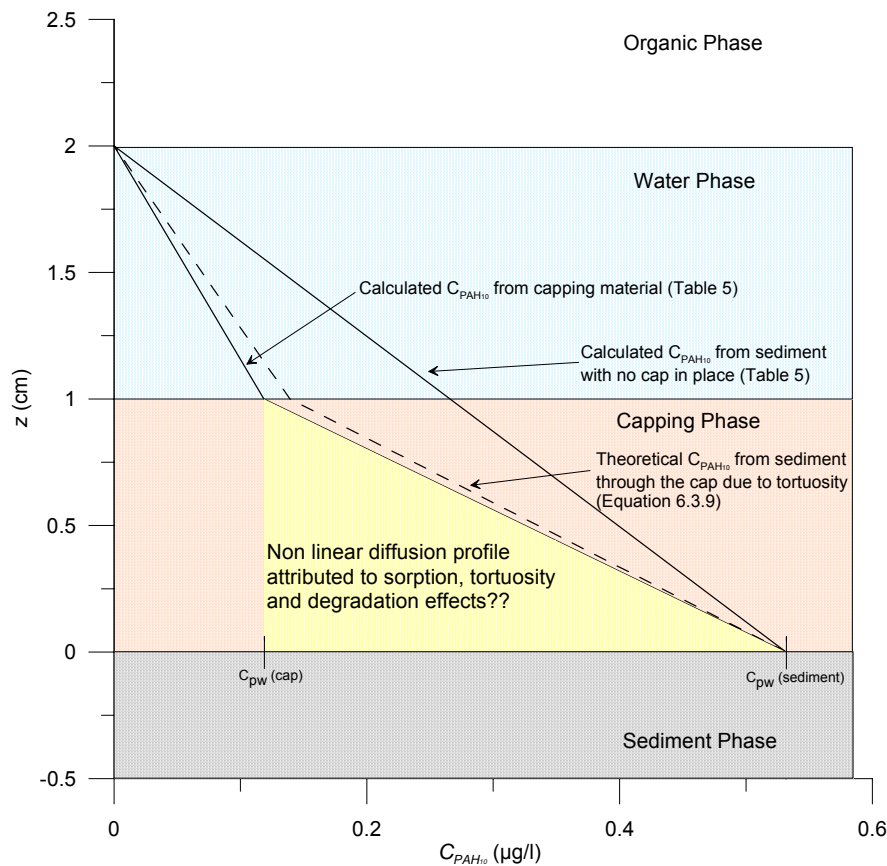
Figure 33: Calculated concentration gradients for flux of PAH through only the water phase and also through the capping phase. The yellow region indicates an area of uncertain behaviour which is most likely not linear. The dotted line indicates the flux of PAH through the water phase adjusted for tortuosity in the capping phase.

By making an adjustment for the porosity of the capping material (36.6%), a new concentration gradient from the sediment can be determined, which takes into account tortuosity (dotted line in Figure 34). The shaded area indicates an area where the concentration gradient in the capping material is unknown and is unlikely to be linear. It is obvious that the effect of tortuosity is enough to account for the reduction in flux between capped and non capped tests, even without the influence of sorption and degradation. This finding further emphasises the findings that no PAH had diffused through the capping phase from the sediment phase during the length of this experiment.

The sorption of PAH (listed in Table 6) may also have had an influence over degradation rates in the capping material. The effect of sorption on the biodegradation rates of PAH, has been studied by Rogers et al (2002), as a means of natural attenuation in contaminated soils. It was previously mentioned that biodegradation was not coupled with anaerobic conditions in sediments. However, biodegradation of PAH may still be occurring in the capping phase. Huesemann et al (2002) found that in most soil types, with the exception of kaolinite clay, the rate of abiotic desorption of PAH was faster than the rate of biodegradation. This indicates that the biodegradation of PAH in the capping material may be limited by microbial factors only and not its availability. The long term biodegradation of PAH may also be enhanced by the development of a biofilm on the surface of cap material grains. It has been noted by Marcell & Eisele (1997) that sorption events on biofilms play a very important and dynamic role in the transport and accumulation of PAH in the aquatic environment. The biodegradation of PAH in the capping material could be further studied as accompanying the retardation of PAH by engineered capping layers, although in this test it will be assumed that the rates of biodegradation were too slow to have an impact on the overall flux of PAH_{10}, during the time scales of these experiments.

A combination of the processes discussed in this section, contributed to a substantial reduction in the flux of PAH by the introduction of a cap. Although, the influence ebullition discussed in System 2 may reduce this integrity and will therefore be discussed next.

System 4 (Flux - Capping Layer – Ebullition of Gas)

The same forces govern bubble entrapment and mobilization in a porous media as control NAPL migration (Reible, 1996), and it is this buoyancy driven migration of gas which may opens new channels for contaminant transport through a capping layer. As discussed, gas bubbles are inherently hydrophobic and tend to accumulate both hydrophobic organic contaminants and colloids from pore water. The transport mechanisms for contaminate transport by bubbles in the sediment phase has been discussed in System 2, although it is the ebullition of gas through the capping layer which is of main concern in this experiment.

Preferential routes generated by gas migration, may provide a means for the migration of gas as well as contaminants to the water phase. Many of these routes were noticed forming above gas fractures in the sediment and can be seen in Figure 34, together with bubble nucleation and a backfilling of the bubble voids. Backfilling seems to be a process in which voids created by the bubbles are eventually filled with capping material. Together with the mixing mentioned in Section 4.2.1, backfilling had a noticeable effect on the sediment-capping interface. It is unsure how deep this backfilling could advance, although observations from the tests seem to indicate that capping material will penetrate all open fishers after bubbles have dissipated. Theoretically, capping material could become mixed with the sediment up to the depth of bubble formation which, as discussed by Huls and Costello (2003) and Kesteren & Kessel (2002), is dependant on the temperature and shear strength of the sediment.
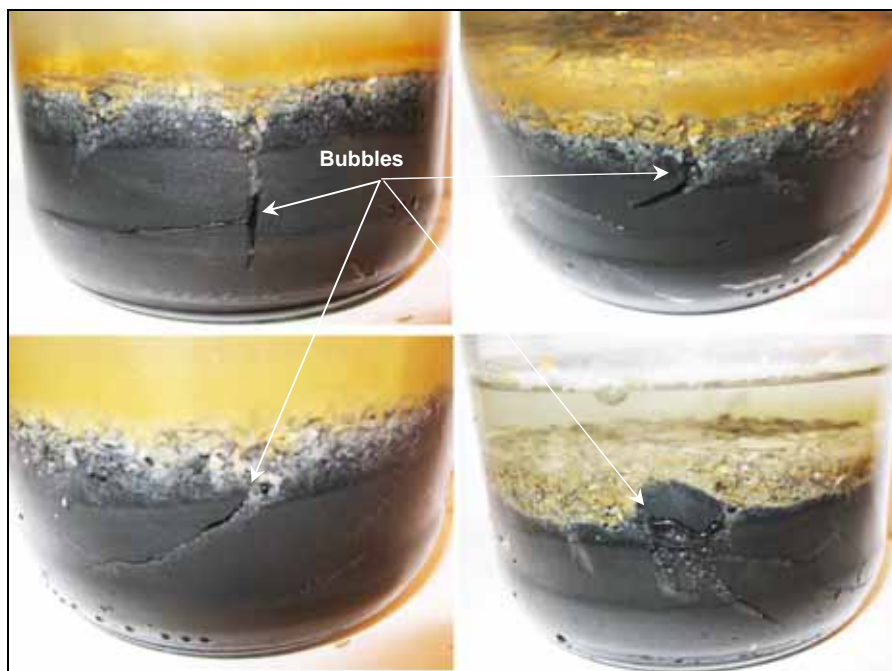
Figure 34: Bubble formation and backfilling of fishers in sediment. The existence of preferential routes is also noticeable.

It is believed that the process of backfilling has two consequences;

- The first is that the diffusion and flushing processes in the bubble voids discussed in System 2 are sequestered

- The second is the creation of larger preferential flow paths through the capping material.

As mentioned the larger preferential flow paths are of greatest concern, due to their possible impact on the flux of PAH through the capping layer.

The process of ebullition creating preferential paths is illustrated very nicely by Figure 35, in which a bubble is seen exiting the void it has recently occupied and thereafter, pushing its way through the capping material. This is a very slow process and as the bubble rises it displaces capping material into the space it previously occupied. It was suggested in System 2 that the escaping bubbles take with them PAH attached to surfactants and in the gas phase of the bubble. Furthermore rising bubbles in the capping phase should follow the same principles discussed in System 2.

Even though it is very likely that these rising bubbles transport PAH into the water column, the results in Section 4.2 tend to suggest that they did not significantly increase the overall flux. Furthermore there is uncertainty as to whether the slight increase in flux seen in Figure 21 was real or only due to uncertainties in the measurements. This small increase in flux may have been attributed to the stripping of PAH from the bubble surface as it passed through the capping phase. The partitioning of PAH to the solid phase of the capping material has been discussed in System 3. However in this case there may need to be an adjustment to the K_d value which takes into account the three transitions which must occur. First, from the bubble surface to the pore water (K_{gw}) and then to the solid phase of the capping material (K_d). Due to the high K_d values of PAH it can be assumed that a certain amount of PAH were stripped from the bubble surface as they passed through the sediment matrix.
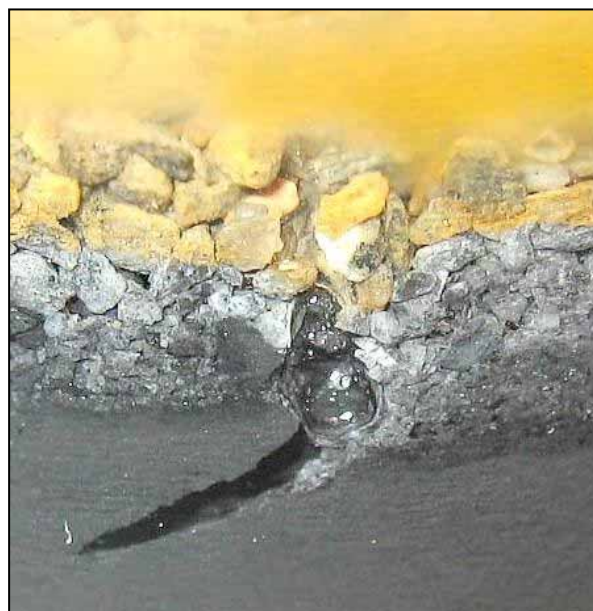
Figure 35: Bubble propagation through the capping material showing the formation of a preferential pathway.

There may exist also the possibility that PAH compounds were filtered directly from the bubble surface as it came in direct contact with the solid phase of the capping material.

The backfilling which occurs when bubbles exit through the capping phase probably reduces the overall increases in flux of PAH, by means of hindering the processes discussed in Figure 29. Especially the flushing action required for the enhanced flux from the sediment interface. The removal of this flushing process may further explain why the increase in flux in those tests with a capping layer was not as high as in those tests without capping layers as seen in Figure 21.
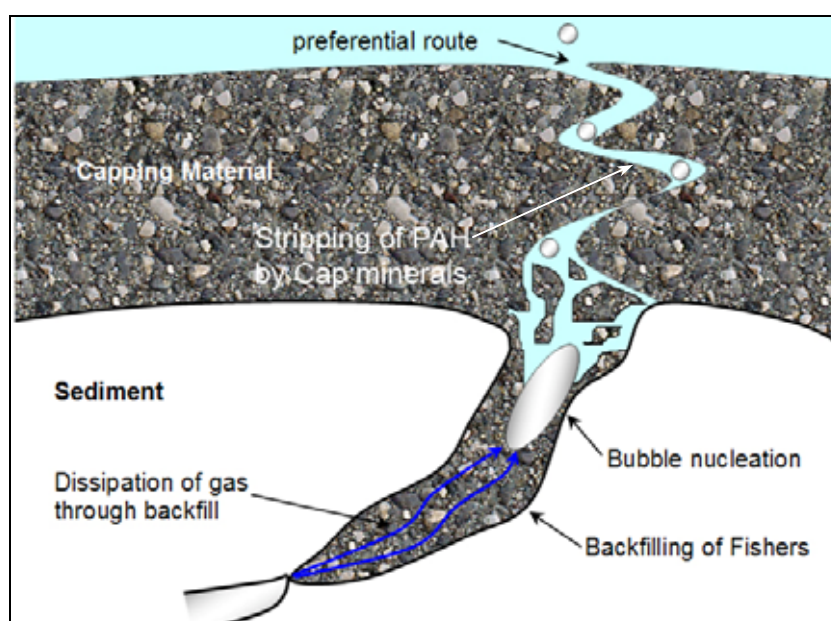
Figure 36: Main processes in System 4 showing that as bubbles rise through the capping material preferential pathways are generated and the backfilling of the bubble void occurs. However PAH are scavenged from the bubbles by the mineral phase of the cap.

Figure 36 summarises the processes involved in the escape of bubbles from the sediment through the capping phase. And although the escape of bubbles occurred, the data presented in Section 4.2.2 indicates that it did not increase the overall flux of PAH. This finding is important as it suggests that processes, which hinder PAH diffusion through the capping phase, are not detrimentally affected by ebullition. Furthermore, the venting of biogenic gas allows for the gradual escape of gas from the sediment phase. If this venting was not permitted to occur, through for example the use of impermeable geomembranes, the gases may accumulate potentially causing greater damage when ultimately they are released.

5 FUTURE RESEARCH

The results obtained in the bench tests described in this report were quite positive, revealing that the ebullition of biogenic gas does not have a detrimental effect on an engineered capping layer. However, the duration of the tests was quite short (150 – 220 days) and it would there-fore, be of interest to perform the same tests over a longer time period. A longer duration may eventually result in the discovery of a breakthrough time, at which point the flux of PAH is constant through the capping phase into the overlying water. This breakthrough time is of great interest, as it describes the expected lifetime of an engineered cap of a particular thick-ness. Furthermore, no research has been found which has investigated the effects ebullition may have on this breakthrough time. It is suspected that the preferential pathways generated by escaping bubbles may slightly increase the eventual flux through a cap, thus reducing its effective life.

If the process of preferential pathway generation could be obstructed, than ebullition would most likely not have a detrimental effect on the breakthrough time. One possible solution could be the introduction of a geomembrane between the sediment and capping phases. The membrane would have to be sufficiently permeable to prevent the trapping of gas, but no so permeable as to allow the escape of bubbles. Tests including a geomembrane between the sediment and capping phase, would therefore be useful to determine if these preferential pathways or perhaps other processes still occur.

The suggestions presented here represent only a couple of the actual investigations into ebullition, which could be performed. Fortunately, there is a great deal of interest around the world in this remediation technique and therefore, research in this field will likely continue.

6 CONCLUSIONS

Chapter 2 discussed the processes in which contaminants can migrate from or be deposited on benthic marine sediments. The basic understanding of these processes is important if decisions are to be made on how to best manage contaminated sediments, which pose risks to both people and the environment. Capping and concealment of these sediments has been found to be very effective option as it fulfils the primary goals of remediation, these being; the elimination of the active movement of contaminated sediment and the isolation of these contaminates. Eliminating particle movement by either erosion or bioturbation means that contaminant migration within a stable cap is limited to porewater processes such as advection and diffusion. Typically contaminants are hydrophobic and therefore, these processes are strongly retarded by sorption processes onto the immobile mineral phase of the capping material.

There have been a number of studies into contaminant migration through remedial caps due to these transport processes, however there is still a number of under defined variables. One of these variables, the ebullition of biogenic gas from sediments, has been presented in this report and the results have been positive. Furthermore, the findings here have supported the results obtained from prior independent studies.

Results have shown that although the ebullition of biogenic gas increases the overall flux of PAH from the sediment in relation to diffusion, this increase is eliminated if the sediment surface is isolated through the construction an engineered capping layer. The overall increase of flux from the sediment surface was facilitated by the formation of water filled fissures created by expanding bubbles. These fissures allowed for an increased flux of PAH partitioned to both the gas phase and surface film on the bubbles and an increase in the effective area of the sediment-water interface available for diffusion. The increase in effective area was generated due to processes tied to the escape of bubbles, which allowed the flushing of these fissures to occur

In the capped tests, it was discovered that fissures opened into the sediment-cap interface, and that the escaping bubbles created preferential pathways through the capping material. Even though bubbles escaped, as in the uncapped tests, the overall increase in diffusional flux of PAH was sequestered. The inhibiting of PAH flux was most likely influenced by tortuosity effects in the sediment phase and the partitioning of the PAH compounds to that phase.

However, the backfilling of the fissures that was witnessed as the bubbles escaped may also have reduced the advective flux of PAH from these structures. Therefore, it is concluded that a combination of these processes resulted in ebullition not increasing the overall flux of PAH in the capped tests resulting in an overall efficiency of 95% for 1 cm of capping material. This result again underpins the usefulness of remedial capping as a safe and reliable remediation method.

It is hoped the findings outlined in this report will help future decision makers, when faced with deciding on the most effective and economic remediation solution, to the ever increasing problem of contaminated sediments in our environment.

7   REFERENCES

Adams, D.D., Fendinger, N.J. & Glotfelty, D.E., 1997, Biogenic gas production and mobilisation of in-place sediment contaminates by gas ebullition, In: Baudo, R., Geisy, J. & Muntau, H. eds., *Sediments: Chemistry and toxicity of in-place pollutants*, Lewis Publishers, Boca Ranton, FL, pp. 215 – 236.

Aller, P.C., 2001, Transport and reactions in the bioirrigated zone, In: Boudreau, B.P. & Jørgensen, B.B., eds., *The Benthic Boundary Layer – Transport Processes and Biochemistry*, New York, Oxford University Press, pp. 144 – 170.

Alves, S.S., Orvalho, S.P. & Vasconcelos, J.M.T., 2005, Effect of bubble contamination on rise velocity and mass transfer, *Chem. Eng. Sci.,* 60 (1). pp. 1 – 9.

Appelo, C.A.J. & Postma, D., 1999, *Geochemistry Groundwater and Pollution*, A.A. Balkema, Netherlands.

Bazhin, N.M., 2002, Theoretical consideration of methane emission from sediments, *Chemosphere*, 50 (2), pp. 191 – 200.

Baron, J.A., Thibodeaux, L.J., Reible, D.D. & Templet, P.H., 1990, Laboratory simulation of diffusion in contaminated marine sediment, *Estuaries*, 13 (1). pp. 81 - 88.

Bear, J., 1982, *Dynamics of fluids in porus media*, American Elsevier: New York.

Berthouex, P.M. & Brown, L.C., 1994, *Statistics for Environmental Engineers*, CRC press, USA.

Boudreau B.P., 2001, Solute Transport above the Sediment-Water interface, In: Boudreau, B.P. & Jørgensen, B.B., eds. *The Benthic Boundary Layer – Transport Processes and Biochemistry*, New York, Oxford University Press, 144-170.

Breedveld, G.D., Oen, A.M.P, Eek, E. & Hauge, A., 2003. Strategy for remediation of Contaminated Fjord Sediments in Norway. *Proceedings of the 2nd International Symposium on Contaminated Sediments*, 26-28 May 2003 Québec City.

Brenner, R.C., Magar, V.S., Ickes, J.A., Abbott, J.E., Stout, S.A., Crecelius, E.A. & Bingler, L.S., 2002, Characterization and Fate of PAH-Contaminated Sediments at the Wyckoff/Eagle Harbor Superfund Site. *Environ. Sci. Technol.*, 36 (12), pp. 2605-2613.

Brock, T.D., Madiga, M.T., Martinko, J.M. & Parker, J., 1994, *Biology of Microorganisms 7th ed.*, Prentice Hall, Inc., New Jersey.

Cappelen, P.I., 2003, Tildekking av forurenset sediment – Sedimentasjon og bæreevne til mudrede masser, *Thesis (M.sc.),* NTNU, Norway.

Cazwmier, W. & Visschedijk, M.A.T., 1997, Gas bubbles in sediments, TNO report no. 97-NM-R1066dm11, In: Kesteren, W.G.M. van; Kessel, T. van, 2002, Gas bubble nucleation and growth in cohesive sediments, Elsevier, *Proceedings in Marine Science, 5, Fine sediment dynamics in the marine* environment, Eds.: Winterwerp, J.C.; Kranenburg, C., pp. 329-341

Costello, M., 2003, Remedial design modelling at a superfund sediment site, In: Pellei, M. & Porta, A. (Eds.), 2003, Remediation of Contaminated Sediments, *Proceedings of the second international conference on remediation of contaminated sediments*: 30 Sep – 3 Oct 2003, Venice, Italy: Battelle Press, Columbous, OH.

Crane, J.L., Smorong, D.E., Pillard D.A., & MacDonald, D.D., 2002. Sediment Remediation Scoping Project in Minnesota Slip, Duluth Harbour. *U.S. Environmental Protection Agency*, Great Lakes National Program Office, Chicago, IL. EPA-905-R02-002.

Davie, M.K., Zatsepina, O.Y. & Buffett, B.A., 2004, Methane solubility in marine hydrate environments, *Marine Geology*, 203 (1-2), pp. 177 – 184.

Di Toro, D.M. & McGrath, J.A., 2000, Technical basis for narcotic chemicals and Polycyclic aromatic hydrocarbon criteria. II. Mixtures and sediments, *Environmental Toxicology and Chemistry*, 19 (8), pp. 1971–1982.

Dyer, K.R., 1986, *Coastal and Estuarine Sediment Dynamics*, John Wiley & Sons, Chichester, UK.

Eek, E., Cappelen, P., Holme, J.K., Breedveld, G.D., Hauge, A., 2003a, Subaqueous disposal and capping of dredged material: Sedimentation and bearing capacity, *Proceedings of the 2nd International Symposium on Contaminated Sediments*, May 26 - 28, 2003 Quebec, Canada.

Eek, E., Pettersen, A., Godøy, O., Oen, A. & Breedveld, G.D., 2003b, Capping of Contaminated Sediments, Redox Reactions and Trace Metal Mobility, In: M. Pellei & Porta, A. Eds., Remediation of Contaminated Sediments—2003. *Proceedings of the Second International Conference on Remediation of Contaminated Sediments*, 30 Sep – 3 Oct 2003, Venice, Italy: Battelle Press, Columbus.

Formica, S.J., Baron, J.A., Thibodeaux, L.J. & Valsaraj, K.T., 1988, PCB transport into lake sediments. Conceptual model and laboratory simulation, *Env. Sci. Technol*, 22 (12), pp. 1435 - 1440.

Gardiner, B.S., Boudreau, B.P. & Johnson, B.D., 2003, Growth of disk-shaped bubbles in sediments, *Geochimica et Cosmochimica Acta*, 67 (8), pp. 1485 – 1494.

Hayduk, W. & Laudie, H., 1974, Prediction of Diffusion Coefficients for Non-Electrolytes in Dilute Aqueous Solutions. *J.AIChE*, 20, 611-615.

Headly, J.V., Boldt-Leppin, B.E.J., Haug, M.D. & Peng, J., 2001, Determination of diffusion and adsorption coefficients for volatile organics in an organophilic clay – sand – bentonite liner, *Can. Geotech. J.,* 38 (4), pp. 809 – 817.

Herrenkohl , M.J., Lunz, J.D., Sheets, R.G. & Wakeman, J.S., 2001, Environmental impacts of PAH and oil release as a NAPL or as contaminated pore water from the construction of a 90-cm in situ isolation cap, *Environ. Sci. Technol.,* 35 (24), pp. 4927 – 4932.

Heyer, J. & Berger, U., 2000, Methane emission from the coastal area in the Southern Baltic Sea, *Estuarine, Coastal and Shelf Science*, 51 (1), pp. 13 – 30.

Hinga, K.R., 2003, Degradation Rates of Low Molecular Weight PAH Correlate with Sediment TOC in Marine Sub tidal Sediments, *Marine Pollution Bulletin*, 46 (4), pp. 466 – 474.

Huesemann, M.H., Hausmann, T.S. & Fortman, T.J., 2002, Microbial Factors Rather Than Bioavailability Limit the Rate and Extent of PAH Biodegradation in Aged Crude Oil Contaminated Model Soils, *Bioremediation Journal*, 6 (4), pp. 321 – 336.

Huettel, M. & Webster, I.T., 2001, Porewater Flow in Permeable Sediments, In: Boudreau, B.P. & Jørgensen, B.B., eds. *The Benthic Boundary Layer – Transport Processes and Biochemistry*, New York, Oxford University Press, 144-170.

Hughes, J.B., Valsaraj, K.T. & Willson, C.S., 2004, In-Situ contaminate and treatment: Engineering cap integrity and reactivity, EPA Grant: R819165-01-0, [online], http://www.hsrc.org/hsrc/html/ssw/hughes04.pdf [Accessed: 09 May 2005].

Huls, H. & Costello, M., 2003, Bench test design evaluation of a remedial wetland cap – with regard to ebullition and its control, *Proceedings of the In-Situ Contaminated Sediment Capping Workshop*, May 12 – 14 2003, Cincinnati OH. [online] http://www.serviceenv.com/Web2005/Docs/Huls%20Webpage%205-20-03.pdf [Accessed: 20 August 2004]

Jepsen, R. McNeil, J. & Lick, W., 2000, Effects of gas generation on the density and erosion of sediments from the Grand River, *J. Great Lakes Res.*, 26 (2), pp. 209 – 219.

Jinno Laboratory, School of Materials Science, Toyohashi University of Technology, 2001, *Polycyclic Aromatic Hydrocarbons (PAHs) Data Base* [online] http://chrom.tutms.tut.ac.jp/JINNO/DATABASE/00database.html [Accessed: 21 April 2005]

Johnson, B.D., Boudreau, B.P., Gardiner, B.S. and Maass, R., 2002, Mechanical response of sediments to bubble growth. *Marine Geology*, 187 (3-4), pp. 347 – 363.

Jørgansen, B.B. & Revsbech, N.P., 1985, Diffusive Boundary Layers of Sediments and Detritus, *Limnol. Oceanogeographer*, 30, pp. 111-122. In: B.P. & Jørgensen, B.B., eds. *The Benthic Boundary Layer – Transport Processes and Biochemistry*, New York, Oxford University Press, 144-170.

Karickhoff, S.W. & Morris, K.R., 1985, Impact of tubificid oligochaetes on pollutant transport in bottom sediments, *Env. Sci. Technol.*, 19 (1), pp. 51 – 56.

Kessel, T. van., 1989, Crack formation in sediments: experimental research. WL report no. Z2314dm21. In: Kesteren, W.G.M. van; Kessel, T. van, 2002, Gas bubble nucleation and growth in cohesive sediments, Elsevier, *Proceedings in Marine Science, 5, Fine sediment dynamics in the marine environment*, Eds.: Winterwerp, J.C.; Kranenburg, C., pp. 329-341

Kesteren, W.G.M. van, 2000, *Gas enhanced transportation from contaminated sediment at Stryker Bay, Duluth* [online], WL/Delft Hydraulics, http://www.wldelft.nl/proj/pdf/4uk00225.scherm.pdf [Accessed 21 July 2004]

Kesteren, W.G.M. van., Kessel, T. van. & Costello, M.J., 2002, Capping of Contaminated Soft Cohesive Sediment Bed in Stryker Bay, Minnesota, In: Winterwerp, J.C. & Kranenburg, C., eds. *Fine Sediment Marine Dynamics in the Marine Environment*, USA, Elsevier

Kesteren, W.G.M. van; Kessel, T. van, 2002, Gas bubble nucleation and growth in cohesive sediments, Elsevier, *Proceedings in Marine Science, 5, Fine sediment dynamics in the marine environme*nt, Eds.: Winterwerp, J.C.; Kranenburg, C., pp. 329-341

Kesteren, W.G.M. van; Kessel, T. van; Costello, M.J., 2003, Site remediation at Stryker Bay, Minnesota, *Proc. Intercoh 2003*, [online] http://www.wldelft.nl/rnd/publ/docs/Ke_Ke_2003a.pdf [Accessed 21 July 2004]

Khodadoust, A.P., Lei, L., Antia, J.E., Bagchi, R., Suidan, M.T. & Tabak, H.H., 2005, Adsorption of Polycyclic Aromatic Hydrocarbons in Aged Harbor Sediments . *J. of Environ. Eng.,* 131 (3), pp. 403 – 409.

Lerman, A., 1979, *Geotechnical Processes Water and Sediment Environments*, John Wiley & Sons, USA.

Lim, P.C., Barbour, S.L. & Fredlund, D.G., 1998, The Influence of Degree of Saturation on the Coefficient of Aqueous Diffusion, *Canadian Geotechnical Journal*, 35 (5), pp. 811 - 827.

Loehr, R.C., Webster, M.T. & Smith, J.R., 2000, Fate of treated and weathered hydrocarbons in soil – long term changes, *Pract. Periodical of Haz., Toxic and Radioactive Waste Mgmt.*, 4 (2), pp. 53 – 59.

Marcell, S. &Eisele, M., 1997, Accumulation of Inorganic and Organic Pollutants by Biofilms in the Aquatic Environment, *Water, Air, & Soil Pollution*, 99 (1-4), pp. 651 – 659.

Millington, R.J. & Quirk, J.P., 1961, Permeability of porous solids, *Trans. Faraday Soc.*, 57, pp. 1200 – 1208. In: Wang, X.Q., Thibodeaux, L.J. & Reible, D.D., 1991, Efficiency of capping contaminated bed sediments in-situ. 1. Laboratory-scale experiments on diffusion-adsorption in the capping layer, *Environ. Sci. Technol.*, 25, pp. 1578 -1584.

Mohan, R.K., Brown, M.P. & Barnes, C.R., 2000, Design criteria and theoretical basis for capping contaminated marine sediments, *Applied Ocean Research*, 22 (2), pp. 85 – 93.

NGI, 2004, *Leaching of Organic Contaminants from Construction Debris – Development of a Diffusion Test Procedure.* Norway: Norwegian Geotechnical Institute Report, (20021082-2).

Nguyen, Q., & Borger, D., 1992, Measuring the flow properties of yield stress fluids, *Ann. Rev. Fluid Mech.* 24, pp 47 – 89.

Quantin, C., Joner, E.J., Portal, J.M., & Berthelin, J., 2005, PAH dissipation in a contaminated river sediment under oxic and anoxic conditions, *Environmental Pollution,* 134 (2). pp – 315 – 322.

Raja, S., Yaccone, F.S., Ravikrishna, R. & Valsaeaj, K.T., 2002, Thermodynamic parameters for the adsorption of aromatic hydrocarbon vapours at the gas-water interface, *J. Chem. Eng. Data*, 47 (5), pp. 1213 – 1219.

Reible, D., 1996, *In Situ Sediment Remediation through Capping: Status and Research Needs,* University of Texas [online] http://www.hsrc-ssw.org/pdf/cap-bkgd.pdf [Accessed 28 March 2005].

Rice, D.D. & Claypool, G.E., 1981, Generation, accumulation, and resource potential of biogenic gas, *AAPG, Bulletin*, 65 (1), pp. 5 – 25.

Rogers, S.W., Ong, S.K., Kjartanson, B.H., Golchin, J. & Stenback, G.A., 2002, Natural attenuation of Polycyclic Aromatic Hydrocarbons – Contaminated Sites: Review, *Pract. Periodical of Haz., Toxic, and Radioactive Waste Mgmt.,* 6 (3), pp. 141-155.

Sander, R., 1999, *Compilation of Henry's Law Constants for Inorganic and Organic Species of Potential Importance in Environmental Chemistry*, Max-Planck Institute of Chemistry, [online] http://www.mpch-mainz.mpg.de/~sander/res/henry.html [Accessed 22 April 2005].

Scardina, P. & Edwards, M., 2001, Prediction and measurement of bubble formation in water treatment, *Journal of Environmental Engineering*, 127 (11), pp. 968 – 973.

Schotmeyer, G.J., 1990, Stability of growing gas bubbles in sediments, GeoDelft report no. 373350/18. In: Kesteren, W.G.M. van; Kessel, T. van, 2002, Gas bubble nucleation and growth in cohesive sediments, Elsevier, *Proceedings in Marine Science, 5, Fine sediment dynamics in the marine environment*, Eds.: Winterwerp, J.C.; Kranenburg, C., pp. 329-341

Schwarzenbach, R.P., Gschwend, P.M. & Imboden, D.M., *Environmental Organic Chemistry* 2nd ed, John Wiley & Sons Inc, USA.

SFT, 1998, Contaminated Marine Sediments (in Norwegian Fjords), *SFT report 98:11*, Norwegian Pollution Control Authority, Oslo.

Sills, G.C. & Gonazlez, R., 2001, Consolidation of naturally gassy soil, *Géotechnique*, 57 (7), pp. 629 – 639.

Sivertsen, A., Eggen, A., Breedveld, G.D., Bjordal, R., & Hauge, A., 2003, Building of the New National Opera House on Contaminated Sediments in Oslo Harbour, Norway, In: M. Pellei & Porta, A. Eds., Remediation of Contaminated Sediments—2003. *Proceedings of the Second International Conference on Remediation of Contaminated Sediments*, 30 Sep – 3 Oct 2003, Venice, Italy: Battelle Press, Columbus.

Smith, J.S. & Valsaraj, K.T., 1997, Bubble column reactors for wastewater treatment. 3. Pilot-scale solvent sublation of pyrene and pentachlorophenol from simulated wastewater, *Ind. Eng. Chem. Res.*, 36, pp. 903 – 914.

Tabak H.H., Govind, R. & Ramani, M., 2001, In Situ Biorestoration of Contaminated Sediments Using Membranes and Gel Beads. In: Leeson, A., Foote, E., Banks, K. & Magar, V. S. (Eds), 2001, *Phytoremediation, Wetlands, and Sediments*, 2001, Battelle Press, USA.

Talbert, B., Thibodeaux, L.J. & Valsaraj, K.T., 2001, Effectiveness of very thin soil layers in chemical release from bed sediment, *Environmental Progress*, 20 (2), pp.103 – 107.

Thibodeaux, L.J. & Bierman, V.J., 2003, The Bioturbation Driven Chemical Release Process, *Environ. Sci. Technol.,* 37 (13), pp 252A-258A.

Thoms et al. (1995), In: Reible, D., 1996, *In Situ Sediment Remediation through Capping: Status and Research Need*s, University of Texas [online] http://www.hsrc-ssw.org/pdf/cap-bkgd.pdf [Accessed 28 March 2005].

Tohma, G.J., Reible, D.D., Valsaraj, K.T. & Thibodeaux, L.J., 1993, Efficiency of Capping Contaminated Sediments in Situ. 2. Mathematics of Diffusion-Adsorption in the capping layer, *Environ. Sci. Technol.,* 27 (12), pp. 2412 – 2419.

US EPA, 2003, *On-line Tools for Site Assessment Calculation* [online] http://www.epa.gov/athens/learn2model/part-two/onsite/index.html [Accessed 22 April 2005]

Vogel, T.M., Oremland, R.S. & Kvenvolden, K.A., 1982, Low-temperature formation of hydrocarbon gases in San Francisco Bay sediment (California, U.S.A.), *Chem. Geology*, 37 (3-4), pp. 289 – 298.

Wang, X.Q., Thibodeaux, L.J. & Reible, D.D., 1991, Efficiency of capping contaminated bed sediments in-situ. 1. Laboratory-scale experiments on diffusion-adsorption in the capping layer, *Environ. Sci. Technol.,* 25 (9), pp. 1578 -1584.

Wright, L. D., Friedrichs, C. T. & Hepworth, D. A., 1997, Effects of Benthic Biology on Bottom Boundary Layer Processes, Dry Tortugas Bank, Florida Keys, *Geo-Marine Letters*, 17 (4), pp. 291–298

Document Statistics

Characters (not spaces)	96 114
Word Count	18 920
Lines	1 719
Paragraphs	567
Sections	23
Chapters	6
Pages	76
Figures	36
Tables	6
References cited	74

LIST OF APPENDICES

Appendix A Details from gas production trials (Section 3.1).

Pan Weight (g)	Wet Weight (g)	Dry Weight (g)	% Water
2.26	62.89	27.51	56.26%

Molecular Weight of Starch $C_6H_{10}O_5$	162.082	g/mol
Molecular Weight of Carbon	12	g/mol
% Carbon i $C_6H_{10}O_5$ (Weight)	44.4 %	

Weights of sediment and starch

Test Number	Glass Weight (g)	Sediment Weight (g)	% Carbon	Dry Weight (g)	Weight $C_6H_{10}O_5$ (g)	Weight Carbon (g)
3-1	537.26	266.14	2.00%	116.42	5.24	2.33
3-2	536.80	142.30	2.00%	62.25	2.80	1.24
3-3	537.27	187.23	2.00%	81.90	3.69	1.64

Solubilities

Compound	Molecular Weight		Solubility (mole fraction solubility of gas in solution)		Where	$\ln X = A + B/T^* + C \ln T^*$
CH_4	16.04246	g/mol	2.81E-05	X		
CO_2	44.0095	g/mol	7.07E-04	X		
O_2	31.9988	g/mol	2.50E-05	X		
N_2	28.0134	g/mol	1.27E-05	X		
H_2	2.0158	g/mol	1.46E-05	X		

Ideal Gas Law Parameters

Test Number	R (J/mol/K)	T (K)	Volume av Gass i Flaske (m^3)	1 atm (Pa)
3-1			9.20E-04	
3-2	8.31	285	9.20E-04	101325
3-3			9.20E-04	

Three gas test jars with gas bags inserted into the ruber membranes

Appendix B TOC and Rock Evaluation Data for Sediment and Cap

(by Applied Petroleum Technology AS)

Sample	S1 (mg/g)	S2 (mg/g)	S3 (mg/g)	Tmax (°C)	PP 8mg/g)	PI (wt ratio)	HI (mg HC/ g TOC)	OI (mg CO2/ g TOC)	TOC (%)	Min C (%)	Oxidation Cycle	TOC (%)	Min C (%)
Cap	0	0,02	0,49	540	0,02	0,05	190	4900	0,01	0,1		0,11	0
Sediment	0,51	13,60	6,80	417	14,11	0,04	313	156	4,35	0,5		4,09	0,3

Appendix C Bench Test 1 – Experimental details

Test	Weight of glass (mg)	Weight of Sediment (mg)	Sediment thickness (mm)	Weight of water (mg)	Water thickness (mm)	Volume of n-Hexane (ml)	n-Hexane Thickness (mm)
1-1	208,11	119,45	28	39,44	11	49,6	12,9
1-2	208,83	109,37	27	39,43	10	49,9	13,0
1-3	208,5	118,38	27	39,21	11	49,8	12,9
1-4	208,69	126,71	30	79,18	20	49,8	12,9
1-5	210,11	118,52	29	78,19	20	49,7	12,9
1-6	209,97	128,33	30	78,05	20	49,5	12,9
1-7	208,51	138,24	32	118,18	31	49,6	12,9
1-8	208,2	128,48	30	119,71	31	49,4	12,8
1-9	209,17	139,25	33	119,02	40	49,6	12,9
1-10	208,78	142,17	33	158,9	41	49,5	12,9
1-11	207,91	141,11	33	158,67	41	49,5	12,8
1-12	208,87	153,29	35	158,68	41	49,4	12,8

Drying Tests

	Pan	Wet	Dry	Water Content (%)
Drying 1	7,02	139,65	70,64	54,4 %
Drying 2	2,26	62,89	29,77	56,3 %

	Bulk Density kg/m^3	Porosity (%)
Capping Properties	1542,77	36,11 %

Appendix D Bench Test 2 – Experimental details

Test	Weight of glass (mg)	Weight of Sediment (mg)	Sediment thickness (mm)	Weight of Cap (mg)	Cap thickness (mm)	Weight of water (mg)	Water thickness (mm)	Volume of n-Hexane (mL)	n-Hexane Thickness (mm)	Volume Air (mL)
2-1	208,6	106,6	28,0			79,7	19,0	49,4	12,8	364,5
2-2	210,1	108,1	27,0			79,4	20,0	49,3	12,8	364,6
2-3	208,4	120,5	30,0			79,4	20,0	49,6	12,9	364,3
2-4	209,1	109,3	26,0			79,0	21,0	49,7	12,9	364,2
2-5	207,8	101,4	26,0			79,9	20,0	49,5	12,8	364,4
2-6	208,5	110,2	27,0			78,6	21,0	49,6	12,9	364,3
2-7	208,3	119,5	30,0			79,4	20,0	49,8	12,9	364,1
2-8	208,8	110,5	28,0			79,4	20,0	49,6	12,9	364,2
2-9	209,3	122,7	30,0			79,2	20,0	49,1	12,8	364,8
2-10	209,7	118,1	28,0			79,7	20,0	49,3	12,8	364,5
2-11	207,6	124,5	30,0			79,0	20,0	49,5	12,9	364,4
2-12	209,4	133,0	30,0			70,7	20,0	49,5	12,9	364,3
2-13	208,1	122,7	30,0			79,3	20,0	49,5	12,9	364,3
2-14	209,1	118,6	28,0			78,7	22,0	49,6	12,9	364,2
2-15	209,0	112,2	27,0			78,5	20,0	49,2	12,8	364,6
2-16	208,6	130,9	30,0			78,3	21,0	49,3	12,8	364,5
2-17	208,3	124,8	30,0			78,5	20,0	48,8	12,7	365,1
2-18	208,9	122,6	29,0			78,7	21,0	49,1	12,8	364,8
2-19	210,6	118,4	25,0	61,2	11,0	51,0	12,0	50,0	13,0	363,9
2-20	209,0	117,0	25,0	61,2	11,0	51,0	11,0	49,8	12,9	364,0
2-21	210,2	112,8	26,0	61,2	10,0	50,1	12,0	49,9	13,0	364,0
2-22	209,5	117,6	25,0	61,2	12,0	51,0	11,0	49,7	12,9	364,1
2-23	208,6	121,0	26,0	61,2	11,0	50,8	12,0	49,8	12,9	364,1
2-24	209,1	96,3	25,0	61,2	9,0	50,0	10,0	49,8	12,9	364,0
2-25	208,8	110,2	25,0	61,2	10,0	51,3	13,0	49,7	12,9	364,1
2-26	208,5	109,1	25,0	61,2	10,0	50,6	11,0	49,5	12,9	364,3
2-27	209,0	106,7	25,0	61,2	10,0	51,0	11,0	49,2	12,8	364,7
2-28	208,0	109,0	25,0	61,2	11,0	50,3	11,0	49,7	12,9	364,2
2-29	208,8	116,3	25,0	61,2	10,0	51,1	13,0	49,3	12,8	364,6
2-30	209,0	108,3	24,0	61,2	10,0	50,2	12,0	49,8	12,9	364,1
2-31	290,2	38,7	25,0	61,2	12,0	51,2	11,0	49,4	12,8	364,4
2-32	208,9	102,1	25,0	61,2	11,0	50,8	10,0	49,6	12,9	364,2
2-33	208,6	94,3	21,0	61,2	12,0	50,8	11,0	49,1	12,8	364,7
2-34	209,8	101,6	24,0	61,2	10,0	50,2	11,0	49,4	12,8	364,5
2-35	208,1	108,6	25,0	61,2	10,0	52,7	11,0	49,2	12,8	364,6
2-36	208,5	108,4	26,0	61,2	11,0	50,3	10,0	49,7	12,9	364,1

Appendix E Bench Test 3 – Experimental details

Test	Weight of glass (mg)	Weight of Sediment (mg)	Sediment thickness (mm)	Weight of Cap (mg)	Cap thickness (mm)	Weight of water (mg)	Water thickness (mm)	Volume of n-Hexane (ml)	n-Hexane Thickness (mm)	Volume Air (mm)
CC-1	211,2	120,2	28,0	55,6	8,0	49,4	11,0	50,0	13,0	363,8
CC-2	210,3	129,6	30,0	55,6	9,0	49,4	12,0	50,0	13,0	363,8
CC-3	211,0	126,3	29,0	55,6	10,0	49,4	10,0	50,0	13,0	363,8
CC-4	210,1	110,2	28,0	55,6	8,0	49,4	6,0	50,0	18,0	344,5
CC-5	211,0	119,7	29,0	55,6	9,0	49,4	10,0	50,0	14,0	359,9
CC-6	210,4	117,2	29,0	55,6	8,0	49,4	10,0	50,0	14,0	359,9
CC-7	211,0	120,9	28,0	55,6	9,0	49,4	11,0	50,0	14,0	359,9
CC-8	209,0	113,0	27,0	55,6	10,0	49,4	11,0	50,0	13,0	363,8
CC-9	211,0	134,2	31,0	55,6	9,0	49,4	11,0	50,0	13,0	363,8
CC-10	210,6	122,4	29,0	55,6	10,0	49,4	9,0	50,0	14,0	359,9
CC-11	209,6	126,1	29,0	55,6	9,0	49,4	11,0	50,0	14,0	359,9
CC-12	210,5	113,7	28,0	55,6	10,0	49,4	10,0	50,0	13,0	363,8
UC-1	210,8	127,8	31,0			35,0	9,0	50,0	14,0	359,9
UC-2	210,1	120,7	30,0			37,0	9,0	50,0	13,0	363,8
UC-3	210,0	121,8	30,0			37,1	10,0	50,0	13,0	363,8
UC-4	210,3	117,5	29,0			37,0	9,0	50,0	15,0	356,1
UC-5	211,0	119,1	30,0			37,0	9,0	50,0	14,0	359,9
UC-6	210,5	119,6	29,0			37,0	10,0	50,0	13,0	363,8
UC-7	211,0	116,0	29,0			37,0	9,0	50,0	14,0	359,9
UC-8	209,4	118,5	29,0			37,0	9,0	50,0	14,0	359,9
UC-9	211,0	115,9	29,0			37,0	9,0	50,0	14,0	359,9
UC-10	210,3	127,6	33,0			37,0	8,0	50,0	13,0	363,8
UC-11	211,7	124,7	30,0			37,0	10,0	50,0	14,0	359,9
UC-12	210,4	134,8	33,0			37,0	9,0	50,0	13,0	363,8
C-1	210,1	130,9	30,0	55,6	10,0	49,4	10,0	50,0	14,0	359,9
C-2	210,3	117,5	28,0	55,6	9,0	49,3	10,0	50,0	14,0	359,9
C-3	210,6	129,2	30,0	55,6	9,0	39,4	10,0	50,0	14,0	359,9
C-4	209,8	129,2	29,0	55,6	10,0	40,4	9,0	50,0	14,0	359,9
C-5	209,5	130,4	30,0	55,6	10,0	48,6	10,0	50,0	13,0	363,8
C-6	209,2	113,5	27,0	55,6	9,0	48,7	10,0	50,0	15,0	356,1
C-7	209,4	114,8	27,0	55,6	10,0	49,2	10,0	50,0	14,0	359,9
C-8	209,7	113,9	27,0	55,6	10,0	48,8	9,0	50,0	14,0	359,9
C-9	210,2	122,9	29,0	55,6	9,0	49,3	9,0	50,0	13,0	363,8
C-10	210,0	117,8	28,0	55,6	10,0	48,6	9,0	50,0	14,0	359,9
C-11	210,2	125,8	29,0	55,6	10,0	49,4	9,0	50,0	14,0	359,9
C-12	209,9	129,6	30,0	55,6	10,0	48,9	10,0	50,0	14,0	359,9
U-1	209,7	111,0	28,0			37,0	9,0	50,0	13,0	363,8
U-2	210,0	115,9	30,0			37,0	8,0	50,0	14,0	359,9
U-3	208,7	116,6	29,0			37,0	9,0	50,0	14,0	359,9
U-4	209,7	122,3	30,0			37,0	9,0	50,0	13,0	363,8
U-5	209,9	124,6	30,0			37,0	10,0	50,0	13,0	363,8
U-6	208,1	118,7	30,0			37,0	9,0	50,0	13,0	363,8
U-7	208,3	116,3	29,0			37,0	9,0	50,0	12,0	367,6
U-8	208,8	111,3	28,0			37,0	9,0	50,0	14,0	359,9
U-9	210,0	109,3	28,0			37,0	9,0	50,0	13,0	363,8
U-10	209,7	111,6	29,0			37,0	8,0	50,0	14,0	359,9
U-11	209,2	112,3	28,0			37,0	10,0	50,0	13,0	363,8
U-12	209,9	109,9	26,0			37,0	10,0	50,0	14,0	359,9

Appendix E Bench Test 3 (cont') – Experimental details

Test	Weight of glass (mg)	Weight of Sediment (mg)	Sediment thickness (mm)	Weight of Cap (mg)	Cap thickness (mm)	Weight of water (mg)	Water thickness (mm)	Volume of n-Hexane (mL)	n-Hexane Thickness (mm)	Volume Air (mL)
BC-1	209,8			55,6	10,0	48,7	10,0	50,0	14,0	359,9
BC-2	209,5			55,6	10,0	48,9	9,0	50,0	13,0	363,8
BC-3	208,7			55,6	11,0	48,8	9,0	50,0	14,0	359,9
V-1	210,0					37,0	10,0	50,0	14,0	359,9
V-2	209,8					37,0	9,0	50,0	13,0	363,8
V-3	208,5					37,0	9,0	50,0	14,0	359,9

Appendix F Bench Test 1 – Results

	Concentration Ratio (R_{OTP})	Naphthalene (µg/ml)	Acenaphthylene (µg/ml)	Acenaphthene (µg/ml)	Fluorene (µg/ml)	Phenanthrene (µg/ml)	Anthracene (µg/ml)	Fluoranthene (µg/ml)	Pyrene (µg/ml)	Benzo (a) anthracene (µg/ml)	Chrysene (µg/ml)	PAH_{10} (µg/ml)
1-1	50	3,0E-02	4,0E-03	4,4E-03	1,3E-02	1,4E-02	5,8E-03	8,6E-03	1,9E-02	6,0E-04	2,2E-03	**1,0E-01**
1-2	49	1,1E-02	8,5E-03	6,1E-03	1,3E-02	5,3E-03	2,6E-03	5,1E-03	1,7E-02	2,6E-03	3,9E-03	**7,6E-02**
1-3	34	1,2E-02	3,6E-03	3,3E-03	7,7E-03	2,4E-03	3,3E-03	3,6E-03	1,7E-02	5,9E-04	3,0E-03	**5,5E-02**
1-4	45	2,9E-02	3,1E-03	4,3E-03	7,8E-03	1,0E-02	4,7E-03	1,1E-02	2,9E-02	4,0E-03	1,8E-03	**1,0E-01**
1-5	46	1,1E-02	5,4E-03	4,8E-03	4,8E-03	3,5E-03	4,1E-03	7,1E-03	2,2E-02	3,9E-03	3,2E-03	**7,0E-02**
1-6	33	2,9E-02	7,2E-03	6,9E-03	1,1E-02	1,5E-02	7,9E-03	1,4E-02	3,0E-02	6,0E-04	2,4E-03	**1,3E-01**
1-7	32	2,6E-02	4,1E-03	9,4E-03	7,2E-03	1,2E-02	5,7E-03	7,2E-03	2,9E-02	9,4E-04	3,1E-03	**1,0E-01**
1-8	48	1,7E-02	2,9E-03	1,1E-02	8,8E-03	9,5E-03	5,5E-03	1,0E-02	2,6E-02	2,1E-04	3,8E-03	**9,4E-02**
1-9	44	2,4E-02	3,9E-03	5,0E-03	8,7E-03	8,7E-03	5,5E-03	9,4E-03	2,2E-02	4,6E-04	2,7E-03	**9,1E-02**
1-10	38	2,3E-02	5,0E-03	8,9E-03	1,4E-02	2,0E-02	1,2E-02	1,9E-02	3,5E-02	1,0E-03	4,2E-03	**1,4E-01**
1-11	44	1,0E-02	3,2E-03	3,2E-03	2,3E-03	3,2E-03	9,0E-04	5,7E-03	1,7E-02	4,5E-04	4,5E-04	**4,6E-02**
1-12	47	3,4E-02	1,7E-03	4,5E-03	4,0E-03	3,8E-02	9,0E-03	2,5E-02	3,0E-02	2,6E-01	5,2E-02	**4,6E-01**

Appendix G Theory – Linear Model with confidence intervals

(Berthouex & Brown, 1994)

The model used in the calculation of the flux of PAH_{10} from the sediments was a linear model with the form;

$$y = \beta_0 + \beta_1 x + e \tag{G.1}$$

where we assume that the errors, e, are normally distributed, with mean zero and constant variance. The parameters were estimated using the *method of least squares*. As the models were calculated with $\beta_0 = 0$ we can ignore this term and we get;

$$y = \beta_1 x \tag{G.2}$$

where the true value of β is the parameter value that minimises S in the least squares estimate;

$$S(\beta) = \sum (y_i - \beta x_i)^2 \tag{G.3}$$

or the algebraic solution for (G.3) gives;

$$b = \frac{\sum x_i y_i}{\sum x_i^2} \tag{G.4}$$

we can now define a confidence intervals for the model namely the prediction of the mean response, η_0, at a particular value x_0 is;

$$\eta_0 = (b_1 x_0) \pm t_{\upsilon, \alpha/2} \left[\left(\frac{1}{n} + \frac{(x_0 - \bar{x})^2}{\sum (x_i - \bar{x})^2} \right) s^2 \right]^{1/2} \tag{G.5}$$

where s^2 is the residual mean square calculated from;

$$s^2 = \frac{S_R}{n - p} \tag{G.6}$$

where S_R is equal to the residual sum of squares, p the number of parameters calculated, n the number of observations, $t_{\upsilon, \alpha/2}$ is the value of the Student's t distribution for $\upsilon = n - p$ and $\alpha = $ confidence limits (95% or $\alpha = 0.05$ for this study).

The confidence interval for the prediction of a future single observation, $\hat{y}_f = b_1 x_f$ is

$$\hat{y}_f = (b_1 x_f) \pm t_{\upsilon, \alpha/2} \left[s^2 + \left(\frac{1}{n} + \frac{(x_f - \bar{x})^2}{\sum (x_i - \bar{x})^2} \right) s^2 \right]^{1/2} \tag{G.7}$$

Appendix H Bench Test 2 - Results

	Concentration Ratio (R_{OTP})	Naphthalene (μg/ml)	Acenaphthylene (μg/ml)	Acenaphthene (μg/ml)	Fluorene (μg/ml)	Phenanthrene (μg/ml)	Anthracene (μg/ml)	Fluoranthene (μg/ml)	Pyrene (μg/ml)	Benzo (a) anthracene (μg/ml)	Chrysene (μg/ml)	PAH_{10} (μg/ml)
2-1	23	2,2E-04	2,2E-04	2,2E-04	8,7E-04	2,2E-04	2,2E-04	8,7E-04	4,3E-04	2,2E-04	2,2E-04	**3,7E-03**
2-2	32	1,6E-04	1,6E-04	1,6E-04	6,3E-04	1,6E-04	1,6E-04	6,3E-04	6,3E-04	1,6E-04	1,6E-04	**3,0E-03**
2-3	26	1,9E-04	1,9E-04	1,9E-04	3,8E-04	1,9E-04	1,9E-04	3,8E-04	7,7E-04	1,9E-04	1,9E-04	**2,9E-03**
2-4	31	5,1E-03	1,6E-03	1,6E-03	3,2E-04	9,6E-04	9,6E-04	2,2E-03	5,4E-03	1,6E-04	1,6E-04	**1,8E-02**
2-5	46	6,9E-03	1,1E-03	1,7E-03	6,5E-04	1,1E-03	1,7E-03	1,9E-03	5,2E-03	1,1E-04	1,1E-04	**2,1E-02**
2-6	24	8,8E-03	1,3E-03	1,3E-03	1,7E-03	2,5E-03	1,7E-03	3,8E-03	7,5E-03	2,1E-04	2,1E-04	**2,9E-02**
2-7*												
2-8	26	1,3E-02	5,0E-03	2,7E-03	7,3E-03	9,2E-03	4,2E-03	6,5E-03	1,3E-02	3,8E-03	6,1E-03	**7,2E-02**
2-9	37	1,7E-02	3,7E-03	1,6E-03	4,8E-03	9,9E-03	4,5E-03	1,2E-02	1,4E-02	3,2E-03	3,5E-03	**7,5E-02**
2-10	29	1,5E-02	5,9E-03	3,1E-03	1,3E-02	9,7E-03	4,2E-03	2,0E-02	2,1E-02	4,5E-03	3,1E-03	**1,0E-01**
2-11	25	1,4E-02	6,8E-03	4,4E-03	1,6E-02	1,5E-02	9,2E-03	5,6E-03	1,8E-02	3,2E-03	2,8E-03	**9,5E-02**
2-12	21	1,7E-02	8,7E-03	5,8E-03	2,0E-02	1,9E-02	1,5E-02	2,1E-02	2,1E-02	4,8E-03	2,9E-03	**1,4E-01**
2-13	39	3,0E-02	1,5E-02	9,7E-03	2,5E-02	2,4E-02	1,3E-02	1,2E-02	2,4E-02	1,3E-02	5,9E-03	**1,7E-01**
2-14	35	3,2E-02	1,1E-02	7,4E-03	2,6E-02	2,3E-02	1,4E-02	1,2E-02	2,3E-02	5,1E-03	3,1E-03	**1,6E-01**
2-15	40	4,2E-02	1,9E-02	1,1E-02	2,3E-02	3,0E-02	2,7E-02	2,2E-02	4,2E-02	7,8E-03	4,3E-03	**2,3E-01**
2-16	41	4,0E-02	1,4E-02	1,4E-02	3,3E-02	5,3E-02	3,4E-02	2,7E-02	5,3E-02	1,6E-02	2,1E-02	**3,1E-01**
2-17	40	4,6E-02	1,5E-02	9,9E-03	2,5E-02	2,5E-02	1,8E-02	1,6E-02	3,8E-02	9,7E-03	8,4E-03	**2,1E-01**
2-18	39	5,3E-02	6,1E-03	1,2E-02	2,9E-02	2,3E-02	1,4E-02	2,4E-02	3,3E-02	1,2E-02	8,2E-03	**2,2E-01**
2-19	35	1,4E-04	1,4E-04	1,4E-04	1,2E-03	1,4E-04	1,4E-04	8,6E-04	1,4E-04	1,4E-04	1,4E-04	**3,2E-03**
2-20	27	1,8E-04	1,8E-04	1,8E-04	1,5E-03	1,8E-04	1,8E-04	7,4E-04	1,8E-04	1,8E-04	1,8E-04	**3,7E-03**
2-21	34	1,5E-04	1,5E-04	1,5E-04	8,8E-04	1,5E-04	1,5E-04	5,9E-04	8,8E-04	1,5E-04	1,5E-04	**3,4E-03**
2-22	27	7,4E-04	1,9E-04	1,9E-04	3,0E-03	1,9E-04	1,9E-04	7,4E-04	1,0E-02	1,9E-04	1,9E-04	**1,6E-02**
2-23	32	1,6E-03	1,6E-04	1,6E-04	1,2E-03	1,6E-04	1,6E-04	6,2E-04	9,4E-04	1,6E-04	1,6E-04	**5,3E-03**
2-25	39	1,0E-03	1,3E-04	1,3E-04	1,8E-03	2,6E-04	1,3E-04	5,2E-04	7,8E-04	1,3E-04	1,3E-04	**5,0E-03**
2-24	28	7,0E-03	1,8E-03	1,1E-03	1,4E-03	3,5E-04	1,8E-04	2,5E-03	7,0E-04	1,8E-04	1,8E-04	**1,5E-02**
2-26#												
2-27	34	4,1E-03	1,5E-03	1,8E-03	2,3E-03	1,5E-04	1,5E-04	1,5E-03	2,9E-04	1,5E-04	1,5E-04	**1,2E-02**
2-28	27	3,7E-03	1,1E-03	2,2E-03	1,6E-02	2,6E-03	1,9E-03	1,5E-03	7,4E-04	1,9E-04	7,4E-04	**3,0E-02**
2-29	22	5,4E-03	2,3E-03	1,4E-03	1,8E-03	9,0E-04	2,3E-04	9,0E-04	9,0E-04	2,3E-04	1,8E-03	**1,6E-02**
2-30	26	4,2E-03	2,7E-03	2,7E-03	1,0E-02	1,1E-03	1,9E-04	7,6E-04	3,8E-04	1,9E-04	1,5E-03	**2,4E-02**
2-31	41	2,5E-02	8,8E-03	6,1E-03	7,9E-03	1,5E-03	1,5E-03	2,9E-03	1,2E-03	7,4E-04	1,2E-03	**5,7E-02**
2-32	49	2,2E-02	4,7E-03	1,0E-03	4,3E-03	2,0E-03	1,6E-03	1,6E-03	6,1E-04	1,0E-04	4,1E-04	**3,8E-02**
2-33	36	8,5E-03	3,0E-03	1,1E-03	6,3E-03	1,6E-03	1,1E-03	2,2E-03	2,7E-04	5,5E-04	5,5E-04	**2,5E-02**
2-34	36	1,1E-02	2,3E-03	2,5E-03	5,6E-03	3,1E-03	2,8E-04	8,4E-04	8,4E-04	5,6E-04	1,4E-04	**2,7E-02**
2-35	46	8,8E-03	1,3E-03	2,6E-03	7,1E-03	2,4E-03	1,1E-04	1,7E-03	2,2E-04	6,5E-04	1,1E-04	**2,5E-02**
2-36	45	6,9E-03	1,6E-03	2,9E-03	8,2E-03	2,9E-03	1,1E-04	4,4E-04	4,4E-04	4,4E-04	4,4E-04	**2,4E-02**

* no results obtained from analysis as all cyclohexane evaporated from test prior to sampling.
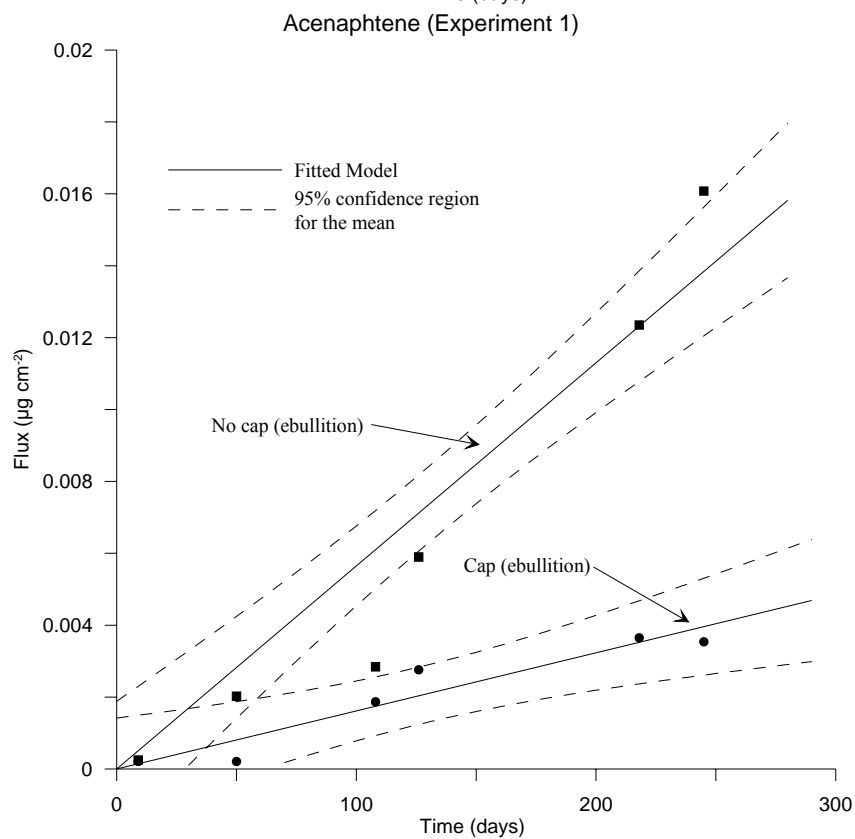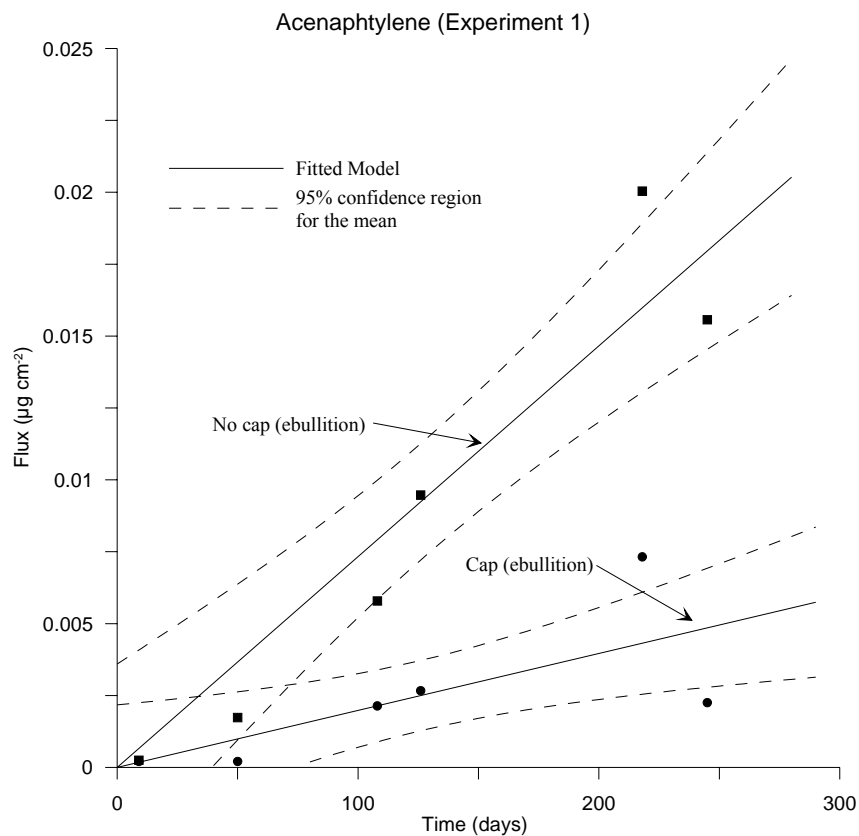# no results obtained due to too low concentration in cyclohexane.
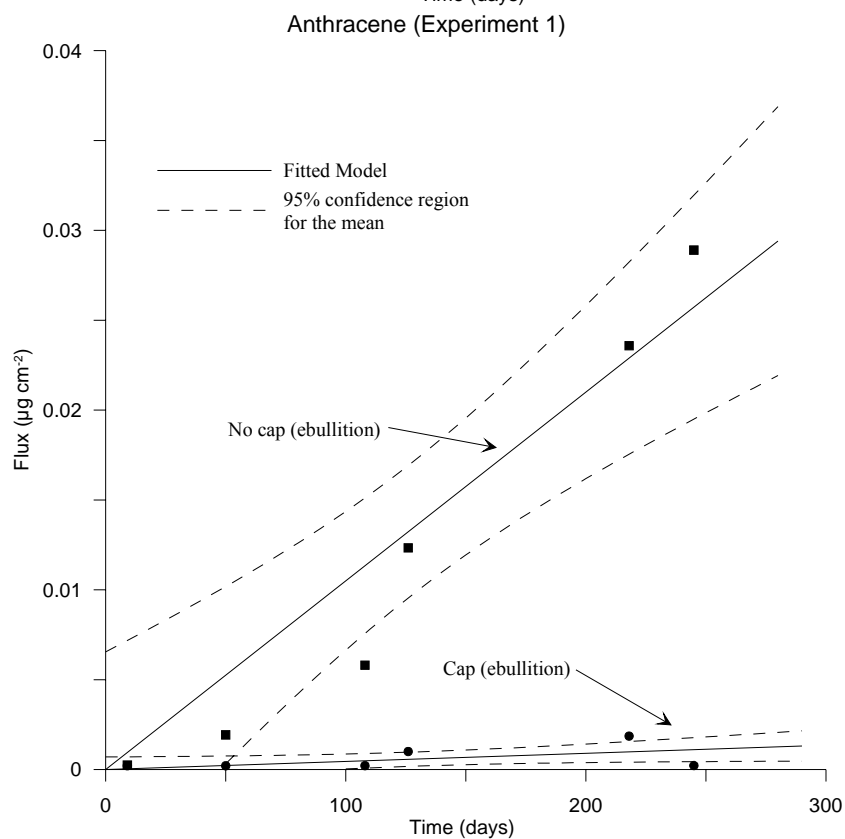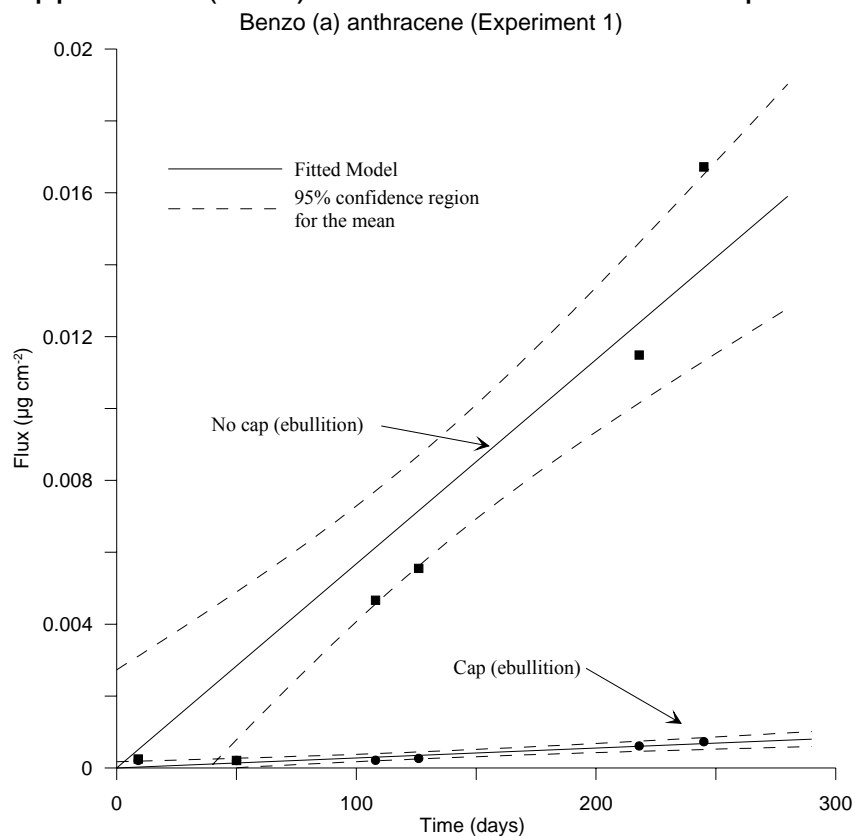
Appendix I Bench Test 3 – Results

	Concentration Ratio (R_{OTP})	Naphthalene (µg/ml)	Acenaphthylene (µg/ml)	Acenaphthene (µg/ml)	Fluorene (µg/ml)	Phenanthrene (µg/ml)	Anthracene (µg/ml)	Fluoranthene (µg/ml)	Pyrene (µg/ml)	Benzo (a) anthracene (µg/ml)	Chrysene (µg/ml)	PAH_{10} (µg/ml)
C1	24	2,1E-04	1,3E-03	2,1E-04	2,1E-04	2,1E-04	2,1E-04	1,3E-03	2,1E-04	2,1E-04	8,4E-04	**4,9E-03**
C2	24	2,1E-04	1,7E-03	2,1E-04	2,1E-04	2,1E-04	2,1E-04	2,1E-04	2,1E-04	2,1E-04	2,5E-03	**5,9E-03**
C3	29	1,7E-04	1,0E-03	1,7E-04	3,4E-04	1,7E-04	1,7E-04	1,7E-04	1,7E-04	1,7E-04	1,4E-03	**3,9E-03**
C4	51	9,8E-05	7,8E-04	9,8E-05	3,9E-04	9,8E-05	9,8E-05	5,9E-04	9,8E-05	5,9E-04	9,8E-05	**3,8E-03**
C5	42	1,2E-04	1,4E-03	2,4E-04	4,8E-04	1,2E-04	1,2E-04	7,1E-04	1,2E-04	1,2E-04	7,1E-04	**4,2E-03**
C6	46	1,1E-04	6,6E-04	1,1E-04	2,2E-04	1,1E-04	1,1E-04	8,8E-04	1,1E-04	4,4E-04	1,1E-04	**2,9E-03**
C7	48	1,7E-03	1,3E-03	2,1E-04	2,1E-04	1,0E-04	1,0E-04	6,3E-04	1,0E-04	8,4E-04	1,0E-03	**6,2E-03**
C8	46	2,0E-03	1,3E-03	2,2E-04	4,4E-04	1,1E-04	1,1E-04	8,7E-04	1,1E-04	2,2E-04	1,1E-04	**5,4E-03**
C9	46	1,1E-04	1,1E-03	6,5E-04	8,7E-04	4,4E-04	2,2E-04	4,4E-04	1,1E-04	2,2E-04	8,7E-04	**5,0E-03**
C10	36	1,4E-04	1,4E-04	1,4E-04	2,8E-04	1,4E-04	1,4E-04	1,4E-04	1,4E-04	2,8E-04	5,6E-04	**2,1E-03**
C11	51	9,9E-05	2,0E-04	5,9E-04	1,2E-03	1,2E-03	9,9E-05	9,9E-05	9,9E-05	2,0E-04	5,9E-04	**4,4E-03**
C12	50	9,9E-05	1,2E-03	9,9E-05	6,0E-04	9,9E-05	9,9E-05	9,9E-05	9,9E-05	9,9E-05	2,0E-04	**2,7E-03**
U1	26	1,9E-04	1,5E-03	1,9E-04	1,1E-03	1,5E-03	1,9E-04	1,9E-04	1,9E-04	1,9E-04	1,9E-04	**5,5E-03**
U2	21	2,4E-04	9,4E-04	2,4E-04	2,4E-04	2,4E-04	2,4E-04	9,4E-04	1,4E-03	2,4E-04	2,4E-03	**7,1E-03**
U3	28	1,8E-04	1,1E-03	1,8E-04	1,8E-04	1,8E-04	1,8E-04	7,2E-04	7,2E-04	1,8E-04	1,1E-03	**4,7E-03**
U4	58	8,6E-05	5,1E-04	1,0E-03	2,7E-03	1,4E-03	1,2E-03	8,6E-05	2,4E-03	5,1E-04	4,5E-03	**1,4E-02**
U5	58	1,7E-04	3,4E-04	1,0E-03	1,0E-03	5,0E-03	6,7E-03	1,7E-04	2,2E-03	1,7E-03	6,9E-03	**2,5E-02**
U6	50	8,0E-04	4,0E-04	6,0E-04	2,0E-04	6,0E-04	1,0E-04	8,0E-04	1,6E-03	1,0E-04	2,0E-03	**7,2E-03**
U7	36	1,7E-03	1,4E-03	2,0E-03	2,8E-04	1,7E-03	1,1E-03	1,1E-03	4,5E-03	1,4E-04	2,2E-03	**1,6E-02**
U8	51	1,6E-03	2,0E-03	1,6E-03	1,6E-03	2,9E-03	2,3E-03	7,8E-04	4,7E-03	9,8E-05	1,8E-03	**1,9E-02**
U9	39	1,3E-04	1,3E-03	1,3E-03	1,6E-03	5,2E-04	1,0E-03	1,3E-03	5,7E-03	1,3E-04	2,1E-03	**1,5E-02**
U10	43	1,2E-04	1,6E-03	2,5E-03	1,6E-03	5,3E-03	2,3E-03	4,6E-04	5,3E-03	2,3E-04	1,8E-03	**2,1E-02**
U11	34	1,5E-04	8,7E-04	4,1E-03	1,5E-03	2,9E-04	2,6E-03	2,0E-03	1,1E-02	1,2E-03	8,7E-04	**2,4E-02**
U12	36	1,4E-04	8,3E-04	5,0E-03	1,9E-03	5,0E-03	4,4E-03	3,0E-04	1,0E-02	5,5E-04	8,3E-04	**2,9E-02**
UC1	21	2,4E-04	1,9E-03	2,4E-04	2,4E-04	2,4E-04	2,4E-04	4,8E-04	1,5E-03	2,4E-04	4,4E-03	**9,7E-03**
UC2	21	2,4E-04	2,9E-03	2,4E-04	2,4E-04	2,4E-04	2,4E-04	9,6E-04	1,4E-03	2,4E-04	2,9E-03	**9,6E-03**
UC3	23	2,2E-04	1,3E-03	2,2E-04	2,2E-04	2,2E-04	2,2E-04	8,7E-04	1,3E-03	2,2E-04	8,7E-04	**5,6E-03**
UC4	24	1,3E-03	1,3E-03	4,2E-03	1,7E-03	2,1E-04	2,1E-04	1,3E-03	5,2E-03	2,1E-04	3,0E-03	**1,9E-02**
UC5	38	1,6E-03	1,0E-03	1,8E-03	2,1E-03	1,3E-04	5,2E-04	1,0E-03	4,2E-03	1,3E-04	5,2E-04	**1,3E-02**
UC6	49	6,1E-04	8,1E-04	1,2E-03	2,0E-03	1,0E-03	8,1E-04	1,0E-03	3,5E-03	1,0E-04	4,1E-04	**1,1E-02**
UC7	38	1,3E-03	2,7E-03	2,1E-03	3,4E-03	1,3E-03	5,3E-04	1,9E-03	8,0E-03	1,3E-04	2,4E-03	**2,4E-02**
UC8	41	2,4E-03	2,2E-03	9,6E-04	1,9E-03	2,9E-03	7,2E-04	4,6E-03	9,4E-03	7,2E-04	2,7E-03	**2,8E-02**
UC9	36	3,4E-03	1,7E-03	2,5E-03	3,4E-03	2,2E-03	8,4E-04	2,8E-03	9,2E-03	1,4E-04	1,4E-03	**2,8E-02**
UC10	51	2,1E-03	9,7E-04	2,3E-03	2,3E-03	2,3E-03	1,4E-03	2,5E-03	1,1E-02	1,2E-03	4,3E-03	**3,0E-02**
UC11	47	2,8E-03	1,7E-03	2,8E-03	5,4E-03	4,3E-03	1,1E-03	4,5E-03	1,1E-02	1,1E-03	3,0E-03	**3,8E-02**
UC12	33	3,6E-03	2,1E-03	2,4E-03	3,6E-03	8,4E-03	2,7E-03	1,3E-02	2,3E-02	3,6E-03	2,1E-03	**6,5E-02**
CC1	21	2,3E-04	9,3E-04	2,3E-04	2,3E-04	2,3E-04	2,3E-04	9,3E-04	2,3E-04	2,3E-04	2,3E-04	**3,7E-03**
CC2	25	2,0E-04	1,2E-03	2,0E-04	2,0E-04	2,0E-04	2,0E-04	2,0E-04	2,0E-04	2,0E-04	1,2E-03	**4,0E-03**
CC3	27	1,9E-04	1,5E-03	1,9E-04	1,9E-04	1,9E-04	1,9E-04	3,7E-04	1,9E-04	1,9E-04	1,5E-03	**4,6E-03**
CC4	2	1,3E-02	2,1E-03	2,1E-03	2,1E-03	2,1E-03	2,1E-03	8,5E-03	2,1E-03	2,1E-03	1,3E-02	**4,9E-02**
CC5	37	1,1E-03	1,4E-04	1,4E-04	5,5E-04	1,4E-03	1,4E-04	8,2E-04	1,4E-04	1,4E-04	1,4E-04	**4,6E-03**
CC6	42	1,4E-03	1,2E-04	2,4E-04	4,8E-04	1,2E-04	1,2E-04	9,6E-04	2,4E-04	1,2E-04	1,2E-04	**3,9E-03**
CC7	39	1,8E-03	1,3E-04	5,1E-04	5,1E-04	1,0E-03	1,3E-04	7,6E-04	1,3E-04	1,3E-04	1,8E-03	**6,9E-03**
CC8	39	1,3E-03	1,3E-04	1,3E-04	5,2E-04	1,3E-04	1,3E-04	7,8E-04	1,3E-04	1,3E-04	1,0E-03	**4,4E-03**
CC9	46	1,1E-03	1,1E-04	1,1E-04	6,5E-04	1,1E-04	1,1E-04	4,4E-04	1,1E-04	1,1E-04	2,4E-03	**5,2E-03**
CC10	49	1,4E-03	1,8E-03	1,0E-04	1,0E-03	1,0E-04	1,0E-04	1,0E-04	1,0E-04	8,1E-04	2,4E-03	**8,0E-03**
CC11	48	2,1E-03	2,1E-03	1,5E-03	1,0E-03	1,0E-04	2,1E-04	8,3E-04	2,1E-04	8,3E-04	1,2E-03	**1,0E-02**
CC12	47	1,1E-04	8,6E-04	1,1E-04	6,4E-04	1,1E-04	1,1E-04	1,1E-04	1,1E-04	2,1E-03	3,0E-03	**7,3E-03**

Appendix I Bench Test 3 – Results (cont')

	Concentration Ratio (R_{OTP})	Naphthalene (µg/ml)	Acenaphthylene (µg/ml)	Acenaphthene (µg/ml)	Fluorene (µg/ml)	Phenanthrene (µg/ml)	Anthracene (µg/ml)	Fluoranthene (µg/ml)	Pyrene (µg/ml)	Benzo (a) anthracene (µg/ml)	Chrysene (µg/ml)	PAH_{10} (µg/ml)
V 1	37	1,2E-06	1,2E-06	1,2E-06	4,8E-06	1,2E-06	1,2E-06	1,2E-06	1,2E-06	1,2E-06	7,2E-06	1,6E-03
V 2	46	9,8E-07	9,8E-07	9,8E-07	3,1E-05	9,8E-07	9,8E-07	2,0E-06	9,8E-07	2,0E-05	9,8E-07	6,0E-03
V 3	39	**1,2E-06**	**1,2E-06**	**1,2E-06**	**4,6E-06**	**1,2E-06**	**1,2E-06**	**6,9E-06**	**1,2E-06**	**1,2E-06**	**6,9E-06**	2,2E-03
BC 1	39	**1,1E-06**	**1,1E-06**	**1,1E-06**	**2,7E-05**	**1,1E-06**	**1,1E-06**	**1,1E-06**	**1,1E-06**	**1,1E-06**	**1,8E-05**	**1,1E-06**
BC 2	49	**9,1E-07**	**9,1E-07**	**9,1E-07**	**1,1E-05**	**1,8E-05**	**9,1E-07**	**9,1E-07**	**9,1E-07**	**9,1E-07**	**3,6E-06**	**9,1E-07**
BC 3	44	1,0E-06	1,0E-06	1,0E-06	1,0E-05	1,0E-06	1,0E-06	1,0E-06	1,0E-06	1,0E-06	1,0E-06	1,0E-06

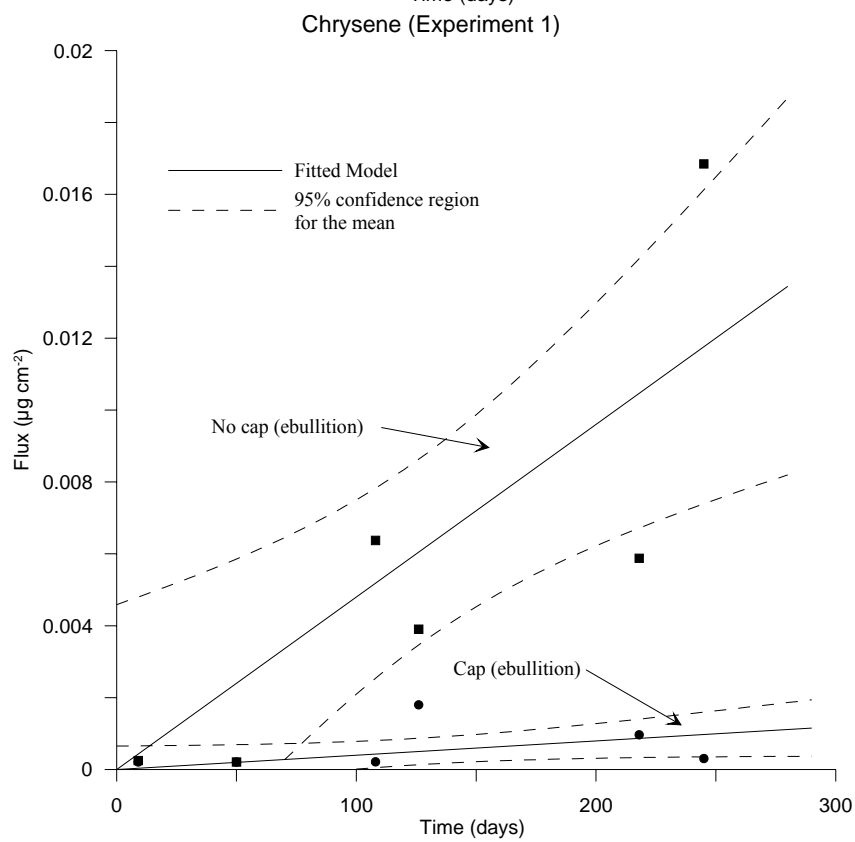## Appendix J Flux vs time for each compound from Test 2.

Acenaphtylene (Experiment 1)

Acenaphtene (Experiment 1)

Appendix J (cont') Flux vs time for each compound from Test 2.
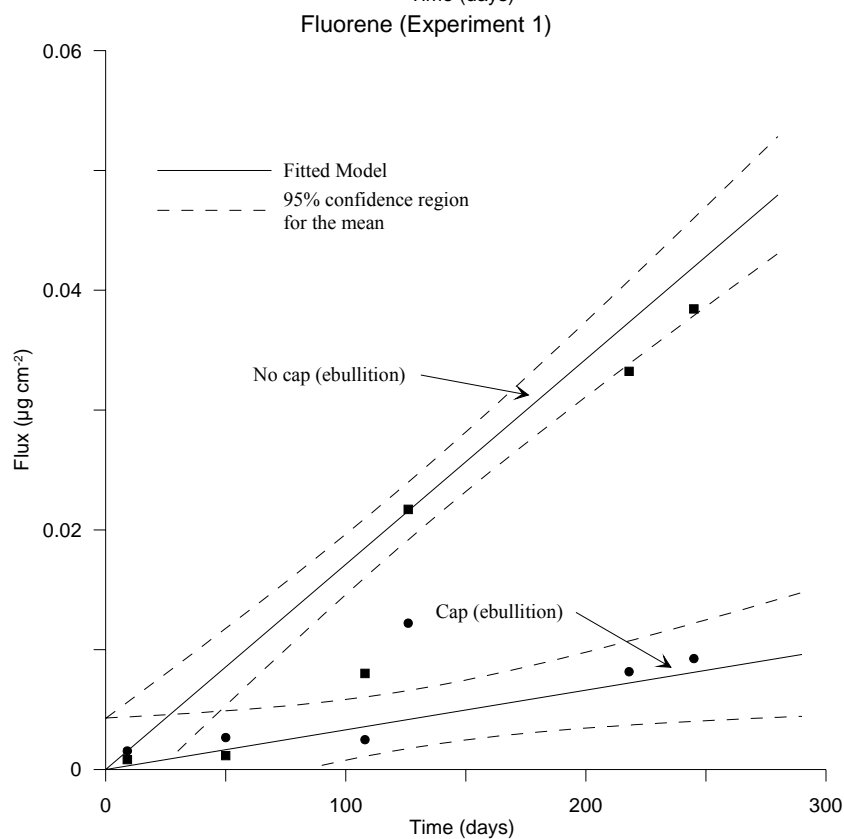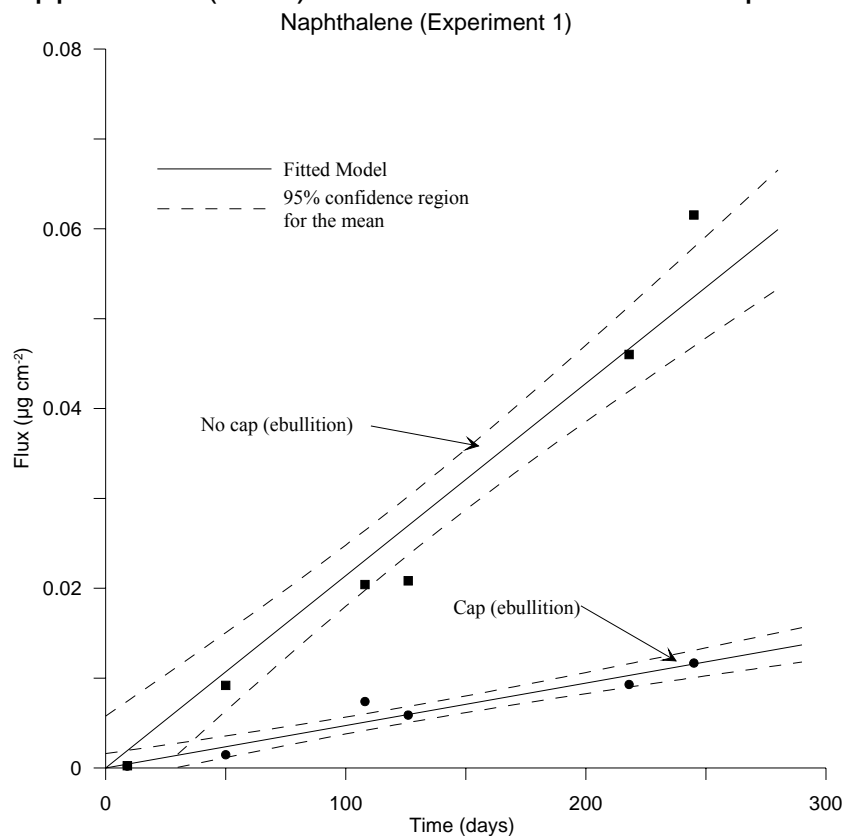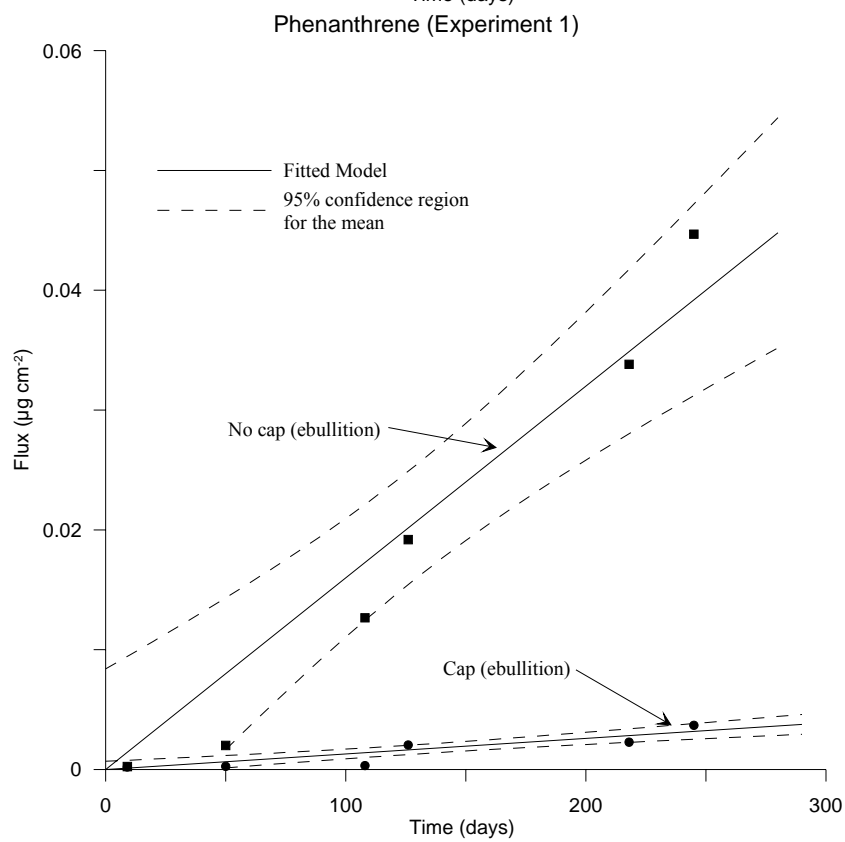
Benzo (a) anthracene (Experiment 1)

Anthracene (Experiment 1)
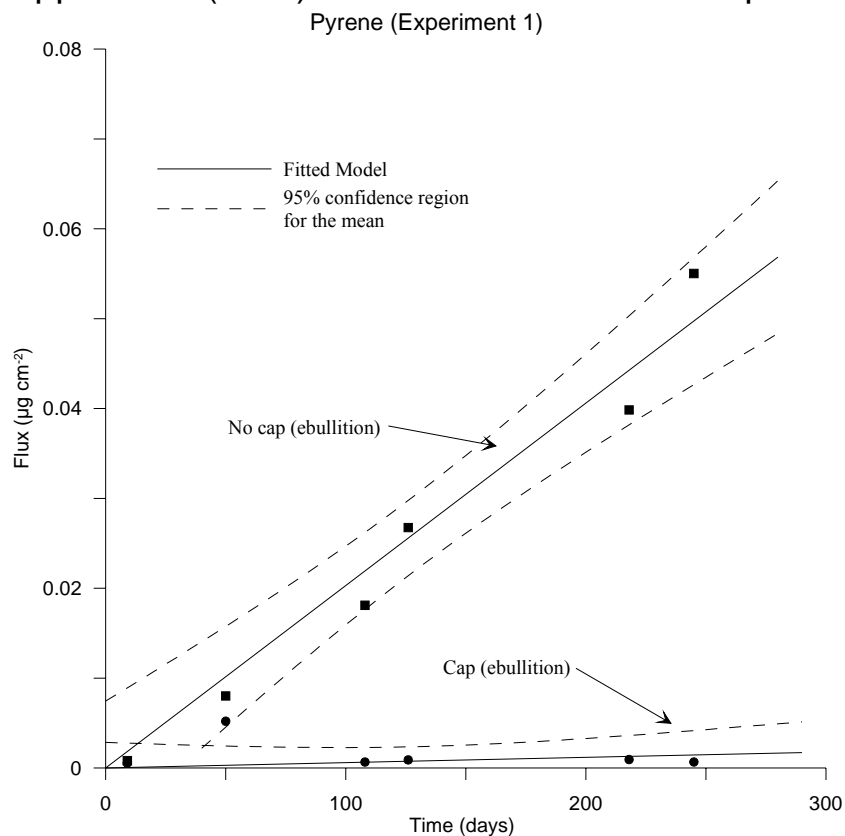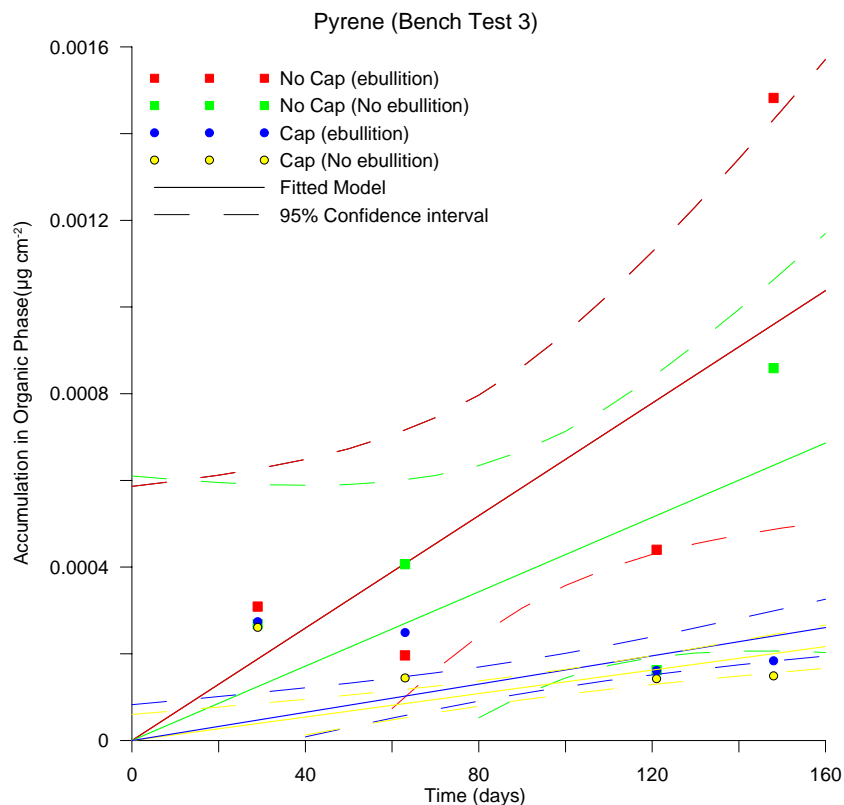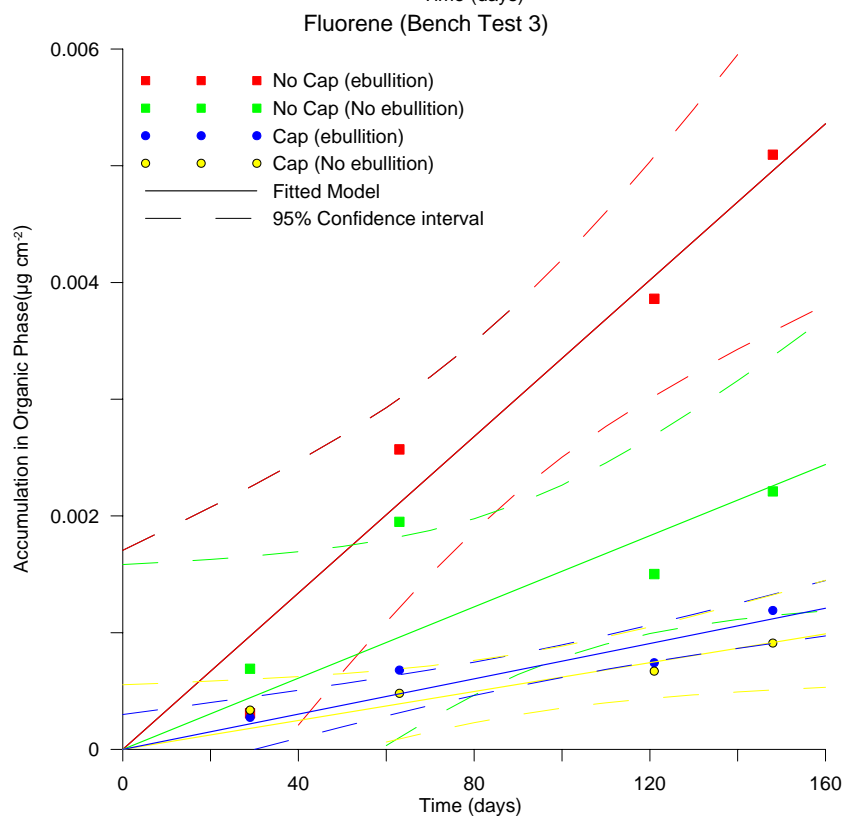
Appendix J (cont') Flux vs time for each compound from Test 2.

Fluoranthene (Experiment 1)

Chrysene (Experiment 1)

Appendix J (cont') Flux vs time for each compound from Test 2.

Naphthalene (Experiment 1)

Naphthalene (Experiment 1)

X-axis: Time (days)
Y-axis: Flux (µg cm^{-2})

Fitted Model
95% confidence region for the mean

No cap (ebullition)
Cap (ebullition)

Fluorene (Experiment 1)

Fluorene (Experiment 1)

X-axis: Time (days)
Y-axis: Flux (µg cm^{-2})

Fitted Model
95% confidence region for the mean

No cap (ebullition)
Cap (ebullition)

Appendix J (cont') Flux vs time for each compound from Test 2.
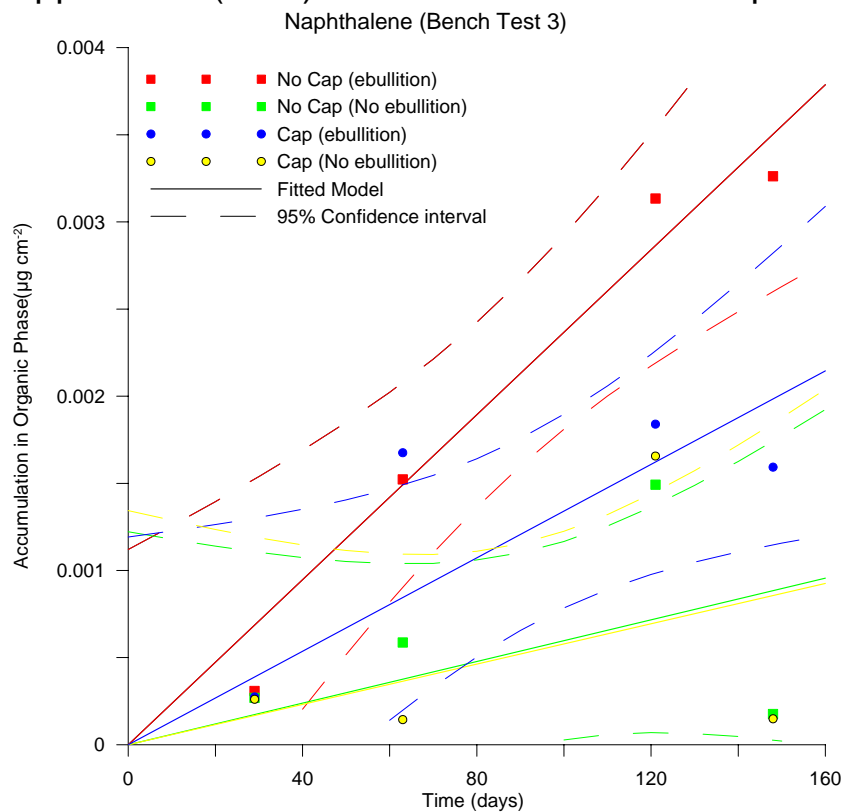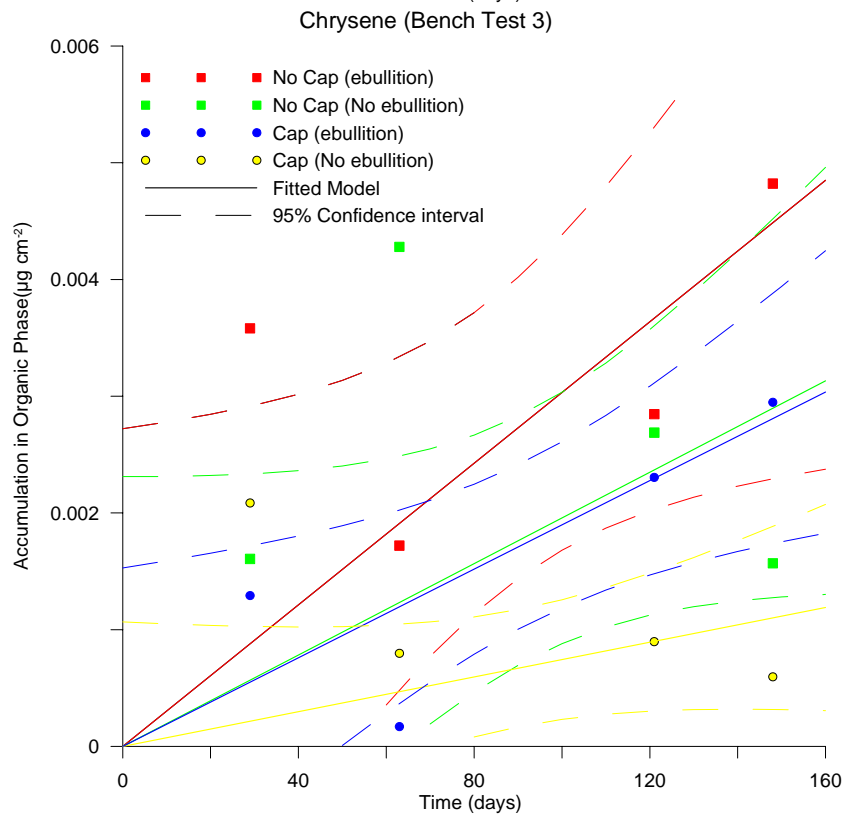

Pyrene (Experiment 1)

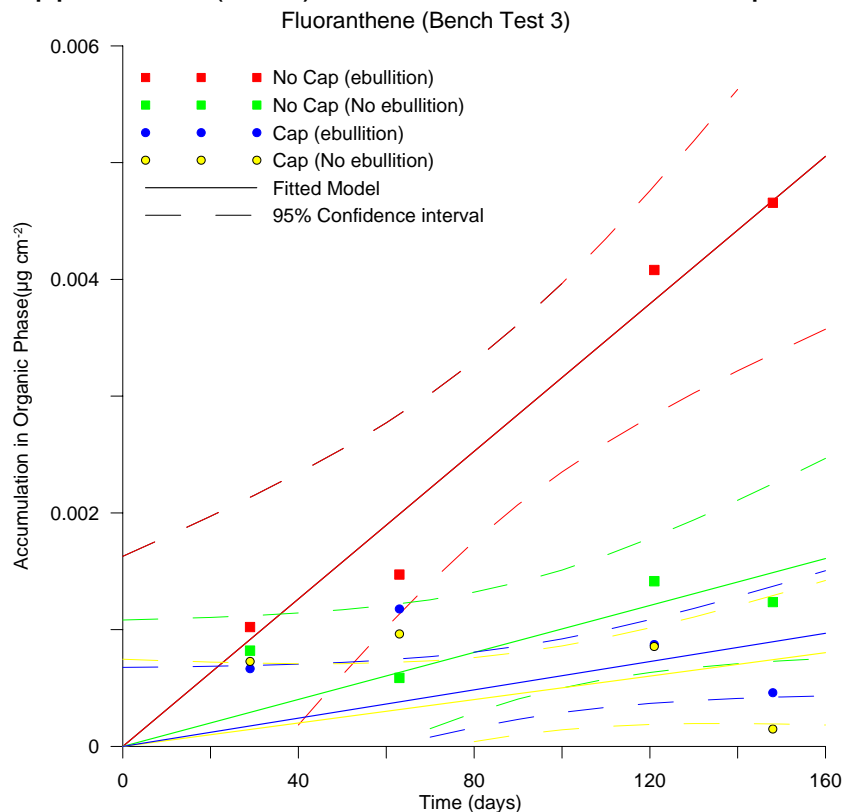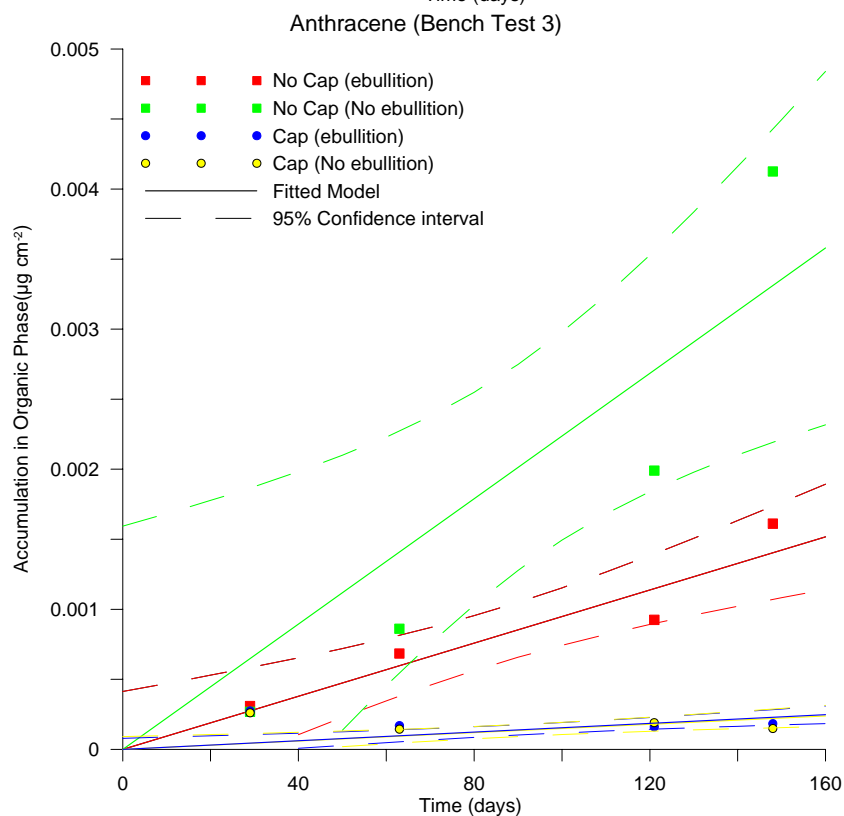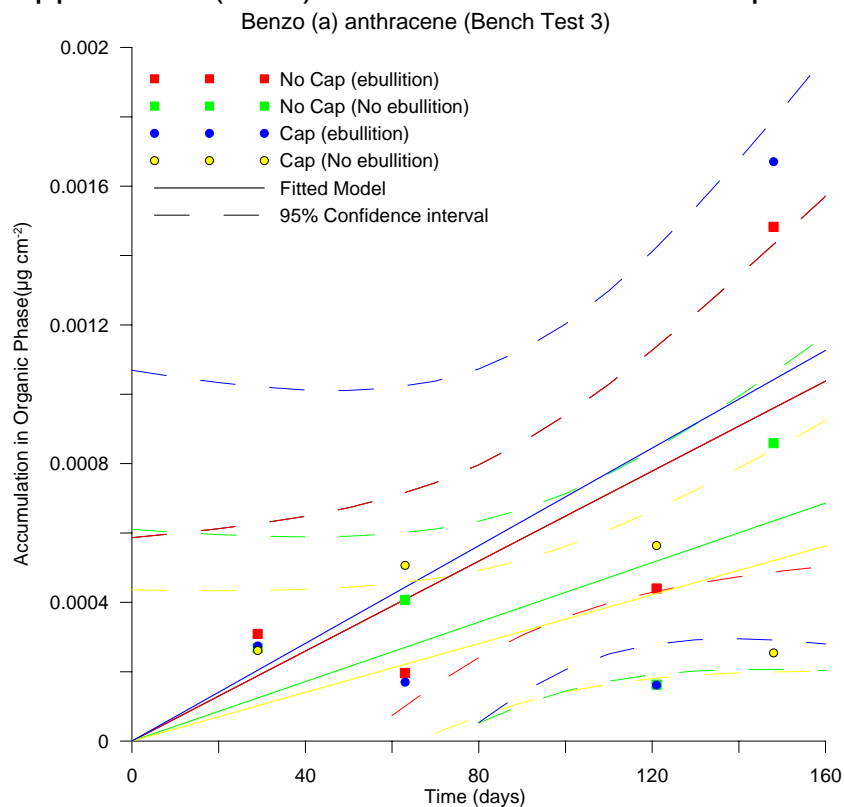Phenanthrene (Experiment 1)
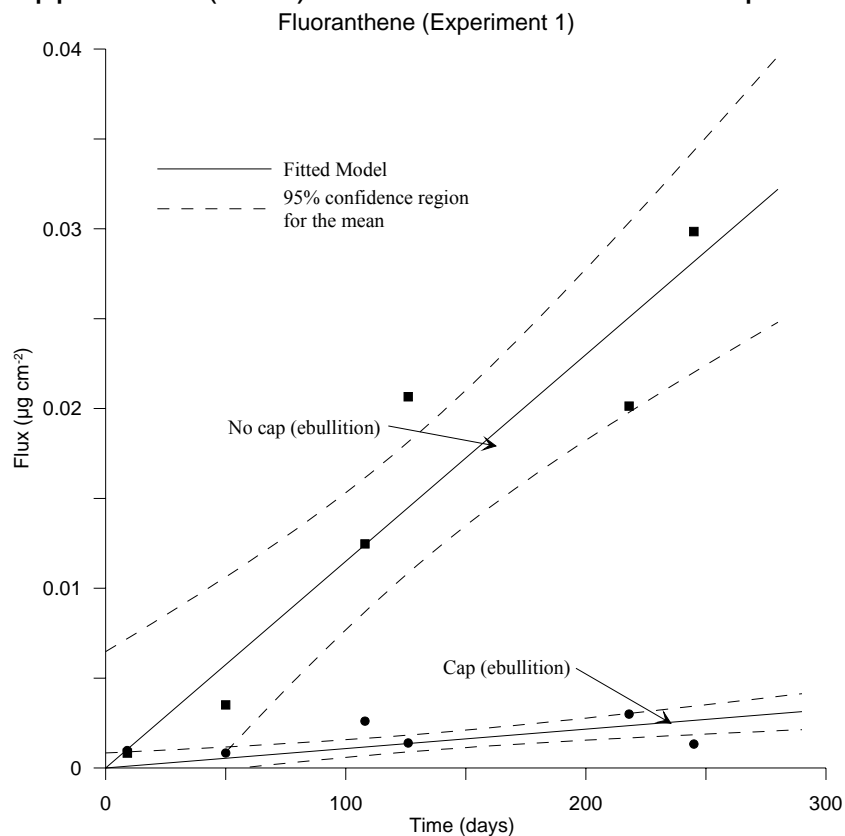
Appendix K Flux vs time for each compound from Test 3.

Pyrene (Bench Test 3)

Phenanthrene (Bench Test 3)

Appendix K (cont') Flux vs time for each compound from Test 3.

Naphthalene (Bench Test 3)

Fluorene (Bench Test 3)

Appendix K (cont') Flux vs time for each compound from Test 3

Fluoranthene (Bench Test 3)

Chrysene (Bench Test 3)

Appendix K (cont') Flux vs time for each compound from Test 3

Benzo (a) anthracene (Bench Test 3)

Anthracene (Bench Test 3)

Appendix K (cont') Flux vs time for each compound from Test 3.

Acenaphtylene (Bench Test 3)

Acenaphtene (Bench Test 3)